

A line confusion-limited millimeter survey of Orion KL

III. Sulfur oxide species

G. B. Esplugues¹, B. Tercero¹, J. Cernicharo¹, J. R. Goicoechea¹, Aina Palau², N. Marcelino³, and T. A. Bell¹

¹ Centro de Astrobiología (CSIC-INTA), Ctra. de Torrejón-Ajalvir, km. 4, E-28850 Torrejón de Ardoz, Madrid, Spain
e-mail: espluguesbg@cab.inta-csic.es

² Institut de Ciències de l'Espai (CSIC-IEEC), Campus UAB-Facultat de Ciències, Torre C5-parell 2, E-08193 Bellaterra, Barcelona, Spain.

³ National Radio Astronomy Observatory, 520 Edgemont Road, Charlottesville, VA 22903, USA.

Received ; accepted

ABSTRACT

Context. We present a study of the sulfur-bearing species detected in a line confusion-limited survey towards Orion KL performed with the IRAM 30-m telescope in the frequency range 80-281 GHz.

Aims. This study is part of an analysis of the line survey divided into families of molecules. Our aim is to derive accurate physical conditions, as well as molecular abundances, in the different components of Orion KL from observed SO and SO₂ lines.

Methods. As a starting point, we assumed LTE conditions obtain rotational temperatures. We then used a radiative transfer model, assuming either LVG or LTE excitation to derive column densities of these molecules in the different components of Orion KL.

Results. We have detected 68 lines of SO, ³⁴SO, ³³SO, and S¹⁸O and 653 lines of SO₂, ³⁴SO₂, ³³SO₂, SO¹⁸O, and SO₂ v₂=1. We provide column densities for all of them and also upper limits for the column densities of S¹⁷O, ³⁶SO, ³⁴S¹⁸O, SO¹⁷O, and ³⁴SO₂ v₂=1 and for several undetected sulfur-bearing species. In addition, we present 2'×2' maps around Orion IRC2 of SO₂ transitions with energies from 19 to 131 K and also maps with four transitions of SO, ³⁴SO, and ³⁴SO₂. We observe an elongation of the gas along the NE-SW direction. An unexpected emission peak appears at 20.5 km s⁻¹ in most lines of SO and SO₂. A study of the spatial distribution of this emission feature shows that it is a new component of a few arcseconds (~5'') in diameter, which lies ~4'' west of IRC2. We suggest the emission from this feature is related to shocks associated to the BN object.

Conclusions. The highest column densities for SO and SO₂ are found in the high-velocity plateau (a region dominated by shocks) and in the hot core. These values are up to three orders of magnitude higher than the results for the ridge components. We also find high column densities for their isotopologues in both components. Therefore, we conclude that SO and SO₂ are good tracers, not only of regions affected by shocks, but also of regions with warm dense gas (hot cores).

Key words. survey-Stars: formation - ISM: abundances - ISM: clouds - ISM: molecules - Radio lines: ISM

1. Introduction

The hot core phase of massive star formation shows a particularly rich chemistry that results from gas-phase chemical reactions and dust grain mantle evaporation. During cloud collapse, depletion of molecules onto dust surfaces takes place. When a new protostar forms, the surrounding gas and dust are heated and molecules sublime from the grain mantles, giving rise to new species in the warm gas and to enhanced abundances of pre-existing species. The existence of molecular outflows and associated shocked regions also plays an important role in the chemical evolution, because they heat up the gas significantly and modify its chemistry.

Orion KL is the closest high-mass star-forming region (≈414 pc, Menten et al. 2007). It is one of the most studied regions owing its chemical complexity and high gas temperature, which lead to a dense and bright line spectrum. In the Orion KL cloud it is useful to differentiate five distinct components, characterized by different physical and chemical conditions (Blake et al. 1987, Persson et al. 2007, Tercero et al. 2010, and references therein): i) the hot core (HC) with 10'' diameter, which contains a high abundance of complex species (Wilson et al. 2000). It is characterized by line widths of $7 \leq \Delta v \leq 15$ km s⁻¹ at v_{LSR} ≈ 5 km s⁻¹. It contains dense and warm gas with T_K ≈ 200 K and n(H₂) ≈ 10⁷

cm⁻³. ii) The plateau (PL), a component with 30'' diameter, is affected by shocks with typical line widths of $\Delta v \approx 20$ -25 km s⁻¹ at v_{LSR} ≈ 6 km/s. Typical temperatures and densities are T_K ≈ 150 K and n(H₂) ≈ 10⁶ cm⁻³, respectively. iii) The high velocity plateau, HVP, (component affected by shocks, with similar temperature and density to the PL) with line widths of $\Delta v \approx 30$ -55 km s⁻¹ at v_{LSR} ≈ 11 km s⁻¹. iv) The compact ridge (CR), with 15'' diameter, centered on v_{LSR} ≈ 7.5 km s⁻¹ with line widths of ~ 4 km s⁻¹. Temperatures are about 110 K and densities ≈ 10⁶ cm⁻³. And v) an extended component, the extended ridge (ER) or ambient cloud, whose emission is characterized by low temperature and density (60 K and 10⁵ cm⁻³, respectively), and line widths similar to the compact ridge, but centered on a velocity of v_{LSR} ≈ 9 km s⁻¹. The luminosity of the Orion Becklin-Neugebauer/Kleinmann-Low complex is ~10⁵ L_⊙ (Gezari et al. 1998). From the model proposed by Wynn-Williams et al. (1984) and without observational evidence, IRC2 was thought to be the main source of luminosity, heating, and dynamics within the region. However, with the detection of two radio continuum point sources, B (coincident with the BN Object) and I (centroid of the Orion SiO maser), it was concluded that the intrinsic luminosity of IRC2 is only a fraction (L ≈ 1000 L_⊙) of the total luminosity of

the complex (Gezari et al. 1998), with source *I* being the main contributor.

In this paper, we continue our analysis of the line survey towards Orion IRc2 in the frequency range 80-281 GHz, first presented by Tercero et al. (2010). Here we concentrate on SO, SO₂, and their isotopologues; we model the different cloud components (hot core, plateau, ridge) and derive their physical and chemical conditions, such as column densities and temperatures. Since Gottlieb & Ball (1973) discovered SO in Orion A, there have been many studies of this molecule, as well as SO₂, in this region, including studies of the gas kinematics (Plambeck et al. 1982), molecular abundances (Blake et al. 1987), and spatial distribution (Sutton et al. 1995). Also we find several interferometric studies of these two molecules such as those from Wright et al. (1996) and Beuther et al. (2005). Sulfur-bearing species are especially sensitive to physical and chemical variations during the lifetime of a hot core (Viti et al. 2001), and therefore are considered good probes of their time evolution (Hatchell et al. 1998). As such, they can be used as tools for investigating the chemistry and physical properties of complex star-forming regions (SFRs) located in dense molecular clouds. On the other hand, it is known that some molecules (SiO, H₂CS, SO, SO₂) show increased abundances in regions affected by shocks (Bachiller et al. 1996) as a result of the action of outflows on the surrounding gas. The study of molecular lines from shocked areas provides valuable information about chemical processes and the physical conditions of the shocked components.

The observations are described in Sect. 2. We present more than 700 detected lines of SO, SO₂, their isotopologues, and their vibrationally excited states. In Section 3 we present the data and compute rotational temperatures as a first LTE approximation. In addition, we present maps of eight emission lines of SO₂, SO, ³⁴SO₂, and ³⁴SO in the 1.3 mm window, over a 2'×2' region around Orion IRc2 (Sect. 3.4). Unlike other studies of SO, we use a non-LTE radiative transfer code (LVG) to derive physical and chemical parameters (Sect. 4). We provide column density calculations for SO and SO₂, and isotopic abundance ratios, which have been improved over previous works due to the much larger number of available lines and to the up-to-date information on the physical properties of the region and molecular constants. Discussions on our results are included in Sect. 5, while Sect. 6 summarizes the main conclusions.

2. Observations

We continue our analysis of the line survey towards Orion IRc2 covering frequency ranges 80-115.5 GHz, 130-178 GHz, and 197-281 GHz, first presented by Tercero et al. (2010). The observations were carried out using the IRAM 30-m radiotelescope during September 2004 (1.3 mm and 3 mm windows), March 2005 (full 2 mm window), and April 2005 (completion of the 1.3 mm and 3 mm windows). Four SiS receivers operating at 1.3, 2, and 3 mm were used simultaneously, with image sideband rejections within ~13 dB (1.3 mm receivers), 12-16 dB (2 mm receivers), and 20-27 dB (3 mm receivers). System temperatures were in the range 200-800 K for the 1.3 mm receivers, 200-500 K for the 2 mm receivers, and 100-350 K for the 3 mm receivers, depending on the particular frequency, weather conditions, and source elevation. For the spectra between 172-178 GHz, the system temperature was significantly higher, 1000-4000 K, owing to the proximity of the atmospheric water line at 183.31 GHz. The intensity scale was calibrated using two absorbers at different temperatures and using the atmospheric transmission model (ATM, Cernicharo 1985; Pardo et al. 2001).

Table 1. IRAM 30m telescope efficiency data along the covered frequency range.

Frequency (GHz)	η_{MB}	HVPBW (")
86	0.82	29.0
100	0.79	22.0
145	0.74	17.0
170	0.70	14.5
210	0.62	12.0
235	0.57	10.5
260	0.52	9.5
279	0.48	9.0

Pointing and focus were regularly checked on the nearby quasars 0420-014 and 0528+134. Observations were made in the balanced wobbler-switching mode, with a wobbling frequency of 0.5 Hz and a beam throw in azimuth of $\pm 240''$. No contamination from the off position affected our observations, except for a marginal amount at the lowest elevations (25°) for molecules showing low-*J* emission along the extended ridge. Two filter banks with 512×1 MHz channels and a correlator providing two 512 MHz bandwidths and 1.25 MHz resolution were used as backends. We pointed the observations towards IRc2 at $\alpha(\text{J2000})=5^{\text{h}} 35^{\text{m}} 14.5^{\text{s}}$, $\delta(\text{J2000})=-5^{\circ} 22' 30.0''$.

The data were processed using the IRAM GILDAS software¹ (developed by the Institut de Radioastronomie Millimétrique). In our analysis we only considered lines with intensities ≥ 0.02 K, covering three or more channels. Spectra with Gaussian line fits are shown in units of antenna temperature T_{A}^* corrected for atmospheric absorption and spillover losses. Figures with results from LVG/LTE analysis are shown in units of main beam temperature T_{MB} , which is defined as

$$T_{\text{MB}} = \left(T_{\text{A}}^* / \eta_{\text{MB}} \right), \quad (1)$$

where η_{MB} is the main beam efficiency. Table 1 shows the half power beam width (HVPBW) and the mean beam efficiencies over the covered frequency range. For further information about the data reduction and line identification, see Tercero et al. (2010).

We also used the 30-m telescope to map a 2'×2' region around IRc2 at 1.3 mm. In this two-dimensional (2D) line survey (Marcelino et al., in prep.), we covered the 1.3 mm window using the nine pixel HERA receiver array (216–250 GHz) and the EMIR single-pixel heterodyne receivers (200–216 and 250–282 GHz). We also mapped a small fraction of the 3 mm band taking advantage of simultaneous observations with the E230 and E090 receivers. Fully sampled maps over 140×140 arcsec², centered on the position of IRc2, were performed in the *on-the-fly* (OTF) mapping mode, scanning both in α and δ with a 4'' spacing, and using position-switching to an emission-free reference position at an offset (-600'', 0'') with respect to IRc2. The observations presented here were obtained in February and December 2008 (HERA), February 2010, and January 2012 (EMIR). We used local oscillator settings at frequencies of 109.983, 221.600, 226.100, 235.100, 239.100, and 258.000 GHz, depending on the observed transition. We used short Wobbler-switching observations on the central position with a slightly different frequency for each setting, in order to remove all features arising from the image side band. We used the WILMA spectrometer backend, with a total bandwidth of 4 GHz (EMIR), 1 GHz (HERA), and a

¹ <http://www.iram.fr/IRAMFR/GILDAS>

spectral resolution of 2 MHz, corresponding to velocity resolutions of 5.4 km s^{-1} at 3 mm and 2.7-2.3 at 1.3 mm. Weather conditions were the typically good winter conditions (with opacities $\sim 0.1 - 0.2$ at 1.3 mm and 1.3-2 mm of precipitable water vapor) resulting in system temperatures of 230-250 K (EMIR) and 300-400 K (HERA), except for observations in February 2010, when conditions were $\tau \sim 0.3-0.4$ and 5 mm of pwv. In this case, system temperatures of 150 K and 300-400 K were obtained at 110 and 239 GHz, respectively. Pointing was checked every hour on strong and nearby quasars, and found to have errors of typically less than 3-4 arcsec.

The basic data reduction consisted of fitting and removing first-order polynomial baselines, checking for image sideband contamination and emission from the reference position. HERA data needed further reduction analysis due to the different performance of each pixel in the array. Spectra from all pixels were averaged to obtain a uniform map gridding of $4''$, taking their different flux calibration and internal pointing errors into account (see Marcelino et al. in prep. for details).

3. Results

In total, the survey covers a bandwidth of 168 GHz, and of the 15,200 detected spectral features, about 10,700 have been identified and attributed to 45 molecules, including 191 isotopologues and vibrationally excited states (Tercero et al. 2010). We identify 20 lines of SO, 21 lines of ^{34}SO , 13 lines of ^{33}SO , and 14 lines of S^{18}O . We also detect 166 lines of SO_2 , 129 lines of $^{34}\text{SO}_2$, 85 lines of $^{33}\text{SO}_2$, 129 lines of SO^{18}O , 74 lines of SO^{17}O , and 78 lines of $\text{SO}_2 \nu_2$. Observed transitions of SO have a range of energy E_{up} between 16 and 100 K and a full width at half maximum (FWHM) of 40 km s^{-1} . In the case of SO_2 the energy range for the observed transitions is 12-1480 K and FWHM of 30-40 km s^{-1} for transitions $J < 25$ and FWHM $\sim 10-20 \text{ km s}^{-1}$ for transitions $J > 25$. All these identifications are shown in Tables A.8 and A.9 (see Appendix). Those tables list the spectroscopic parameters² of each transition, together with the observed line properties of the detected lines.

SO was the first molecule with a $^3\Sigma$ electronic ground-state detected in space by radio techniques (Gottlieb & Ball 1973). Its rotational levels are characterized by the rotational angular momentum quantum number, N , and the total angular momentum quantum number, J , which includes the contribution of the angular momentum of two unpaired electrons. For ^{33}S and ^{17}O , the nuclear quadrupolar momentum couples with the rotation to produce a hyperfine splitting of the rotational levels. Selection rules for the electric dipole transitions are: $\Delta N = \pm 1$, $\Delta F = 0, \pm 1$, and $\Delta J = 0, \pm 1$, in the absence of external fields. In the case of inter-

mediate coupling, transitions are allowed for $\Delta N = \pm 3$. The magnetic dipole transitions occur with the selection rules: $\Delta N = 0, \pm 2$ and $\Delta J = 0, \pm 1$. However, these transitions are extremely weak compared to the electric dipole transitions. We have estimated that the magnetic dipole allowed transitions SO will have intensities $\sim 1-6 \text{ mK}$, i.e., lines within the confusion limit of Orion ($T_{\text{A}}^* = 20 \text{ mK}$).

SO_2 is an asymmetric molecule. The rotational energy levels are characterized by the three quantum numbers J , K_{-1} , and K_{+1} . Since triatomic molecules are planar, the dipole moment components can only occur in the a- and b-axis directions. The selection rules for a-type transitions are $\Delta J = 0, \pm 1$, $\Delta K_{-1} = 0, \pm 2$, and $\Delta K_{+1} = \pm 1, \pm 3$. For b-type transitions: $\Delta J = 0, \pm 1$, $\Delta K_{-1} = \pm 1, \pm 3$, and $\Delta K_{+1} = \mp 1, \mp 3$. SO_2 has its dipole moment along the b axis of the molecule. The nuclear quadrupolar momentum of ^{33}S and ^{17}O also couples with the rotation leading to hyperfine structure.

As a starting point, we fitted each observed line with Gaussian profiles using CLASS to derive the contribution of each cloud spectral component (see Sect. 3.1). We assumed that the emission is optically thin and the observed lines are thermalized at a given temperature that was derived from rotational diagrams (see Goldsmith & Langer 1999), providing rotational temperatures for the different components of the cloud (Sect. 3.3). In Sect. 4 we use a radiative transfer code for a more advanced analysis of the LTE and non-LTE emission of SO and SO_2 species.

3.1. Line profiles

Figures 1, 2, 3, and 4 show the line profiles of some observed transitions of SO and SO_2 , together with Gaussian fit results. To avoid degeneration, we fixed radial velocities (v_{LSR}) considering the characteristic values of each component of Orion KL. And we left the line width, the integrated intensity, and the antenna temperature as free parameters in the fits (in the results, we took the typical ranges of line widths into account for each component found in the bibliography, discarding those with large differences). In addition to the contribution from the usual components listed above, we also observe an unexpected emission peak centered on a velocity of $\approx 20.5 \text{ km s}^{-1}$. We discuss its origin in Sects. 3.2 and 5.2.

We have detected 20 rotational transitions of SO, eight of which are blended with lines of other species. Figure 1 shows the contribution of the different cloud components to the emerging profile. We tried to fit the lines by considering only one plateau instead of two (at high and low velocity). First we centered this single plateau component on a velocity around 6-7 km s^{-1} , but with this we could not fit the part of the line profiles covering high ($> 20 \text{ km s}^{-1}$) velocities. With an increase in the line width of the fit, we reproduced this part of the profiles, but we overestimated the part of the lines that covers negative velocities. We found the opposite behavior if we fixed the single plateau component at higher velocities. Therefore we deduced that the best fits were obtained by considering two plateau components: one at low velocity, PL, ($\sim 6.5 \text{ km s}^{-1}$) and the other at high velocity, HVP, ($\sim 12 \text{ km s}^{-1}$). We observe that the emission mainly arises from these both plateau components. For transitions with angular momentum quantum number $N \lesssim 5$, the strongest emission is found from the HVP, while for $N \gtrsim 5$ PL presents the highest contribution to the emission. The contribution from the ER is very small. In this LTE analysis of SO, we have not considered the compact ridge component since its contribution is difficult to distinguish from the contribution from the HC. The parameters

² Spectroscopic parameters for SO (dipole moment $\mu = 1.535 \text{ D}$) have been obtained from Clark & DeLucia (1976), Tiemann (1982), Lovas et al. (1992), Cazzoli et al. (1994), Klaus et al. (1996), Bogey et al. (1997), Powell & Lide (1964), and Martin-Drumel (2012). For ^{34}SO and S^{18}O ($\mu = 1.535 \text{ D}$) from Tiemann (1974), Tiemann (1982), Lovas et al. (1992), Klaus et al. (1996), Bogey et al. (1982), and Powell & Lide (1964). And for ^{33}SO ($\mu = 1.535 \text{ D}$) from Klaus et al. (1996), Lovas et al. (1992), and Powell & Lide (1964). In the case of SO_2 and $^{33}\text{SO}_2$ ($\mu = 1.633 \text{ D}$), the spectroscopic parameters were taken from Müller et al. (2000) and Patel et al. (1970). For $^{34}\text{SO}_2$ ($\mu = 1.633 \text{ D}$) from Belov et al. (1998) and Patel et al. (1979). For the isotopologue SO^{18}O ($\mu_a = 0.0328 \text{ D}$, $\mu_b = 1.633 \text{ D}$) obtained from Belov et al. (1998) and for SO^{17}O ($\mu_a = 0.02 \text{ D}$, $\mu_b = 1.633 \text{ D}$) from Müller et al. (2000). For the vibrational state $\text{SO}_2 \nu_2 = 1$, ($\mu = 1.626 \text{ D}$) from Müller & Brünken (2005) and from Patel et al. (1979), and for $^{34}\text{SO}_2 \nu_2 = 1$, ($\mu = 1.626 \text{ D}$) from Maki & Kuritsyn (1990).

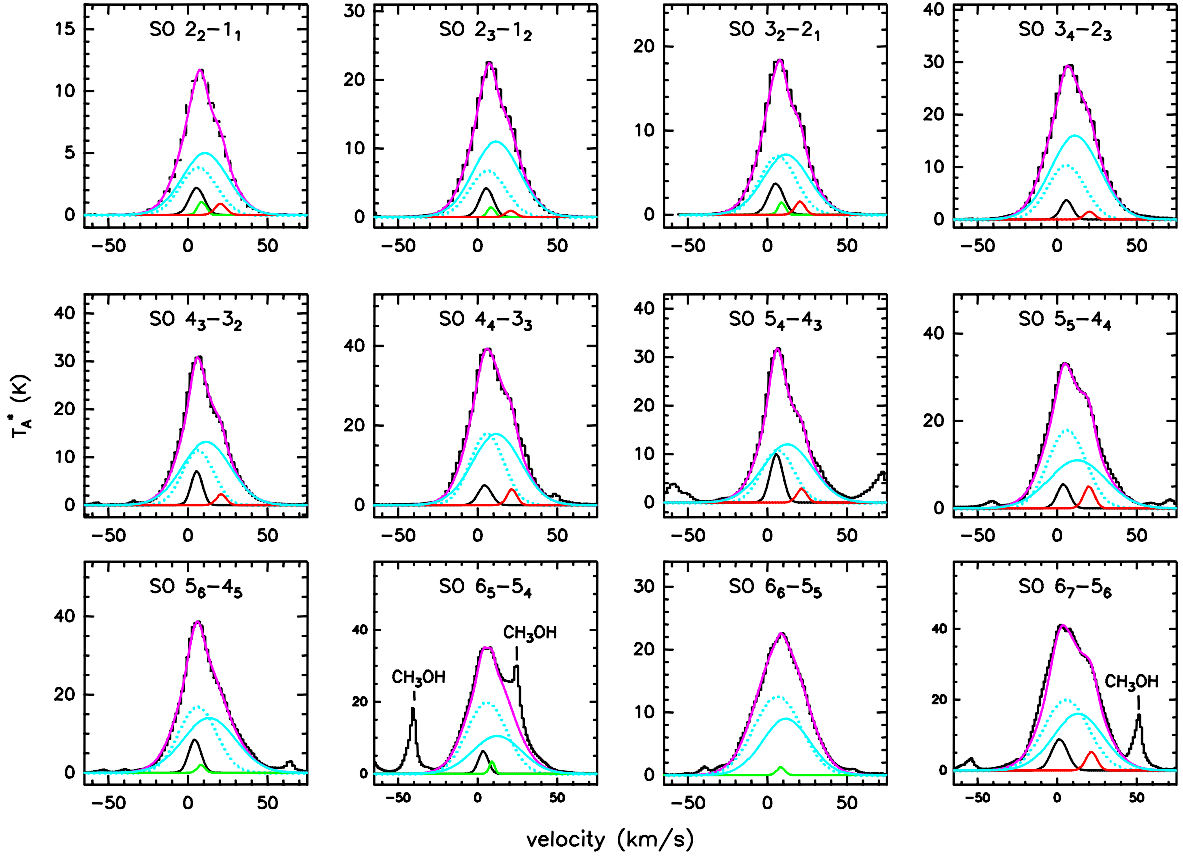


Fig. 1. Gaussian fits to the observed SO lines. Dashed line for the plateau, cyan (solid line) for the high-velocity plateau, black for hot core, green for extended ridge, and red for the contribution of the component at 20.5 km s^{-1} . The total fit is shown in magenta. The data are the black histogram spectra.

obtained from Gaussian fits for some of the SO lines are listed in Table A.1 (see Appendix).

For SO_2 we have clearly identified 166 rotational transitions (see Figs. 2, 3, and 4). As indicated by their broad line profiles, we see that most of the emission comes from the plateau components, especially for transitions $J < 20$ where the HVP plays an important role. However, for transitions $J > 20$ the HC dominates. The parameters obtained for each component from Gaussian fits for SO_2 lines are listed in Tables A.2 and A.3 (see Appendix). Comparing this with SO lines, we see that the line profiles of both species are very similar.

3.2. The 20.5 km s^{-1} feature and absorption at 15 km s^{-1}

Unlike the other species detected in the survey, we clearly observe an emission peak at $\approx 20.5 \text{ km s}^{-1}$ in most SO and SO_2 lines. From Gaussian fits, we find that the line widths are $\sim 7.5 \text{ km s}^{-1}$. This feature presents an increase in the line intensity with frequency (i.e., with smaller beam). Figure 5 shows the integrated intensity, W , as a function of the frequency for the 20.5 km s^{-1} component for SO lines. We see that, for the same line width, W increases with frequency with a dependence as ν^2 . This means that the size of the region responsible for this velocity component is only a few arcseconds in diameter ($< 9''$, smaller than the IRAM 30-m beam at the highest frequencies). The emission of this component could come from the interaction of the outflow with the ambient cloud; however, it should be noted that while in Orion-KL the v_{LSR} of the different components varies approximately between 3 and 10 km s^{-1} , Scoville et

al. (1983) inferred that the *BN* (Becklin-Neugebauer) object in Orion presents a significantly higher LSR velocity of around 21 km s^{-1} , therefore another possibility is that this feature located at 20.5 km s^{-1} arises from the *BN* source.

On the other hand, between the main emission peak of the line profiles of SO and SO_2 and this emission peak at 20.5 km s^{-1} , we observe a dip at $\approx 15 \text{ km s}^{-1}$. Tercero et al. (2011) also find a velocity component at 15.5 km s^{-1} in SiS emission lines ($\nu=0$), and one component of the SiO maser emission ($\nu=1$). Since the opacity is high for some lines of SO and SO_2 , as well as for SiO, another possibility is that this dip may be the result of self-absorption. This could suggest that the SO and SO_2 dips at 15.5 km s^{-1} are produced by the same gas observed in SiS. In Section 5 we draw firmer conclusions about the origin of the dip at 15.5 km s^{-1} and of the peak at 20.5 km s^{-1} from maps of SO and SO_2 .

3.3. Rotational diagrams

The results from the Gaussian fits have been used to build rotational diagrams for each species. This method involves the representation of the upper level column density normalized by the statistical weight of each rotational level versus the upper level energy, assuming optically thin emission filling the beam (see, e.g., Goldsmith & Langer et al 1999). The expression used to obtain the rotational diagrams, taking an optical depth (C_τ) different to unity into account, is

$$\ln(\gamma_u W/g_u) = \ln(N) - \ln(C_\tau) - \ln(Z) - (E_u/kT), \quad (2)$$

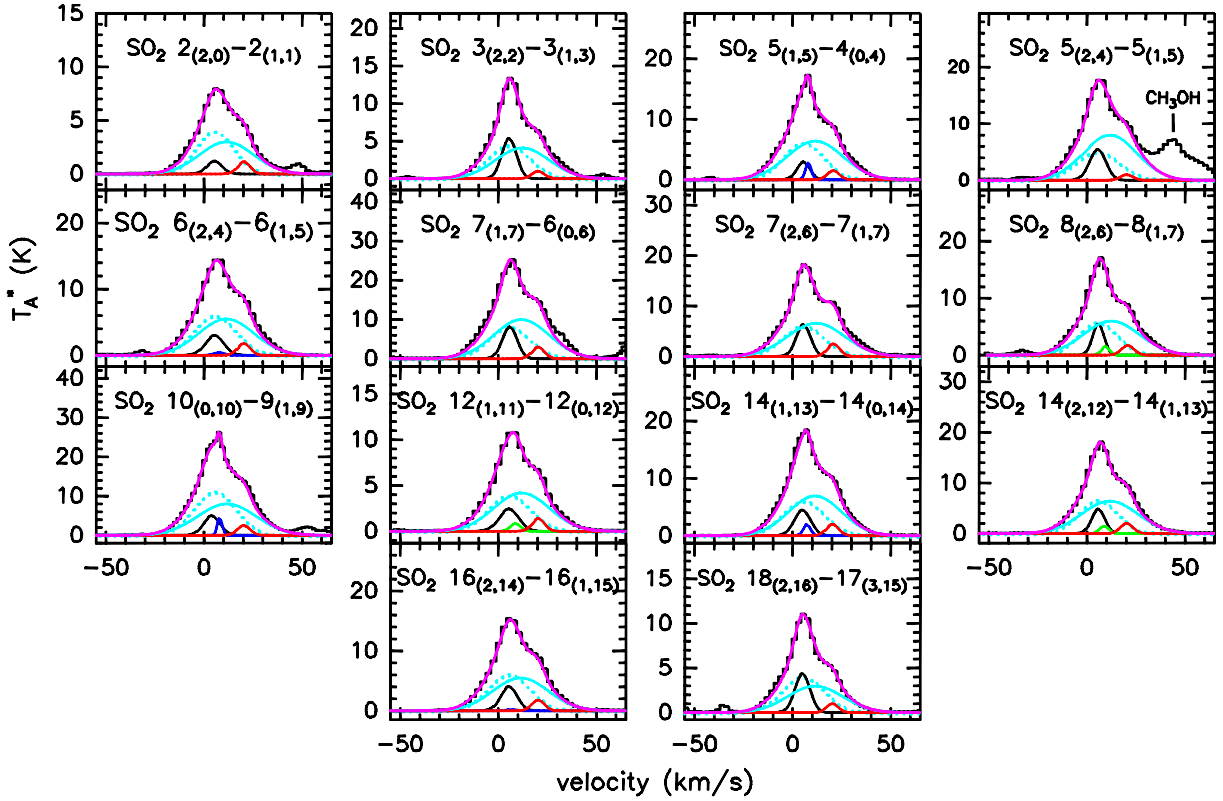


Fig. 2. Gaussian fits for the SO₂ lines (2 mm data). The total fit is shown in magenta. Plateau is represented with the dashed line, high-velocity plateau in cyan (solid line), hot core in black, compact ridge in blue, extended ridge in green, and 20.5 km s⁻¹ component in red. The data are the black histogram spectra.

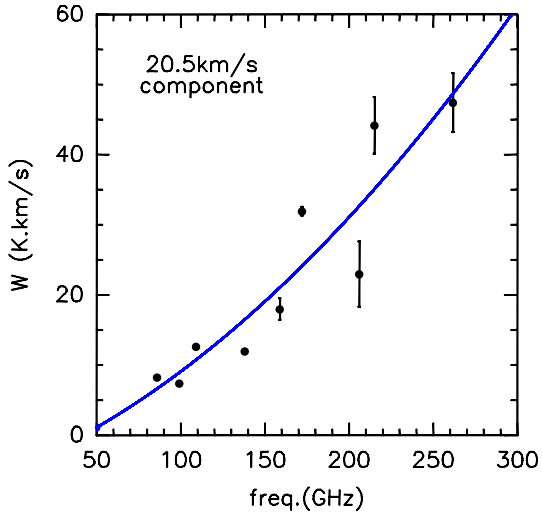


Fig. 5. Integrated line intensities of the 20.5 km s⁻¹ component as a function of the line frequency for SO transitions.

where W is the integrated line intensity, g_u is the statistical weight of each level, N the column density, Z the partition function, E_u the level energy, k the Boltzman constant, T the temperature considering local thermodynamic equilibrium, and γ_u a constant that depends on the transition frequency and the Einstein coefficient A_{ul} (see Goldsmith & Langer 1999 for more details). Each cloud component is considered separately in the analysis. The rotational diagrams, shown in Figs. A.1 and A.2 (see Appendix), were obtained considering only lines without contamination from other species. The rotational tempera-

tures obtained from SO₂ lines are plateau (PL)=120±20 K, hot core (HC)=190±60 K, high-velocity plateau (HVP)=110±20 K, compact ridge (CR)=80±30 K, extended ridge (ER)=83±40 K and 20.5 km s⁻¹ component=90±20 K. The results from SO lines are (PL)=130±20 K, (HC)=288±90 K, (HVP)=111±15 K, (ER)=107±40 K, and 20.5 km s⁻¹ component=51±10 K. These results are shown in Table A.4 (see Appendix), together with the derived column densities and the optical depths. For each component, the obtained rotational temperatures for both molecules are consistent with each other, except for the HC where we obtain a large difference between both temperatures. This could indicate a temperature gradient in the hot core, or simply that the obtained rotational temperature could be overestimated due to the high scatter in the SO data. It would be necessary to have values of this species at higher energies in order to obtain firmer conclusions. We observe that HVP presents a similar rotational temperature to the component of the plateau with lower velocity (PL). For the CR, we obtained a low temperature, probably due to the beam dilution, which is not corrected for in the rotational diagrams. From the diagrams, we also deduce that the new component at 20.5 km s⁻¹ is not a very warm region.

3.4. 2'×2' maps around IRC2

From the 2D line survey data of Orion KL, (Marcelino et al. in prep.), we produced integrated intensity maps of several SO and SO₂ transitions over different velocity ranges. Figure 7 shows the transitions 4_(2,2)-3_(1,3), 11_(1,11)-10_(0,10), and 14_(3,11)-14_(2,12) of SO₂; Fig. 6 shows the transitions 6₆-5₅ and 3₂-2₁ of SO; and Fig. 8 shows the transition 6₇-5₆ of ³⁴SO and the transition 28_(3,25)-28_(2,26) of ³⁴SO₂. Velocity intervals in the figures

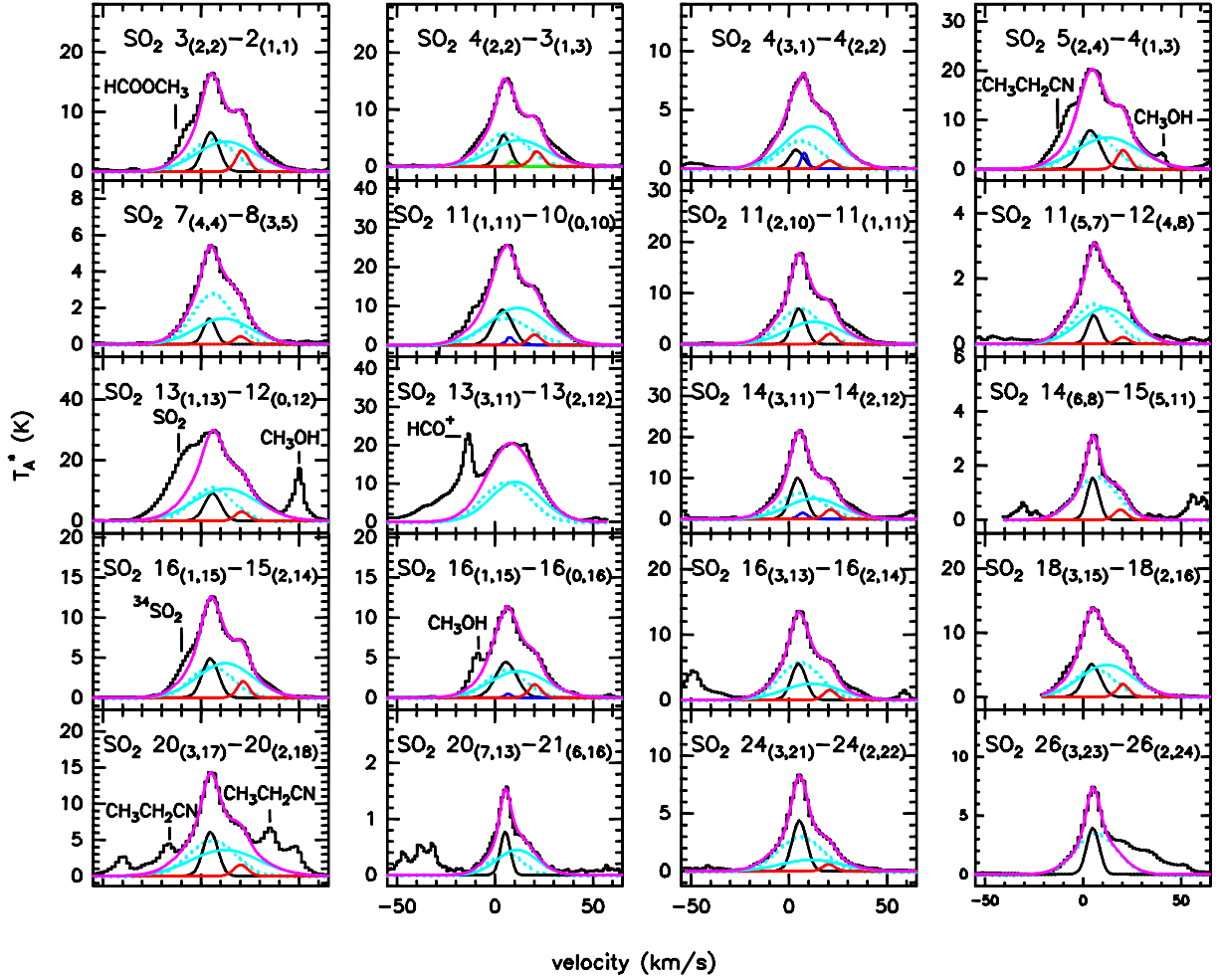


Fig. 3. Gaussian fits for the SO₂ lines (1.3 mm data). The total fit is shown in magenta. Plateau is represented with the dashed line, high-velocity plateau in cyan (solid line), hot core in black, compact ridge in blue, extended ridge in green, and 20.5 km s⁻¹ component in red. The data are the black histogram spectra.

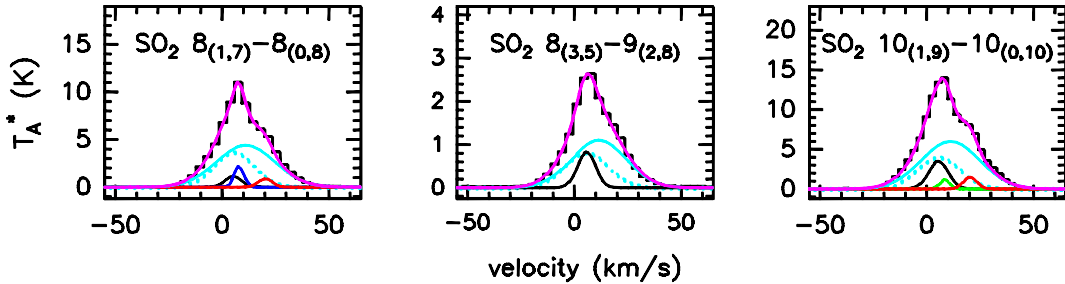


Fig. 4. Gaussian fits for the SO₂ lines (3 mm data). The total fit is shown in magenta. Plateau is represented with the dashed line, high-velocity plateau in cyan (solid line), hot core in black, compact ridge in blue, extended ridge in green, and 20.5 km s⁻¹ component in red. The data are the black histogram spectra.

have been chosen to represent different source components. For all species and transitions, the strongest contribution arises from the velocity ranges 3–7 km s⁻¹ and 10–14 km s⁻¹, belonging to the HC and the HVP, respectively. The range 3–7 km s⁻¹ also includes PL velocities. These maps show elongated emission along the direction NE–SW. This agrees with Plambeck et al. (2009), who find (from SiO $J=2-1$ observations with an angular resolution of 0.45'') that the strongest emission arises from a bipolar outflow covering velocities from -13 to 16 km s⁻¹ along the NE–SW direction. This distribution is clearly seen in the maps of ³⁴SO and of SO (see lower panel in Fig. 6), espe-

cially in the ranges 7–10 km s⁻¹ (ridge) and 10–14 km s⁻¹ (HVP). Since the line widths corresponding to the HVP are the widest, with FWHM~ 30–40 km s⁻¹, altogether this suggests that the gas of the high velocity plateau is expanding in the direction NE–SW. On the other hand, the spatial distribution of ³⁴SO₂ is less extended and usually shows a peak to the NE of IRc2 (also seen in SO₂ and SO at velocities 3–7 km s⁻¹). For this species, the NE–SW distribution is better traced by the 20.5 component. This different behavior should be due to the high energy level ($E_{\text{up}}=402.1$ K) compared to the other mapped transitions, revealing the most compact and hottest regions in the KL cloud.

Also evident on the maps is the new component at 20.5 km s^{-1} . From Figs. 7 and 6 we observe that its emission peak is located between the HC and BN positions.

4. Analysis

4.1. LVG models of the SO lines

In this section we analyze the non-LTE excitation and radiative transfer of SO lines. Following the study started by Tercero et al. (2010), we use an LVG (large velocity gradient) code, MADEX, developed by Cernicharo (2012) assuming that the width of the lines is due to the existence of large velocity gradients across the cloud, so that the radiative coupling between two relatively close points is negligible, and the excitation problem is local. The LVG models are based on the Goldreich & Kwan (1974) formalism. The final considered fit is the one that reproduces more line profiles better from transitions covering a wide energy range, within a $\sim 30\%$ of the uncertainty in line intensity. For each component of the cloud, we assume uniform physical conditions (kinetic temperature, density, line width, radial velocity, and source size) that we choose taking into account the parameters obtained from the Gaussians fits of the line profiles, the rotational diagrams (with the derived rotational temperatures), and the mapped transitions.

Only for the HC do we consider LTE, which means that most transitions will be thermalized to the same temperature ($T_{\text{rot}} \approx T_{\text{K}}$). If this condition was not satisfied, but we kept considering LTE approximation, the temperatures would be overestimated, and this would produce a variation in the column densities. We cannot estimate whether they would be overestimated or underestimated since we do not know the population of each level. However, the HC of Orion presents a condition of temperature ($T_{\text{K}} > 200 \text{ K}$) and density ($n(\text{H}_2) \approx 10^7 \text{ cm}^{-3}$), which make the LTE assumption in this component feasible. Corrections for beam dilution are also applied for each line depending on the different beam sizes at different frequencies. Therefore, we fix all the above parameters (see Table 2) leaving only as a free parameter the column density for each component. For the density, $n(\text{H}_2)$, we have adopted fixed values taken from typical values quoted in the literature. In order to determine the uncertainty of the values of hydrogen density and of temperature (T_{K}), we have run several models varying only the values for these parameters and fixing the rest.

Comparing the intensity differences between the spectra and the obtained line profiles for each case of T and n , we deduce an uncertainty of 20 and 15% for the temperature and the hydrogen density, respectively. Although the parameter which could introduce higher uncertainty in the line profiles is the considered source size for each component, due to it varies depending on the molecular emission used for its determination. We fixed this parameter, as well as the hydrogen density, taking into account also the values used by Tercero et al. (2011) in her models of SiO and SiS. Other sources of uncertainty in the model predictions arise from the spatial overlap of the different cloud components. However, it has been possible to model their contribution thanks to the wide range of frequency and to the large number of lines from different isotopologues. We also find as a source of uncertainty the modest angular resolution of any single-dish line survey, pointing errors (errors as small as $2''$ could introduce important changes in the contribution from each cloud component to the observed line profiles, especially at 1.3 mm), and line opacity effects. This last source of uncertainty becomes important when lines arising from the plateau are optically thick, causing

an underestimation of the column densities of the components that are surrounded by the plateau (compact ridge, hot core, and the 20.5 km s^{-1} component) along the line of sight (Schultz et al. 1999). In Tercero et al. (2010), these sources of uncertainty are explained in more detail. We estimate an uncertainty in our model intensity predictions of 25% for SO and ^{34}SO , and 35% for SO_2 , $^{34}\text{SO}_2$, ^{33}SO , S^{18}O , $^{33}\text{SO}_2$, and SO^{18}O lines (higher uncertainty for SO_2 with respect to SO because of considering LTE instead of LVG approximation).

4.1.1. SO

To model the rotational lines of SO (listed in Table A.8, see Appendix), we used the collisional rates from Lique et al. (2006) for collisions with H_2 . Figure 9 shows our best fit model. The component with the highest SO column density is the HVP, with $N(\text{SO}) = (5 \pm 1) \times 10^{16} \text{ cm}^{-2}$ (see Table 3), although in the HC we also find a high column density with $N(\text{SO}) = (9 \pm 3) \times 10^{15} \text{ cm}^{-2}$. We find that the PL and the 20.5 km s^{-1} component also contribute to the emission, but with a column density that is one order of magnitude lower than the HVP. We did not need to consider any contribution from the CR for SO. We could fit the narrow component by considering only the contribution from a single ridge (the extended ridge) at a temperature $T_{\text{K}} = 60 \text{ K}$. This agrees with the previous SO analysis in Sect. 3.1.

The model indicates that some SO lines with emission coming mainly from the high-velocity plateau are optically thick. The optical depths are $\tau = 1.1\text{--}1.4$ for the transitions $6_5\text{--}5_4$ and $6_6\text{--}5_5$, and $\tau = 1.4\text{--}1.8$ for the transitions $5_6\text{--}4_5$ and $6_7\text{--}5_6$. This means that the column densities obtained for the HC and 20.5 km s^{-1} components, which are surrounded by the plateau, must be considered as lower limits, because the gas in the plateau components can absorb the emission from them. The HVP column density also has to be considered as a lower limit due to this opacity effect. We have also calculated the SO column density from the column density of ^{34}SO , whose lines are optically thin, and from the solar abundance ratio $^{32}\text{S}/^{34}\text{S} = 23$ (Anders & Grevesse 1989). As we expected, Table 3 shows that the column densities of SO obtained from ^{34}SO are higher than those obtained from the fits. This confirms the presence of opacity effects on SO lines. We notice that the SO lines $2_1\text{--}1_2$, $5_4\text{--}4_4$, 6_5-- , and $9_8\text{--}8_8$ present a poor fit. This is because of the low Einstein coefficients A_{ul} and, mainly, to the low line strengths S ($< 4 \times 10^{-6} \text{ s}^{-1}$ and < 0.35 , respectively) of these lines, which provides small fits. The profile lines that we observe for these transitions are probably caused by stronger emission from other species.

Compared with values obtained in previous studies, such as those of Turner et al. (1991) or Blake et al. (1987), who derived (from source-averaged) $N(\text{SO}) \sim 3 \times 10^{16} \text{ cm}^{-2}$ in the plateau and $N \sim 3 \times 10^{15} \text{ cm}^{-2}$ in the HC, we see our results agree. If we compare these results with our obtained column densities from ^{34}SO , we see that the plateau remains in agreement with these previous studies, but our column density in the HC is one order of magnitude higher.

From the spatial distribution of the SO emission (Fig. 6), we find the integrated intensity peak to be in the velocity ranges $3\text{--}7 \text{ km s}^{-1}$ and $10\text{--}14 \text{ km s}^{-1}$ for both transitions. These ranges correspond to emission arising mainly from the HC and the HVP, respectively, which agrees with the results obtained for the column densities in these regions. The transition with lowest energy (upper panel) shows a concentric emission distribution around Irc2, while for the transition with higher energy, the emission distribution is elongated toward NE-SW direction. We also ob-

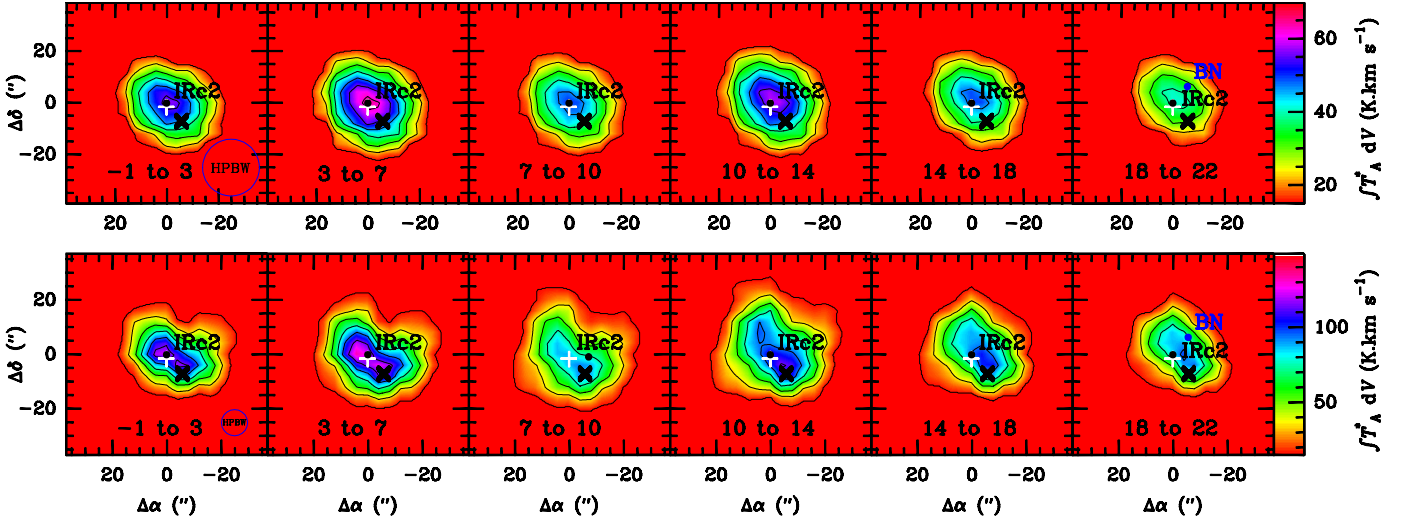


Fig. 6. SO-integrated intensity maps over different velocity ranges (indicated at the bottom of each panel in km s^{-1}). Row 1 shows the transition 3_2-2_1 ($E_{\text{up}}=21.1$ K, $A_{\text{ul}}=1.1 \times 10^{-5}$ s^{-1} , $S=1.5$). The interval between contours is 8 K km s^{-1} and the minimum contour is 15 K km s^{-1} . Row 2 shows the transition 6_6-5_5 ($E_{\text{up}}=56.5$ K, $A_{\text{ul}}=2.2 \times 10^{-4}$ s^{-1} , $S=5.8$). The interval between contours is 20 K km s^{-1} and the minimum contour is 15 K km s^{-1} . The white cross indicates the position of the hot core and the black cross the position of the compact ridge.

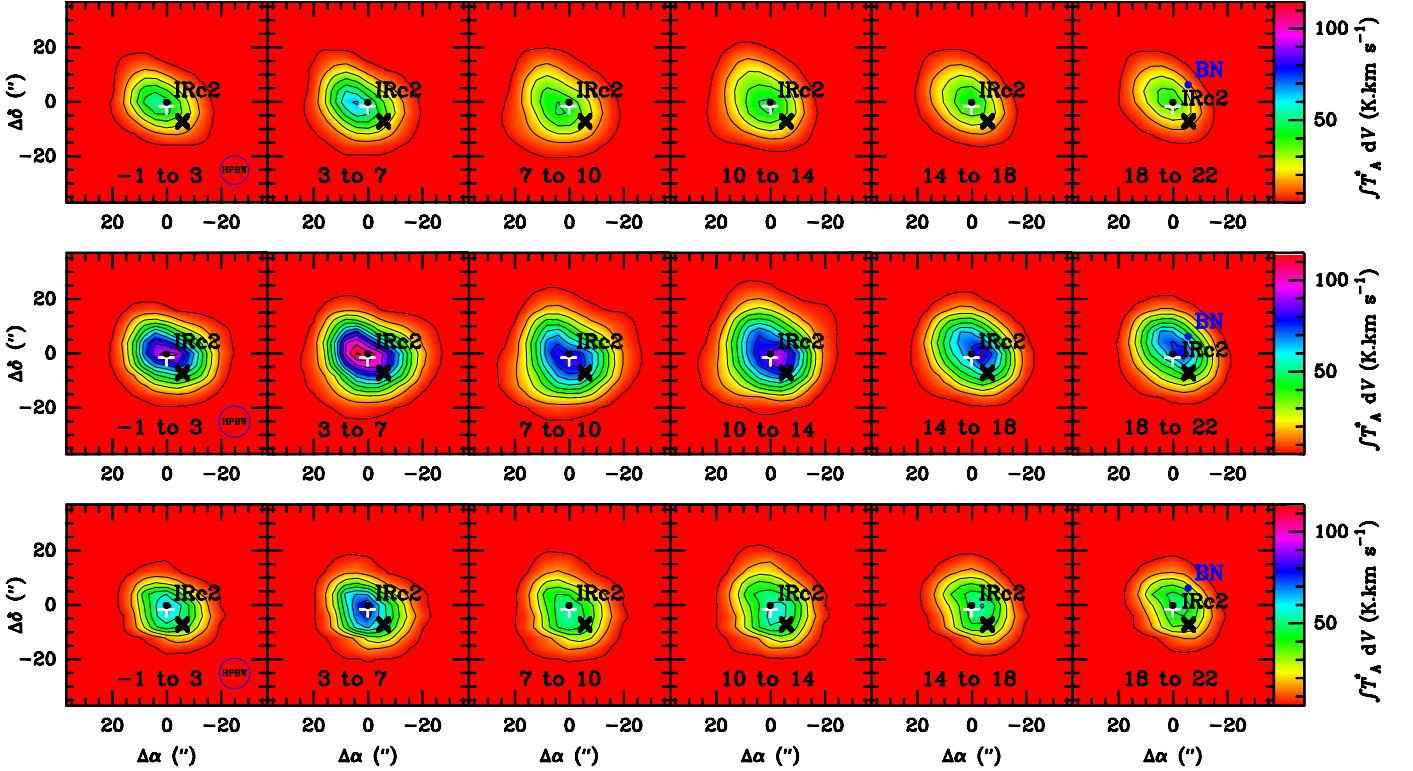


Fig. 7. SO_2 -integrated intensity maps over different velocity ranges (indicated at the bottom of each panel in km s^{-1}). Row 1 shows the transition $4_{(2,2)}-3_{(1,3)}$ (energy $E_{\text{up}}=19$ K, Einstein coefficient $A_{\text{ul}}=7.7 \times 10^{-5}$ s^{-1} , and line strength $S=1.7$), row 2 the transition $11_{(1,11)}-10_{(0,10)}$ ($E_{\text{up}}=60.4$ K, $A_{\text{ul}}=1.1 \times 10^{-4}$ s^{-1} , $S=7.7$), and the last row shows the transition $14_{(3,11)}-14_{(2,12)}$ ($E_{\text{up}}=119$ K, $A_{\text{ul}}=1.1 \times 10^{-4}$ s^{-1} , $S=8.1$). The interval between contours is 10 K km s^{-1} , the minimum contour is 5 K km s^{-1} and the maximum 155 K km s^{-1} . The white cross indicates the position of the hot core and the black cross the position of the compact ridge.

serve that, for high energies, the emission peak in the velocity range $3-7$ km s^{-1} is shifted toward the NE of the HC.

4.1.2. ^{34}SO , ^{33}SO , and S^{18}O

Figure 10 shows our best fit model for several rotational lines of ^{34}SO , which are listed in Table A.8 (see Appendix). We find that the HVP is also responsible for most of the emission, together with the PL and the 20.5 km s^{-1} component. According

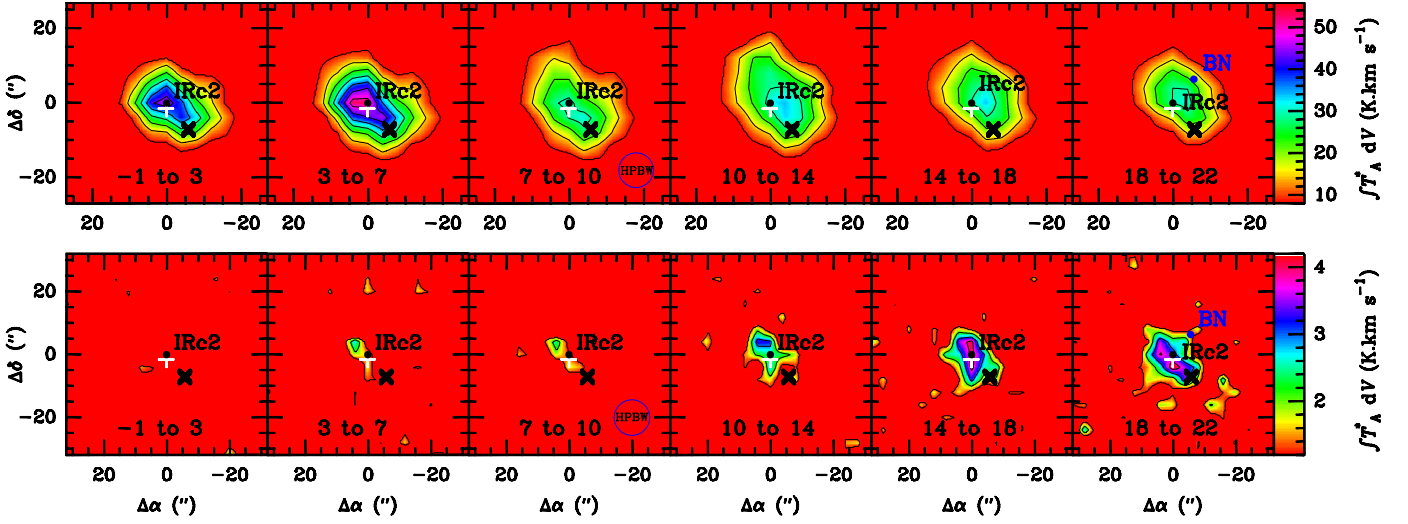


Fig. 8. ^{34}SO and $^{34}\text{SO}_2$ -integrated intensity maps over different velocity ranges (indicated at the bottom of each panel in km s^{-1}). Row 1 shows the transition 6_7-5_6 of ^{34}SO ($E_{\text{up}}=46.7$ K, $A_{\text{ul}}=2.2\times 10^{-4}$ s^{-1}). The contour interval is 7 K km s^{-1} and the minimum contour is 8 K km s^{-1} . Row 2 shows the transition $28_{(3,25)}-28_{(2,26)}$ of $^{34}\text{SO}_2$ ($E_{\text{up}}=402.1$ K, $A_{\text{ul}}=1.5\times 10^{-4}$ s^{-1}). The interval between contours is 0.9 K km s^{-1} , and the minimum contour is 1.2 K km s^{-1} . The white cross indicates the position of the hot core and the black cross the position of the compact ridge.

Table 2. Physical parameters adopted for the Orion KL cloud components.

Component	Source diameter ($''$)	Offset (IRc2) ($''$)	$n(\text{H}_2)$ cm^{-3}	T_{K} (K)	Δv_{FWHM} (km s^{-1})	v_{LSR} (km s^{-1})
Extended ridge (ER)	120	0	10^5	60	4	8.5
Compact ridge (CR)	15	7	10^6	110	3	8
High-velocity plateau (HVP)	30	4	10^6	100	30	11
Plateau (PL)	20	0	5×10^6	150	25	6
Hot core (HC)	10	2	1.5×10^7	220	10	5.5
20.5 km s^{-1} component	5	2	5×10^6	90	7.5	20.5

to our models, all transitions are optically thin with $\tau < 0.4$, therefore this result is not considered to be a lower limit. The 20.5 km s^{-1} component presents a similar column density to the HVP, and as for SO, its contribution is greater for higher J . In the HC we also find a strong contribution to the emission, however in the ER we find the lowest column density with $N(^{34}\text{SO}) = (7 \pm 2) \times 10^{12}$ cm^{-2} .

For the case of ^{33}SO we observe in Fig. A.3 (see Appendix) that lines are partially blended with other species, which produces a large uncertainty in the derived fit. In addition, the hyperfine structure is noticeable in these transitions, adding more complexity to the line profiles. The fits for this isotopologue were done by adopting the calculated frequencies, intensities, and energies for hyperfine levels up to $N=30$ provided by the CDMS catalogs. We obtain similar column densities for all components, with $N(^{33}\text{SO}) = (3-6) \times 10^{14}$ cm^{-2} (see Table 3).

As was the case for ^{33}SO , some lines of S^{18}O are blended with other species (Fig. A.4 and Table A.8, see Appendix). In this case we also find similar column densities for all the components, $N(\text{S}^{18}\text{O}) = (1-5) \times 10^{14}$ cm^{-2} , except for the CR, the ER, and the 20.5 km s^{-1} component, where we do not find contribution to the emission.

4.1.3. S^{17}O , ^{36}SO , and $^{34}\text{S}^{18}\text{O}$

Owing to the presence of other more intense species, we have detected neither S^{17}O nor ^{36}SO in this survey, but from

our data we derive upper limits for their column densities of $N(\text{S}^{17}\text{O}) < 1.3 \times 10^{14}$ cm^{-2} and $N(^{36}\text{SO}) < 1.6 \times 10^{14}$ cm^{-2} , respectively. We note that C^{36}S was detected by Mauersberger et al. (1996) in Orion. They found $^{32}\text{S}/^{36}\text{S} \approx 3500$ which is consistent with our upper limit. We have not detected $^{34}\text{S}^{18}\text{O}$ either; however, assuming the same physical conditions as those for the main isotopologue, we obtain an upper limit for its column density of $N(^{34}\text{S}^{18}\text{O}) < 1.4 \times 10^{14}$ cm^{-2} .

4.2. LTE models of the SO_2 lines

Due to the lack of collisional rates for levels with energies higher than 90 K, we have assumed LTE excitation to derive the SO_2 column densities. As stated before, this can overestimate or underestimate the calculated column densities. Given that we have collisional rates for SO, we ran our SO models again but considering LTE approximation, in order to compare the results. We observed that the new fits underestimated the line profiles, especially for low transitions. Probably this also happens with the SO_2 case, so we should consider our SO_2 column densities as lower limits. Table A.9 (see Appendix) lists the 166 observed rotational lines. Figures 11, 12, 13, and 14 show a sample of 90 observed lines (ordered by increasing energy) with our best fits overlaid.

The main contribution to the emission of SO_2 comes from the HVP (affecting mainly the lines with energies $E < 400$ K), with a column density of $N(\text{SO}_2) = (1.3 \pm 0.5) \times 10^{17}$ cm^{-2} . The

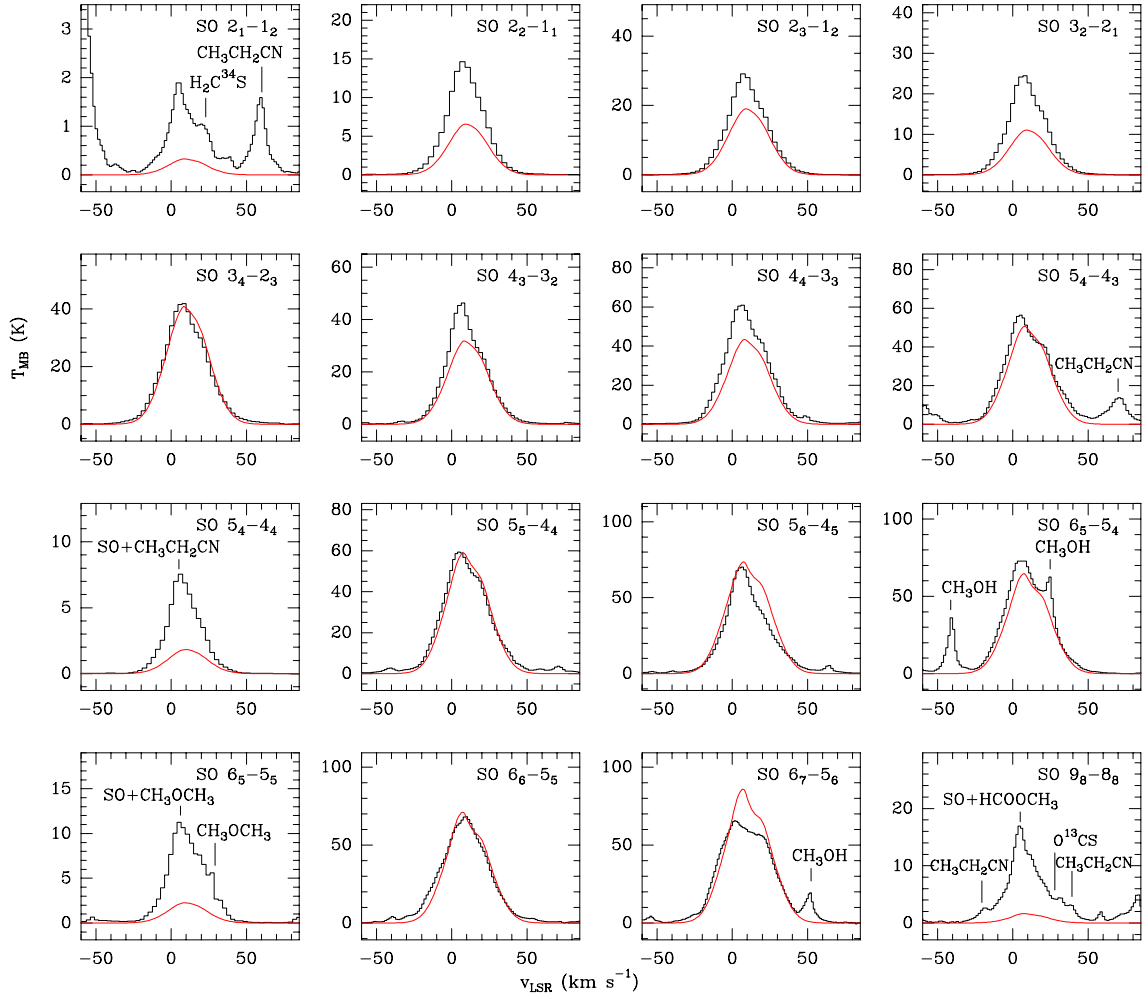


Fig. 9. Observed lines of SO (black histogram) and best fit LVG model results (red).

Table 3. Column densities, N , for SO and its isotopologues obtained from LVG model fits.

Component	SO $N \times 10^{15} (\text{cm}^{-2})$	^{34}SO $N \times 10^{15} (\text{cm}^{-2})$	$\text{SO}^{(a)}$ $N \times 10^{15} (\text{cm}^{-2})$	^{33}SO $N \times 10^{15} (\text{cm}^{-2})$	S^{18}O $N \times 10^{15} (\text{cm}^{-2})$
Extended ridge (ER)	0.018 ± 0.005	0.007 ± 0.002	0.16 ± 0.05
High-velocity plateau (HVP)	45 ± 10	4 ± 1	92 ± 23	0.25 ± 0.06	0.24 ± 0.08
Plateau (PL)	5 ± 1	3.0 ± 0.8	69 ± 19	0.5 ± 0.2	0.10 ± 0.04
Hot core (HC)	9 ± 3	2.2 ± 0.5	20 ± 11	0.4 ± 0.1	0.5 ± 0.2
20.5 km s^{-1} component	5 ± 1	3.5 ± 0.8	81 ± 19	0.6 ± 0.2	...

Notes. ^(a) Values calculated from the solar abundance ratio $^{32}\text{S} / ^{34}\text{S} = 23$ and from the column densities obtained for ^{34}SO (optically thin lines).

hottest region (the HC) also presents a similar high value, $N(\text{SO}_2) = (1.0 \pm 0.4) \times 10^{17} \text{ cm}^{-2}$. We find that the CR presents a column density of $N(\text{SO}_2) \sim 10^{15} \text{ cm}^{-2}$, whereas the 20.5 km s^{-1} component presents the lowest contribution to the emission (Table 4).

If we compare our results for SO_2 with those of SO, we find that SO_2 column densities are about one order of magnitude larger in all components, except in the 20.5 km s^{-1} component, where SO presents a higher contribution to the emission. As for SO, we also calculated the SO_2 column densities from $^{34}\text{SO}_2$ (optically thin lines) and the $^{32}\text{S}/^{34}\text{S}$ solar abundance ratio (Table 4). Except for the plateau components, we obtain that the column densities of SO_2 obtained from $^{34}\text{SO}_2$ are larger than those ob-

tained from fits, suggesting they are opacity effects on the SO_2 lines. Comparing with previous results, Blake et al. (1987) obtained (source-averaged) that SO_2 presents a column density in the plateau, $N \sim 10^{16} \text{ cm}^{-2}$. Schilke et al. (2001) derived (beam-averaged) for the same region $N(\text{SO}_2) = 9.7 \times 10^{16} \text{ cm}^{-2}$, which is very similar to our result in the high velocity plateau. For the HC, Sutton et al. (1995) found (also source-averaged) a column density, $N(\text{SO}_2) \sim 9 \times 10^{16} \text{ cm}^{-2}$. Our results agree with these values; however, the large number of transitions that we observed let us determine more accurately that it is the lower temperature plateau component, i.e. the HVP, which contributes more to the emission of SO_2 .

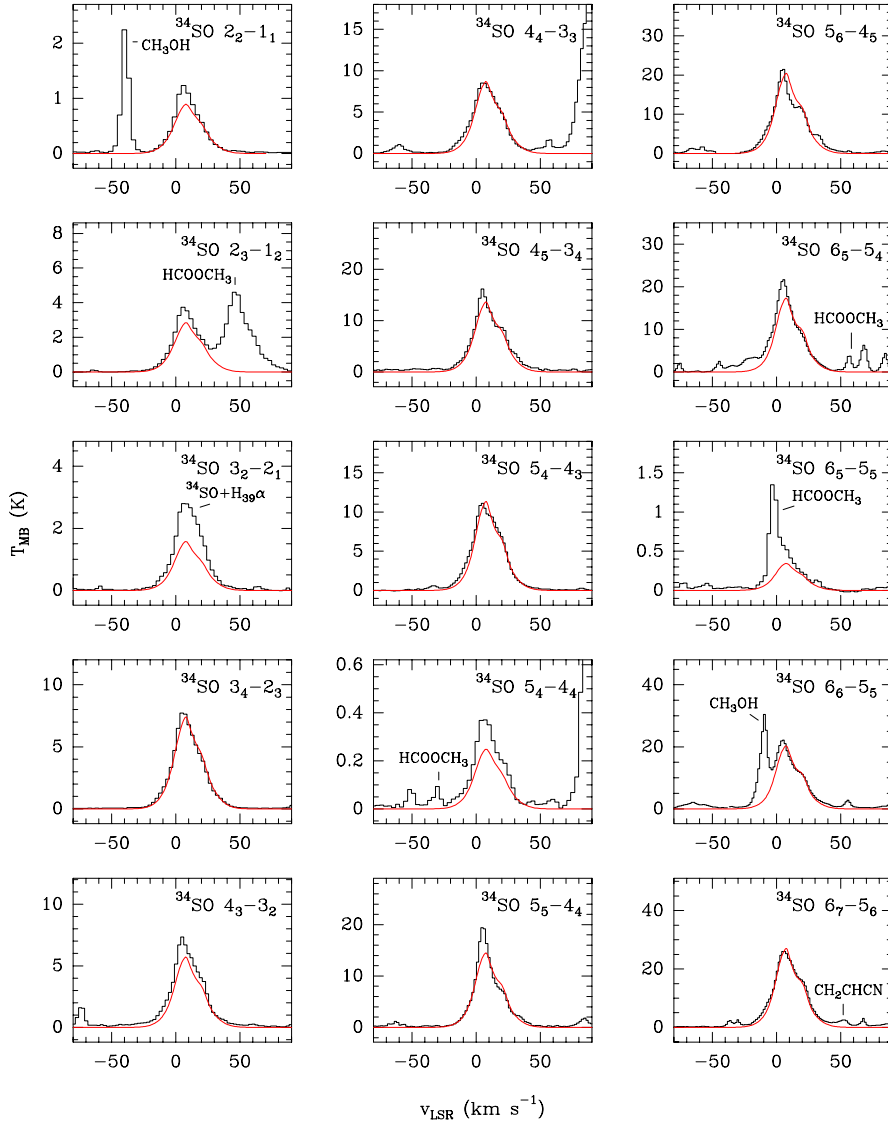


Fig. 10. Observed lines of ^{34}SO (black histogram) and best fit LVG model results (red).

From the spatial distribution of the SO_2 emission (Fig. 7), we find the maximum integrated line intensity between the velocity ranges $3\text{--}7\text{ km s}^{-1}$ and $10\text{--}14\text{ km s}^{-1}$, as well as for SO. These velocity ranges correspond to emission of the HC and the HVP, respectively, which agrees with the column density results obtained above. The emission peak is located towards the NE of IRC2 for the range $3\text{--}7\text{ km s}^{-1}$, while the emission peak for the HVP range is located $\sim 4''$ to the SW of IRC2. Emission from the 20.5 km s^{-1} component presents similar integrated intensity to the ridge (range of $7\text{--}10\text{ km s}^{-1}$). On the other hand, the map of $^{34}\text{SO}_2$ (Fig. 8) shows the strongest peak emission located northeast of IRC2 for all velocity ranges, although extended emission is seen to the southwest of IRC2, between 10 km s^{-1} and 22 km s^{-1} . The $^{34}\text{SO}_2$ transition shown in Fig. 8 has an upper energy level of $\sim 400\text{ K}$ and therefore may trace only the hottest component of the gas.

4.2.1. $^{34}\text{SO}_2$

We have detected 130 rotational lines of $^{34}\text{SO}_2$ (Table A.9 in Appendix). A sample of more than 30 lines is shown in Fig. 15.

This isotopologue, whose lines are optically thin, has the highest contribution to its emission from the HC, with $N(^{34}\text{SO}_2) = (1.0 \pm 0.4) \times 10^{16}\text{ cm}^{-2}$. The other components with high column densities are the HVP and the PL with $N(^{34}\text{SO}_2) = (7 \pm 2) \times 10^{15}\text{ cm}^{-2}$ and $N(^{34}\text{SO}_2) = (6 \pm 2) \times 10^{14}\text{ cm}^{-2}$, respectively. Particularly interesting is the column density found in the ER, which presents the same order of magnitude as the PL. The same behavior is also observed in the isotopologues $^{33}\text{SO}_2$ and SO^{18}O , where the column densities in the ER are only 3 to 12 times lower than in PL. This could be due to the strong emission emerging from the HVP and HC affecting the excitation of the energy levels of this isotopologue in the ER, which means that line photons emitted from the inner components will be scattered by the lower density gas in the ER component (radiative scattering). For the compact ridge, we find the emission contributes mainly to the lines at low frequencies. The column density for $^{34}\text{SO}_2$ obtained in the 20.5 km s^{-1} component is about 100 times lower than for ^{34}SO (see Table 4).

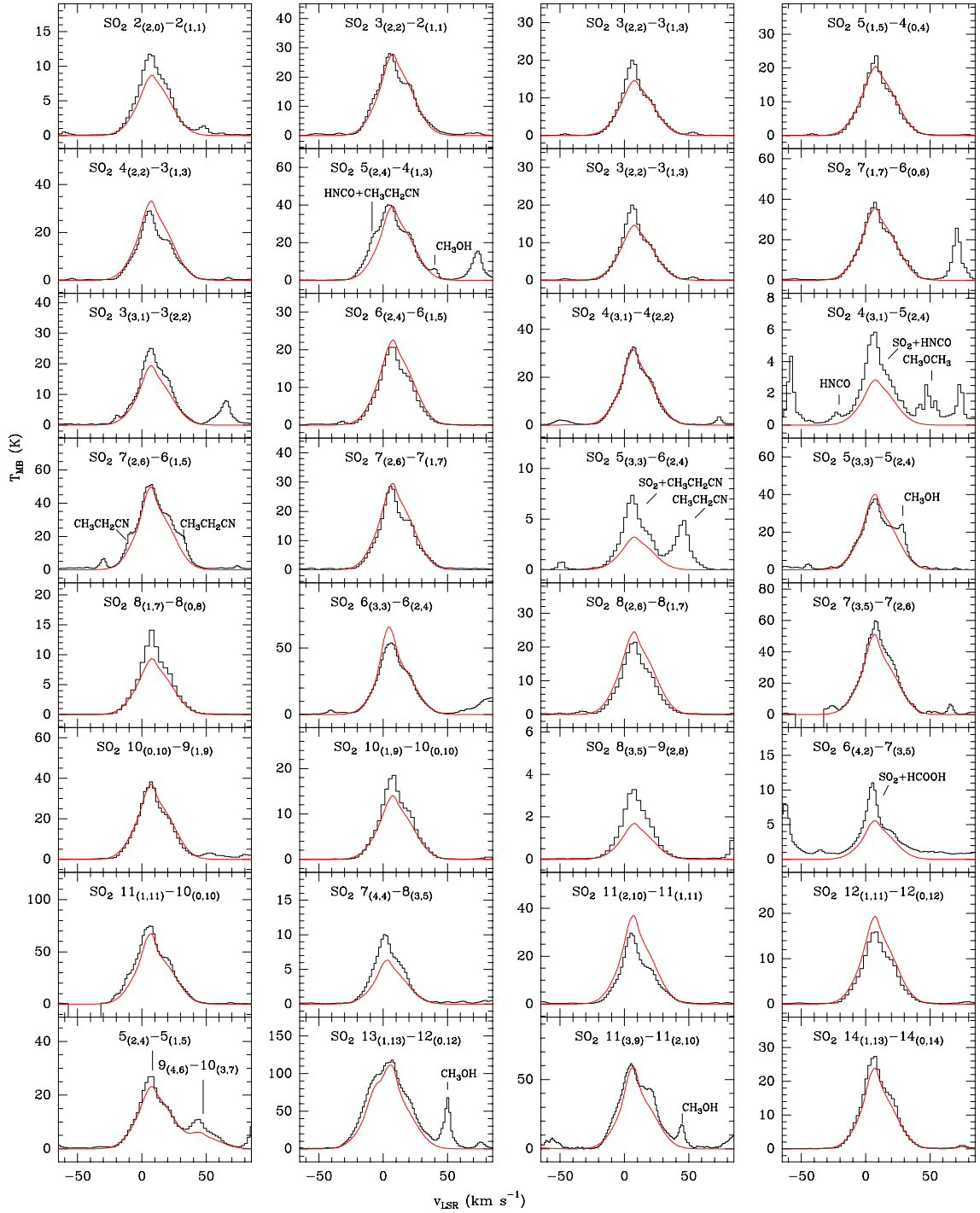


Fig. 11. Observed lines (black histogram) of SO_2 with upper state energies lower than 400 K, ordered by increasing energy from top left to bottom right. Best fit LTE model results are overlaid in red.

4.2.2. $^{33}\text{SO}_2$, SO^{18}O , and SO^{17}O

Figure A.5 (see Appendix) shows transitions of $^{33}\text{SO}_2$ in the frequency range covered at 1.3, 2, and 3 mm. Several of these are blended with other species, which makes the derived fits a bit biased. As for ^{33}SO , hyperfine structure affects the line profiles; however, we did not consider it in the $^{33}\text{SO}_2$ model, so the derived column densities could be underestimated.

The most important contribution to the emission of $^{33}\text{SO}_2$ comes from the hot core, with $N(^{33}\text{SO}_2)=(4\pm 1)\times 10^{15}\text{ cm}^{-2}$, and from the HVP. The lowest contribution to the emission arises

from the 20.5 km s^{-1} component, with $N(^{33}\text{SO}_2)=(9\pm 3)\times 10^{12}\text{ cm}^{-2}$.

For SO^{18}O (Fig. A.6, see Appendix), the highest column density is also found in the HC, with $N(\text{SO}^{18}\text{O})=(1.5\pm 0.5)\times 10^{15}\text{ cm}^{-2}$. The high-velocity plateau also presents an important contribution to the emission across the frequency range, whereas the PL mainly affects lines at 2 mm. The weakest contribution is from the ER, with $N(\text{SO}^{18}\text{O})\sim 10^{13}\text{ cm}^{-2}$.

Figure A.7 shows the spectra that contain some frequencies of SO^{17}O , together with our best model. The maximum contribution to the emission of this isotopologue arises from the hot core

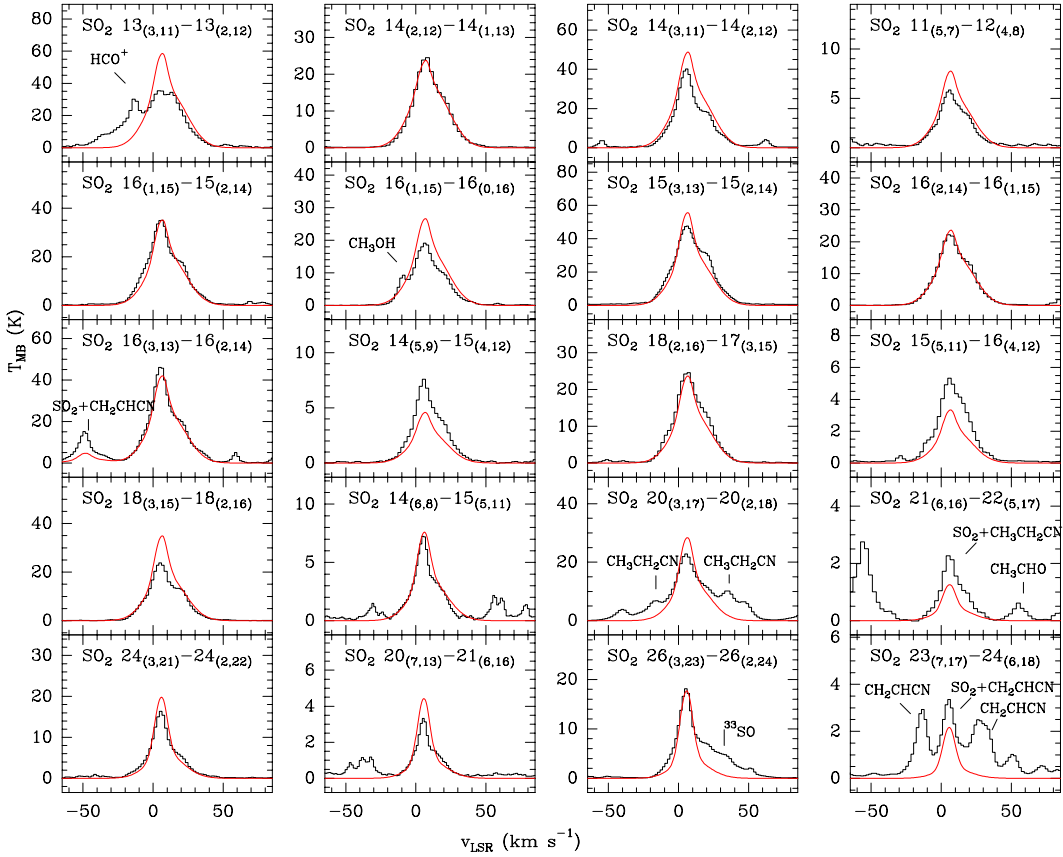


Fig. 12. Observed lines of SO₂ (black histogram) with upper state energies lower than 400 K (continued), ordered by increasing energy from top left to bottom right. Best fit LTE model results are overlaid in red.

with $N(\text{SO}^{17}\text{O})=(8\pm 3)\times 10^{14}\text{ cm}^{-2}$. We find that the PL and HVP also contribute to the emission, but about four to eight times less than the HC. However, because all lines are weak ($T_{\text{MB}}<0.3\text{ K}$) and blended with other species, we should consider these results as upper limits.

4.2.3. SO₂ $\nu_2=1$

Figure 16 shows some of the detected lines of vibrationally excited SO₂ ν_2 , which are also listed in Table A.9 (see Appendix). The hot core is responsible for most of the emission of this vibrational mode, with a column density one order of magnitude higher than in the other components. From the column densities in the HC for SO₂ in its ground and vibrationally excited states, we can estimate a vibrational temperature, considering that

$$\frac{\exp(-E_{v_x}/T_{\text{vib}})}{f_v} = \frac{N(\text{SO}_2\nu_x)}{N(\text{SO}_2)}, \quad (3)$$

where E_{v_x} is the energy of the vibrational state ($E_{\nu_2}=745.1\text{ K}$), T_{vib} is the vibrational temperature, $N(\text{SO}_2\nu_x)$ is the column density of SO₂ in the excited vibrational state, $N(\text{SO}_2)$ the total column density, and f_v is the vibrational partition function, given by

$$f_v = 1 + \exp(-E_{\nu_3}/T_{\text{vib}}) + 2 \exp(-E_{\nu_2}/T_{\text{vib}}) + \exp(-E_{\nu_1}/T_{\text{vib}}). \quad (4)$$

Taking into account that $N(\text{SO}_2)=N_{\text{(ground)}}\times f_v$, we only need the energy of the vibrational state and the calculated column densities to derive the vibrational temperature.

We obtain $T_{\text{vib}}=(230\pm 40)\text{ K}$ for SO₂ $\nu_2=1$. This value is similar to the kinetic temperature we assumed for the HC component (220 K). It is unlikely that the $\nu_2=1$ level at 745 K above the ground is excited by collisions. The main pumping mechanism could be IR radiation from the HC. A similar situation was found by Tercero et al. (2010) for OCS and other species.

4.2.4. ³⁴SO₂ $\nu_2=1$

Figure A.8 (see Appendix) shows some observed lines of ³⁴SO₂ $\nu_2=1$. The strongest emission comes from the hot core with $N(^{34}\text{SO}_2\nu_2=1)=(7\pm 2)\times 10^{14}\text{ cm}^{-2}$, although we also find a small contribution from the HVP and the CR, with $N(^{34}\text{SO}_2\nu_2=1)\sim 5\times 10^{13}\text{ cm}^{-2}$ for both. These contributions mainly affect the lines at 2 mm. Since all the lines we detect are very weak and mixed with other species, we should consider these results as upper limits.

4.3. Isotopic and molecular abundances

From the derived column densities of SO, SO₂, and their isotopologues, we can estimate abundance ratios. These are shown in Table A.5 (see Appendix). We compare these ratios with solar isotopic abundance values from Anders & Grevesse (1989).

³²S/³⁴S: from the SO₂ lines we obtain a column density ratio for the PL of ³²S/³⁴S=16±10, in agreement with previous studies (³²S/³⁴S≈16 by Johansson et al. 1984, ³²S/³⁴S≈13-16 by Blake et al. 1987, and ³²S/³⁴S=15±5 by Tercero et al. 2010). For the HVP, ³²S/³⁴S=20±13, which is similar to the value for the solar isotopic abundance ratio and to the result deduced by Persson

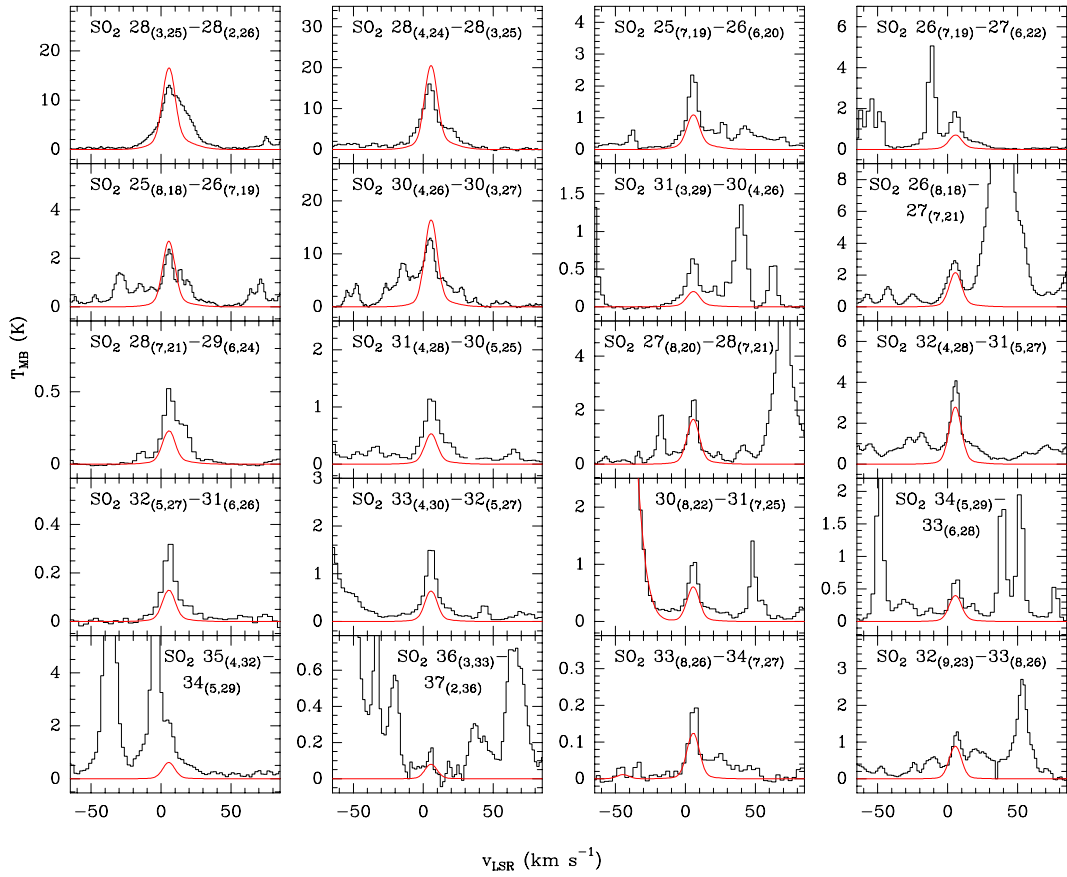


Fig. 13. Observed lines of SO₂ (black histogram) with upper state energies between 400 K and 700 K, ordered by increasing energy from top left to bottom right. Best fit LTE model results are overlaid in red.

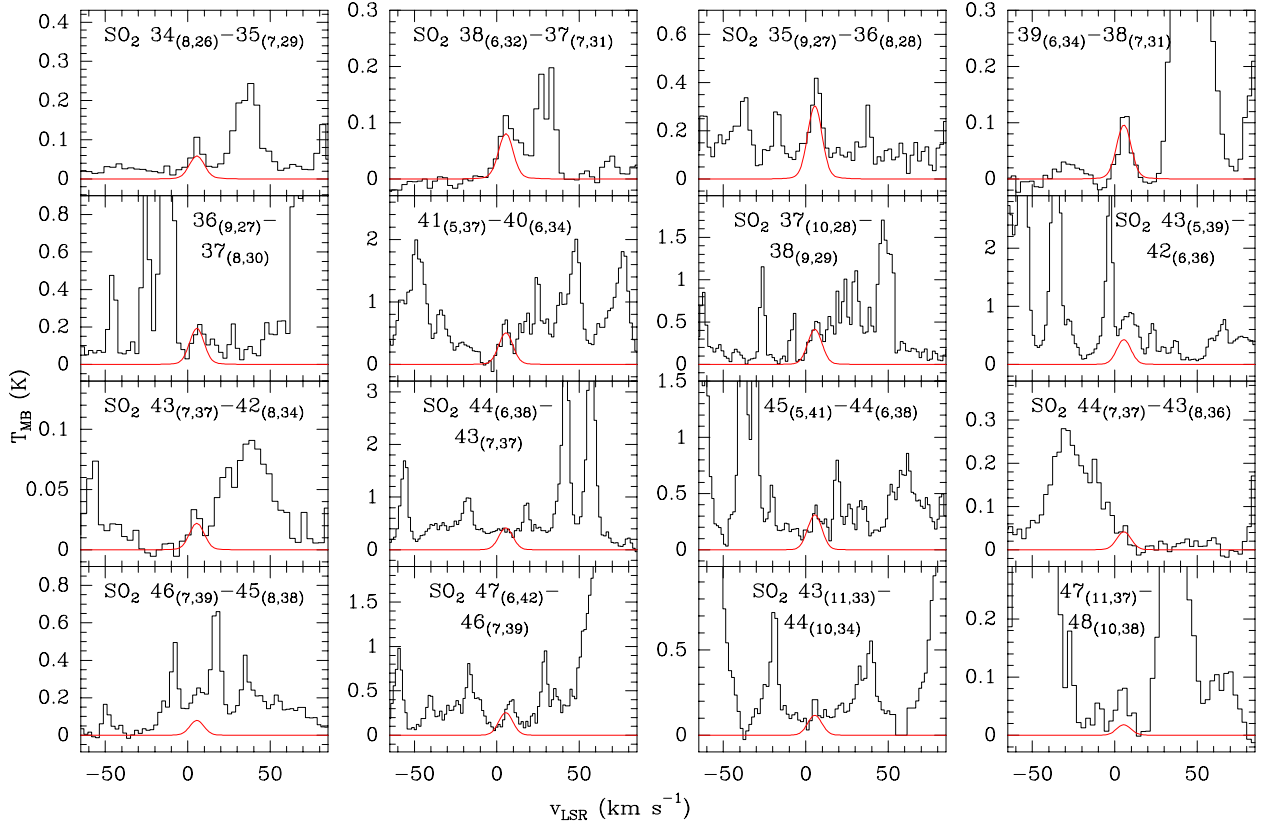


Fig. 14. Observed lines of SO₂ (black histogram) with energies higher than 700 K, ordered by increasing energy from top left to bottom right. Best fit LTE model results are overlaid in red.

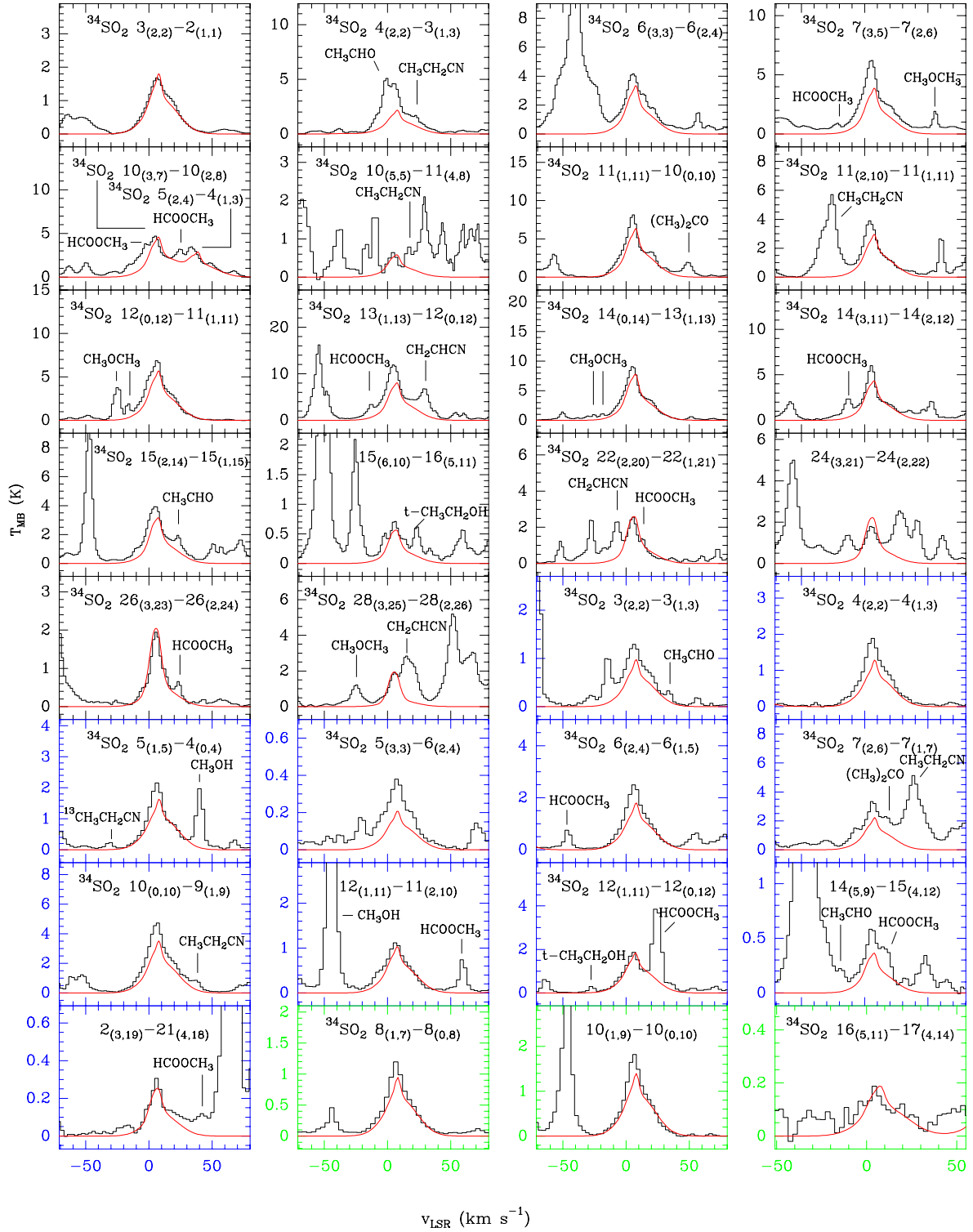


Fig. 15. Observed lines of $^{34}\text{SO}_2$ (black histogram). Best fit LTE model results are shown in red. Boxes with black, blue and green borders correspond to lines observed at 1.3, 2, and 3 mm, respectively.

et al. (2007) where $^{32}\text{S}/^{34}\text{S} \approx 23 \pm 7$. From the SO lines, with the exception of the HVP, we obtain low ratios for $^{32}\text{S}/^{34}\text{S}$ in comparison with the solar abundance, which could be due to opacity effects on the SO lines.

$^{32}\text{S}/^{33}\text{S}$: from $N(\text{SO})/N(^{33}\text{SO})$ we obtain $^{32}\text{S}/^{33}\text{S} = 180 \pm 80$ for the HVP. This value agrees with the solar isotopic abundance ratio, 127, from Anders & Grevesse (1989). For the other three components, the obtained ratios are very low compared to the

solar abundance, probably also due to the opacity effects for SO lines. These values should be considered as lower limits. We find similar behavior for the ratio $N(\text{SO}_2)/N(^{33}\text{SO}_2)$.

$^{34}\text{S}/^{33}\text{S}$: from $N(^{34}\text{SO}_2)/N(^{33}\text{SO}_2)$ we obtain $^{34}\text{S}/^{33}\text{S} = 4 \pm 3$ for the 20.5 km s^{-1} component and $^{34}\text{S}/^{33}\text{S} = 3\text{--}7$ for the ridge (ER and CR), the HVP, and the HC. These values are similar to the solar abundance ratio (5.5). From $N(^{34}\text{SO})/N(^{33}\text{SO})$ the

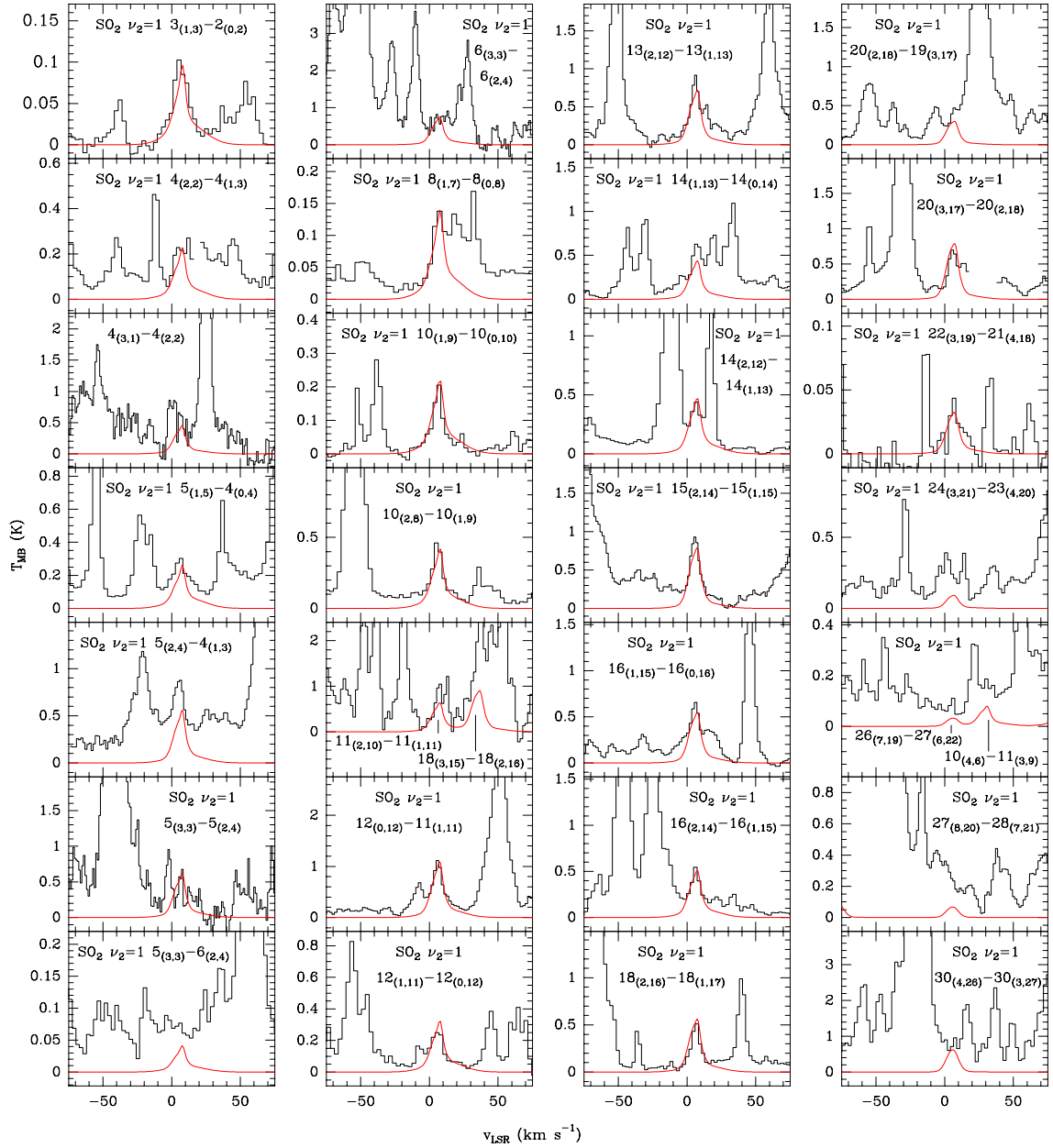


Fig. 16. Observed lines of $\text{SO}_2 \nu_2=1$ (black histogram). Best fit LTE model results are shown in red.

obtained ratio is $^{34}\text{S}/^{33}\text{S}=6\pm 3$ for the HC and both plateau components.

$^{16}\text{O}/^{18}\text{O}$: our results for this ratio in the plateau agree with those obtained by Tercero et al. (2010), who derived $^{16}\text{O}/^{18}\text{O}=250\pm 135$ in the plateau from a study of OCS in this region. The compact ridge also presents similar ratio to that obtained by them. However, all these values are lower than the solar isotopic abundance (≈ 500).

SO/SO_2 : in Fig. 18 we present the ratio $N(\text{SO})/N(\text{SO}_2)$ for the different components, as well as for the different isotopologues of SO and SO_2 . We find that SO_2 is more abundant than SO in all components, except in the 20.5 km s^{-1} component. In the HVP, SO_2 is three times more abundant than SO, while in the HC is up to 11 times more. However, in the 20.5 km s^{-1} component, SO is ~ 30 times more abundant than SO_2 .

$^{34}\text{SO}/^{34}\text{SO}_2$: in the region affected by shocks, this ratio implies that $^{34}\text{SO}_2$ is more abundant (~ 1.7 times) than ^{34}SO . In the hot core, we also find that $^{34}\text{SO}_2$ is more abundant (5 times) than

^{34}SO , whereas in the ER the ratio is much larger ($^{34}\text{SO}_2$ is 14 times more abundant). As was found for SO/SO_2 , the main difference is in the 20.5 km s^{-1} component, where ^{34}SO is ~ 100 times more abundant than $^{34}\text{SO}_2$.

Table A.6 shows the molecular abundances, X , of SO and SO_2 with respect to hydrogen in each component. They were derived using H_2 column density by means of the C^{18}O column density, from the isotopic abundance $^{16}\text{O}/^{18}\text{O}$, and assuming that CO is a good tracer of H_2 and therefore their abundance ratio is roughly constant. The column densities for H_2 are 7.5×10^{22} , 7.5×10^{22} , 2.1×10^{23} , 6.2×10^{22} , $4.2\times 10^{23} \text{ cm}^{-2}$, and 1.0×10^{23} for the ER, CR, PL, HVP, HC, and the 20.5 km s^{-1} component, respectively (see Tercero et al. 2011). We observe that the highest abundance of SO is obtained in the HVP, whereas in the HC and in the PL this abundance is ~ 30 times lower. The extended ridge presents the lowest abundance of sulfur monoxide. The abundance of this molecule in the 20.5 km s^{-1} component is about twice larger than in the HC. SO_2 is also more abundant in the

Table 4. Column densities, N , for SO_2 and its isotopologues, obtained from LTE model analysis.

Component	SO_2 $N \times 10^{15}$ (cm^{-2})	$^{34}\text{SO}_2$ $N \times 10^{15}$ (cm^{-2})	$^{(a)}\text{SO}_2$ $N \times 10^{15}$ (cm^{-2})	$^{33}\text{SO}_2$ $N \times 10^{15}$ (cm^{-2})	SO^{18}O $N \times 10^{15}$ (cm^{-2})	SO^{17}O $N \times 10^{15}$ (cm^{-2})	$\text{SO}_2 \nu_2=1$ $N \times 10^{15}$ (cm^{-2})	$^{34}\text{SO}_2 \nu_2=1$ $N \times 10^{15}$ (cm^{-2})
Extended ridge	0.23±0.06	0.10±0.04	2.3±0.7	0.04±0.001	0.020±0.007	0.007±0.003	0.013±0.003	...
Compact ridge	1.2±0.4	0.5±0.2	12±2	0.07±0.02	0.03±0.01	0.007±0.003	0.20±0.05	0.05±0.02
High-velocity plateau	130±50	7±2	161±46	1.0±0.3	0.9±0.3	0.10±0.04	0.4±0.1	0.06±0.02
Plateau	10±3	0.6±0.2	14±3	0.5±0.2	0.06±0.02	0.03±0.01
Hot core	100±40	10±4	230±60	4±1	1.5±0.5	0.9±0.3	4±1	0.7±0.2
20.5 km s ⁻¹ comp.	0.17±0.06	0.04±0.01	0.8±0.2	0.009±0.003

Notes. ^(a) Values calculated from the solar abundance ratio $^{32}\text{S} / ^{34}\text{S}=23$ and from the column densities obtained for $^{34}\text{SO}_2$ (optically thin lines).

HVP (between 8 and 600 times more abundant than in the rest of components). With respect to hydrogen, SO_2 is about one order of magnitude more abundant than SO in the HC and in the ER, while in both plateaus sulfur dioxide is only two-three times more abundant than SO.

4.4. Other sulfur-bearing molecules

We provide here upper limits for the column densities of several sulfur-bearing molecules not detected in our survey. We have assumed the same spectral components as for SO and SO_2 (HC, PL, HVP, CR, and ER) and an LTE approximation, due to the lack of available collision rates. Table 2 shows the adopted temperature values, among other parameters, for each component, and Table A.7 (see Appendix) shows the results obtained, the dipole moment of each species, and references for the spectroscopic constants. The upper limit of column density for each species were obtained summing the contribution of all the components.

SO^+ : first detected in the interstellar medium towards the supernova remnant IC443 (Turner et al. 1992), it was proposed as a tracer of dissociative shocks, although later surveys carried out in dark clouds, star-forming regions, and high velocity molecular outflows suggest that this reactive ion is not associated with shock chemistry (Turner et al. 1994). SO^+ presents a high abundance in PDRs like NGC 7023 and in the Orion Bar (Fuente et al. 2003). In Orion KL, we obtain an upper limit to its column density of $N(\text{SO}^+) \leq 2.5 \times 10^{14} \text{ cm}^{-2}$, providing an abundance ratio of $N(\text{SO})/N(\text{SO}^+) \geq 2080$. This result implies that UV radiation does not play an important role in this region.

(*cis*)- HOSO^+ : it is the most stable isomeric form of this ion. This species has not yet been detected in the interstellar medium, but its large dipole moment (1.74 D), its easy formation through H_3^+ reacting with SO_2 and the fact that it does not react with H_2 make this ion an excellent candidate for being detected, mainly in hot regions where the parent SO_2 is very abundant. The upper limit calculated for this ion is $N(\text{cis-HOSO}^+) \leq 3.6 \times 10^{13} \text{ cm}^{-2}$.

SSO: this molecule has not been detected yet in the interstellar medium, but it is a plausible candidate, since the oxides SO and SO_2 are particularly abundant, especially in star-forming regions. Disulfur monoxide (SSO) was spectroscopically studied first by Meschi & Myers (1959) who detected rotational transitions in the ground vibrational state and in the $\nu_2=1$ state. Later, Thorwirth et al. (2006) carried out a millimeter and submillimeter wave investigation of SSO in the ground vibrational state to frequencies as high as 470 GHz. We have not detected SSO in our line survey, but we obtain an upper limit for its column den-

sity of $N(\text{SSO}) \leq 7.6 \times 10^{14} \text{ cm}^{-2}$, providing an abundance ratio of $N(\text{SO})/N(\text{SSO}) \geq 1155$.

OSiS: silicon oxysulfide was first characterized in the gas phase at high spectral resolution by Thorwirth et al. (2011). It possesses a large dipole moment ($\mu_a=1.47 \text{ D}$) and its bond distances are very short in comparison with those of SiO and SiS. It has not been detected yet in the interstellar medium, and we obtained an upper limit for the column density of this molecule in Orion KL of $N(\text{OSiS}) \leq 6.3 \times 10^{13} \text{ cm}^{-2}$. Tercero et al. (2010) found that in Orion KL the total column density for SiS in the ground state is $N(\text{SiS})=(1.4 \pm 0.4) \times 10^{15} \text{ cm}^{-2}$. This result provides an abundance ratio of $N(\text{SiS})/N(\text{OSiS}) \geq 22$.

S_3 : thiozone is a bent chain with a bond to the apex S whose rotational spectrum was first measured by McCarthy et al. (2004). S_3 has not yet been observed in the interstellar medium; however, it is an excellent candidate for astronomical detection in rich interstellar sources. In addition, S_3 may also exist in the atmosphere of Io, where S_2 has already been detected in the ultraviolet. Owing to the presence of more intense lines from other species we have not detected S_3 in our line survey. We provide an upper limit for its column density of $N(\text{S}_3) \leq 1 \times 10^{15} \text{ cm}^{-2}$.

S_4 : tetrasulfur is a singlet planar trapezoid whose rotational spectrum was observed for the first time by McCarthy et al. (2004). S_4 has a substantial dipole moment, 0.87 D, hence an intense rotational spectrum across the entire radio band. The upper limit column density we calculated for this molecule is $N(\text{S}_4) \leq 7 \times 10^{14} \text{ cm}^{-2}$.

CH_3SOCH_3 : Barnes et al. (1994) obtained this molecule in the laboratory while investigating the gas-phase reaction of OH with the oxidation of dimethyl sulfide at room temperature. Dimethyl sulfoxide has not been observed yet in the interstellar medium, but we provide an upper limit for its column density of $N(\text{CH}_3\text{SOCH}_3) \leq 1 \times 10^{14} \text{ cm}^{-2}$.

H_2CSO : sulfine was first identified in 1976 as a product of the pyrolysis of a variety of sulfur-bearing precursors. H_2CSO is a planar molecule of C_s symmetry. Joo et al. (1995) analyzed its infrared spectrum at high resolution. We provide an upper limit for the column density for this undetected molecule in the interstellar medium of $N(\text{H}_2\text{CSO}) \leq 3 \times 10^{13} \text{ cm}^{-2}$.

HNSO: thionylimide is a semi-stable molecule that adopts a *cis*-planar structure of C_s symmetry in the ground state. HNSO is the simplest molecule in the group of organic nitrogen-sulfur compounds. We calculated an upper limit for its column density of $N(\text{HNSO}) \leq 4.1 \times 10^{14} \text{ cm}^{-2}$, which provides an abundance ratio $N(\text{SO})/N(\text{HNSO}) \geq 2600$.

$\text{o-H}_2\text{S}_2$: the rotational spectrum of disulfane (H_2S_2) has been measured in the far-infrared, millimeter, and submillimeter (Winnewisser et al. 1966). The density of its spectrum is en-

hanced by the presence of low-lying torsional and S-S stretching modes. We did not observe this molecule in our line survey but we provide an upper limit for its column density of $N(\text{o-H}_2\text{S}_2) \leq 1.6 \times 10^{14} \text{ cm}^{-2}$.

SSH and H_2SO_4 : these molecules have not yet been detected in the interstellar medium. The calculated upper limits for their column densities are $N(\text{SSH}) \leq 7.1 \times 10^{13} \text{ cm}^{-2}$ and $N(\text{H}_2\text{SO}_4) \leq 1.3 \times 10^{14} \text{ cm}^{-2}$, respectively.

CH_3SSH : methyl hydrodisulfide has not been observed in the interstellar medium. Tyblewski et al. (1986) studied its rotational spectrum, together with that of CH_3SSD , between 18 and 40 GHz providing rotational constants. We derive an upper limit for its column density of $N(\text{CH}_3\text{SSH}) \leq 2.6 \times 10^{14} \text{ cm}^{-2}$.

(*tr*)-HCSSH: the spectrum of dithioformic acid has been studied by Bak et al. (1978), who assigned the rotational transitions of this species in its ground state to a *trans* and *cis* rotamer. We provide an upper limit for the column density of (*tr*)-HCSSH (more stable) $N \leq 3.6 \times 10^{13} \text{ cm}^{-2}$.

5. Discussion

There have been many spectral line surveys of Orion KL aimed at determining the physical and chemical structure of this region (e.g., Blake et al. 1987, Sutton et al. 1995, Schilke et al. 2001). The survey analyzed here was first presented by Tercero et al. (2010), covers the widest frequency range of all of them (80–281 GHz). Due to this wide range and to the large number of observed transitions of SO, and particularly of SO_2 , it has been possible not only to determine the structure of the cloud (gas temperature, gas density, size of components, etc.) with better accuracy (the 3 mm window shows best the coldest regions, such as the ER, whereas the 1.3 mm window probes the warmest regions), but also to demonstrate the need for considering a density and temperature gradient in the HC of Orion KL. From rotational diagrams, we found a large difference (~ 100 K) between the rotational temperatures of SO and SO_2 , indicating the possibility of a hotter inner region to the HC. We draw the same conclusion from the fits for SO_2 lines with energies $E > 400$ K. To obtain better fits for lines with energies $E > 700$ K, we considered a high column density for the HC, which overestimates in the fit for the lines with energy around 400 K (see Figs. 12 and 13). But by considering an additional inner component to the HC with higher temperature, it would probably be possible to obtain a better fit to the lines with high energies, while avoiding overestimation of lines with intermediate energies. To test this possibility, we fit the SO_2 line profiles with energies $E > 700$ K considering a hotter ($T_K = 280$ K) HC (affecting only the highest energy transitions), with $n(\text{H}_2) = 5 \times 10^6 \text{ cm}^{-3}$, located at 5.5 km s^{-1} , and with $\Delta v_{\text{FWHM}} = 7 \text{ km s}^{-1}$. For a SO_2 column density of $(4 \pm 1) \times 10^{16} \text{ cm}^{-2}$, we improve the line profile fits of these high energies transitions (see Fig. 17). This shows the existence of a temperature and density gradient in the HC of Orion KL. However, its structure should be determined accurately with observations of SO and SO_2 (and mainly of its isotopologues³, which are optically thin) at higher frequencies with telescopes such as APEX.

On the other hand, the large number of observed lines of the ^{34}S and ^{33}S isotopologues has allowed us to calculate column densities and isotopic and molecular abundances that are key to understanding the chemical evolution of this region.

³ The energies of the observed isotopologues in this survey are < 680 K.

5.1. SO and SO_2 as tracers of shocks and hot gas

In Section 4 we showed that an important contribution to the emission of SO and SO_2 comes from the HC component of Orion KL. In Fig. 18 we plotted the ratio of $N(\text{SO})/N(\text{SO}_2)$ for the different components, as well as for the different isotopologues of SO and SO_2 . The figure shows that the column density of SO_2 in the HC is higher than that for SO. We should take into account that our column densities for SO_2 may have been slightly underestimated because of using an LTE model to infer the column density (instead of LVG, as was used for SO). For that reason, we considered a higher uncertainty (35%) in the model intensity predictions for SO_2 , than for SO (20%), as said previously. Moreover, the opacity may affect SO and SO_2 differently, which would in turn affect their column density ratio. But if we consider the result of the ratio $^{34}\text{SO}/^{34}\text{SO}_2$ in the hot core, we observe that SO_2 continues to be more abundant than SO. This could indicate that SO_2 is a better tracer of warm gas than SO.

Our results are consistent with predictions from chemical models of hot cores (e.g., Hatchell et al. 1998). Viti et al. (2004a) modeled the evaporation of ices near massive stars and found that SO_2 becomes more abundant than SO in the hot core from 31,500 years after the formation of a high-mass star. For shorter timescales, SO is much more abundant than SO_2 . Thus, the SO/SO_2 ratio could be regarded as a chemical clock (which should decrease with time), and our results showing a lower SO/SO_2 ratio for the HC component seem to suggest a late stage for the hot core evolution in Orion KL.

On the other hand, the ratio of SO/SO_2 is higher in the PL and the HVP than in the HC and the ER (see Fig. 18), and in particular for the PL, this ratio reaches values close to or even higher than 1. Since SO is a well-known outflow tracer (e.g., Chernin et al. 1994; Codella & Scappini 2003; Lee et al. 2010; Tafalla et al. 2010), and SO seems to be more enhanced than SO_2 in shocks (from an observational point of view, e.g., Codella & Bachiller (1999), Jiménez-Serra et al. (2005), and from a theoretical point of view, e.g., Viti et al. (2004b); Benedettini et al. (2006), for timescales $\sim 10,000$ yr), it seems very feasible that the high SO/SO_2 ratios measured in the (high velocity) plateau are the consequence of a definite enhancement of the SO abundance with respect to SO_2 , due to shocks propagating into the surrounding medium of Orion KL.

5.2. Nature of the 15 km s^{-1} dip and 20.5 km s^{-1} velocity component

To properly fit the SO and SO_2 spectra in Orion KL, a new velocity component at 20.5 km s^{-1} had to be included in the model (see Section 3.2). In addition, a possible dip at 15.5 km s^{-1} in the SO and SO_2 spectra has been identified. The dip at 15.5 km s^{-1} could be self-absorption due to the high opacity of the observed transitions. However, in all cases, the line strength S is uncorrelated with the amount of absorption. For example, the transition $11_{(1,11)}-10_{(0,10)}$ of SO_2 , with a line strength of $S = 7.7$ and Einstein coefficient $A_{ul} = 1.1 \times 10^{-4} \text{ s}^{-1}$, would be expected to display more self-absorption and therefore a lower integrated intensity than the transition $4_{(2,2)}-3_{(1,3)}$ with $S = 1.7$ and $A_{ul} = 7.7 \times 10^{-5} \text{ s}^{-1}$, but we see the opposite (especially in the range at $14.5-16.5 \text{ km s}^{-1}$). In addition, we obtain in Fig. 7 a high integrated intensity in the velocity range $14-18 \text{ km s}^{-1}$, when the integrated intensity in the ranges $10-14 \text{ km s}^{-1}$ and $18-22 \text{ km s}^{-1}$ is also large. Altogether, this suggests that the emission at 15 km

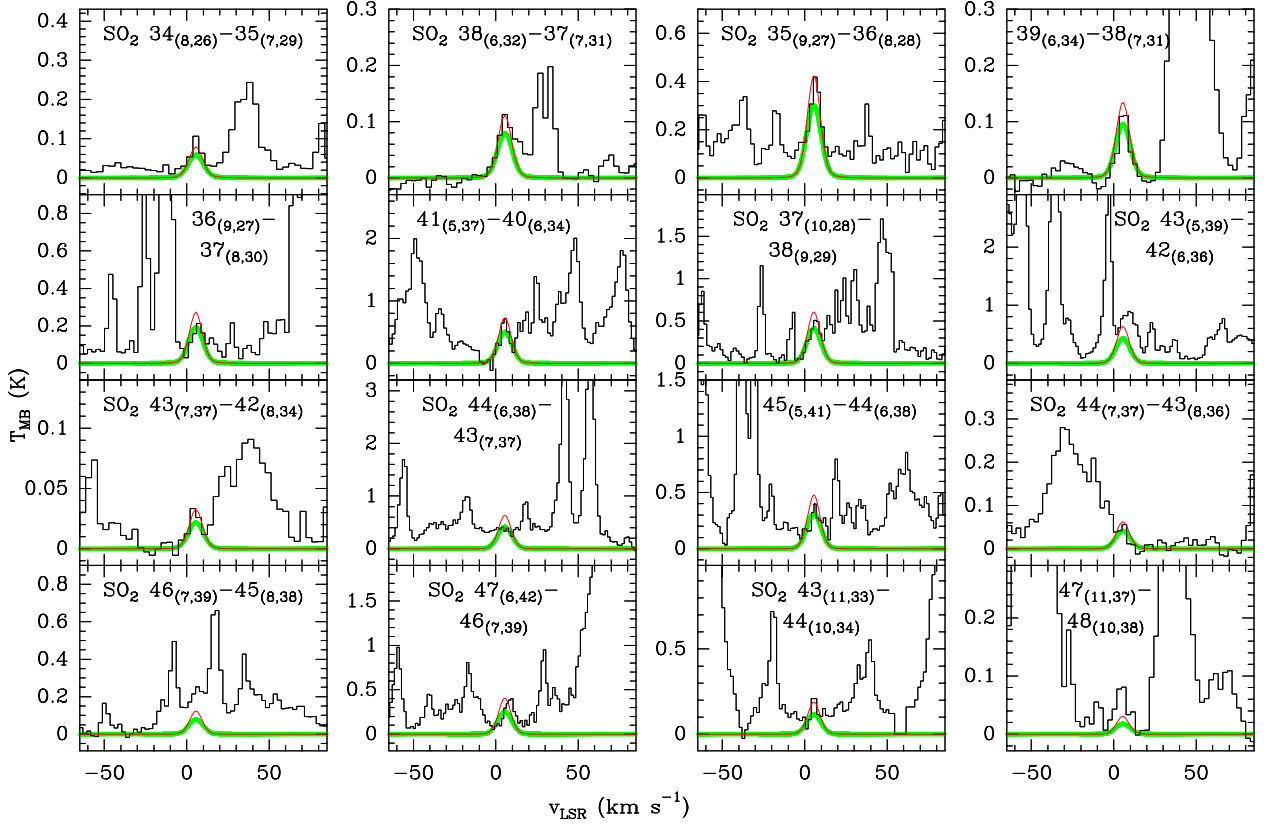


Fig. 17. Observed lines of SO₂ (black histogram) with energies higher than 700 K, ordered by increasing energy from top left to bottom right. Best fit LTE model results considering a hot core at $T_K=220$ K (green curve) and with a hot core at $T_K=280$ K (red curve).

s^{-1} is only the sum of contributions of emission coming from the HVP and the 20.5 km s^{-1} component.

With respect to the nature of the emission at 20.5 km s^{-1} , Fig. 18 shows that the column density ratio of SO/SO₂ of this component is about two to three orders of magnitude higher than the other velocity components in Orion KL. This is also true for the $^{34}\text{SO}/^{34}\text{SO}_2$ and $^{33}\text{SO}/^{33}\text{SO}_2$ ratios, suggesting that it is not an opacity effect. Such a high ratio could be due in part to filling factor problems, if the 20.5 km s^{-1} component is much more compact in SO₂ than in SO⁴, and/or could be the result of applying a different method (LVG for SO vs LTE for SO₂) to infer the column densities. However, the large difference compared to the other components suggests that it is a definite chemical effect, and since the SO/SO₂ ratio is higher in regions associated with shocks such as the HVP and the PL (Sect. 5.1), the 20.5 km s^{-1} component could be related to shocks as well, maybe associated with the explosive dynamical interaction that took place in Orion KL (Gómez et al. 2005, Zapata et al. 2011a) and more specifically to shocks associated with the BN object. This is consistent with the fact that the BN object in Orion presents significantly high CO and ¹³CO emission at $\sim 20 \text{ km s}^{-1}$ (Scoville et al. 1983). Observations combining both single-dish and interfer-

ometric data are required to definitely identify the spatial region in Orion KL emitting the bulk of emission at 20 km s^{-1} .

6. Summary and Conclusions

This study is part of a series of papers with the goal of analyzing the physical and chemical conditions of Orion KL. The study is divided into different molecular families, and here we have focused on the emission lines of SO and SO₂ and their isotopologues. We have analyzed the IRAM 30-m line survey of Orion KL observed by Tercero et al. (2010), which covers the frequency range 80-281 GHz. We identified more than 700 rotational transitions of these molecules, including lines from the vibrational state $\nu_2=1$ of SO₂ and the isotopologue SO¹⁷O, detected for the first time in the interstellar medium. This large sample has let us improve our knowledge about the physical and chemical conditions in Orion KL, especially due to the observation of a large number of SO₂ transitions at high energies. The analysis of SO and SO₂ was carried out using an LTE and LVG radiative transfer model, taking the physical structure of the source into account (hot core, compact ridge, extended ridge, and plateau components).

First, we fit SO and SO₂ lines with Gaussian profiles to obtain an approximate T_{rot} value in each component. We detected a dip at $\sim 15 \text{ km s}^{-1}$ in most of the lines and an emission peak centered on 20.5 km s^{-1} . For the dip at 15 km s^{-1} , we discarded self-absorption as a possible cause, concluding instead that the weak emission is due to the sum of small contributions coming from the high velocity plateau and from the 20.5 km s^{-1} feature, which corresponds to an unresolved component ($\sim 5''$ di-

⁴ In fact, interferometric maps of ³⁴SO in Orion KL reveal emission only from 1 to 15 km s^{-1} (Beuther et al. 2005), indicating that the emission from the 20 km s^{-1} component has probably been filtered out by the interferometer. Given the minimum baseline of the interferometric observations (Beuther et al. 2005), the largest angular scale detectable is $\sim 6''$ (following the Appendix in Palau et al. 2010), similar to the size adopted in this work for the 20.5 km s^{-1} component.

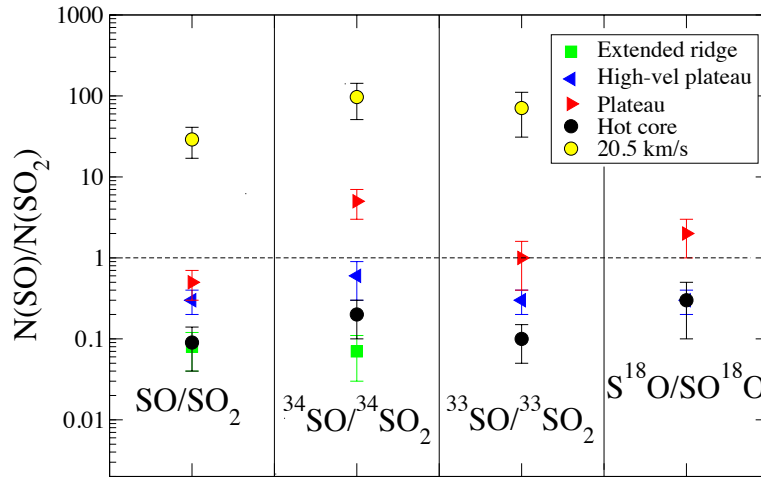


Fig. 18. Ratio $N(\text{SO})/N(\text{SO}_2)$ for each component and for the different isotopologues of SO and SO_2 .

ameter), with line width of $\sim 7.5 \text{ km s}^{-1}$ and with an especially high column density of SO in comparison to SO_2 . Its rotational temperature is $50 \pm 10 \text{ K}$ from SO lines and $90 \pm 20 \text{ K}$ from SO_2 lines. For the rest of the components, the rotational temperatures obtained from SO_2 lines are: plateau (PL) = $120 \pm 20 \text{ K}$, hot core (HC) = $190 \pm 60 \text{ K}$, high velocity plateau (HVP) = $110 \pm 20 \text{ K}$, compact ridge (CR) = $80 \pm 30 \text{ K}$, and extended ridge (ER) = $83 \pm 40 \text{ K}$. The results from SO lines are: (PL) = $130 \pm 20 \text{ K}$, (HC) = $288 \pm 90 \text{ K}$, (HVP) = $111 \pm 15 \text{ K}$, and (ER) = $107 \pm 40 \text{ K}$.

The second part of the analysis was carried out using a radiative transfer code. For the case of SO, we analyzed its non-LTE excitation, however, for SO_2 we assumed LTE excitation due to the lack of collisional rates for energies higher than 90 K (we observe SO_2 lines with energies up to 1500 K). We found that most of the emission of SO_2 and SO arises from the high-velocity plateau, with column densities of $N(\text{SO}_2) = (1.3 \pm 0.3) \times 10^{17} \text{ cm}^{-2}$ and $N(\text{SO}) = (5 \pm 1) \times 10^{16} \text{ cm}^{-2}$, respectively, and from the hot core, in particular in the case of SO_2 , whose column density is similar to that obtained in the high-velocity plateau. These values are up to three orders of magnitude higher than the column densities obtained for the ridge components. These results let us conclude that SO and SO_2 are not good tracers only of shock-affected areas, but also of hot dense gas. In addition, from the ratios $^{34}\text{SO}/^{34}\text{SO}_2$, $^{33}\text{SO}/^{33}\text{SO}_2$, and $\text{S}^{18}\text{O}/\text{SO}^{18}\text{O}_2$ in the different components of the cloud, we observe that in the high-velocity plateau (region affected by shocks) sulfur dioxide is up to five times more abundant than SO. The same trend is found in the hot core.

We have also carried out $2' \times 2'$ mapping around Orion IRC2 in a number of lines of SO, SO_2 , and their ^{34}S isotopologues. In Sect. 3.4 we presented maps of three transitions of SO_2 (Fig. 7), two transitions of SO (Fig. 6), one transition of ^{34}SO and one of $^{34}\text{SO}_2$ (Fig. 8). We plotted different velocity ranges for each transition to explore the spatial distribution of the emission. In agreement with our column density results, we found the maximum integrated intensities in the range containing the hot core ($3\text{--}7 \text{ km s}^{-1}$) and in the range $10\text{--}14 \text{ km s}^{-1}$ (corresponding to the high velocity plateau), whose emission peak is centered approximately $4''$ to the southwest of IRC2. In all mapped transitions, but especially in those of SO and ^{34}SO , we observe an elongation of the gas along the NE-SW direction. In these maps, we also detected a strong emission in the velocity range located at 20.5 km s^{-1} . From the spatial distribution of this feature and from the analysis of the line profiles, we suggest that this emis-

sion is probably related to shocks associated to the *BN* source or to a gas cloudlet ejected in the explosive event that could have taken place in Orion KL.

In this paper, we have also demonstrated the need to consider a temperature and density gradient in the hot core of Orion KL, with a comparison between fits of SO_2 line profiles at high energies, assuming two different temperatures ($T_K = 220 \text{ K}$ and $T_K = 280 \text{ K}$) in the hot core. Only with the low temperature it was not possible to obtain good line fits for $E > 700 \text{ K}$, without avoiding overestimation for lines with intermediate energies. In addition, the large difference between the rotational temperatures in the hot core and the need to consider a large contribution to the SO_2 isotopologue emission in the extended ridge support the conclusion of the presence of temperature and density gradients in Orion KL. However, it would be necessary to also consider emission lines (mainly from isotopologues) spanning a wider frequency range with observations from other telescopes, such as APEX, in order to determine these gradients accurately. Moreover, to describe this molecular cloud in greater detail while avoiding spectral confusion would require interferometric observations with higher spectral resolution and higher sensitivity (such as those provided by ALMA).

Acknowledgements. We thank the Spanish MICINN for funding support through grants AYA2006-14876, AYA2009-07304, and CSD2009-00038. J.R.G. is supported by a Ramón y Cajal research contract. A.P. is supported by a JAE-Doc CSIC fellowship co-funded with the European Social Fund under the program "Junta para la Ampliación de Estudios", by the Spanish MICINN grant AYA2011-30228-C03-02 (co-funded with FEDER funds), and by the AGAUR grant 2009SGR1172 (Catalonia). T. A. B. is supported by a JAE-Doc research contract.

References

- Anders, E. & Gevesse, N., 1989, *GeCoA*, 53, 197.
- Bachiller, R., 1996, *A&A*, 34, 111-54.
- Bak, B., Nielsen, J., & Svanholt, H., 1978, *J. Mol. Spectrosc.*, 69, 401.
- Barnes, I., Becker, K. H., & Patroescu, I., 1994, *GeoRL*, 21, 2389-2392.
- Behrend, J., Mittler, P., Winnemissner, G., & Yamada, K. M. T., 1990, *J. Mol. Spectrosc.*, 141, 265-280.
- Belov, S. P., Tretyakov, M. Y., Kozin, I. N., et al. 1998, *J. Mol. Spectrosc.*, 191, 17.
- Benedettini, M., Yates, J. A., Viti, S., & Codella, C., et al. 2006, *MNRAS*, 370, 229.
- Beuther, H., Zhang, Q., & Greenhill, L. J., et al. 2005, *ApJ*, 632, 355-370.
- Blake, G., Sutton, E. C., Masson, C. R., & Phillips, T. G., 1987, *ApJ*, 315, 621.
- Bogey, M., Demuynck, C., & Destombes, J. L., et al. 1982, *Chem. Phys.*, 66, 99.
- Bogey, M., Civis, S., Delcroix B., et al. 1997, *J. Mol. Spectrosc.*, 182, 85.
- Cazzoli, G., Cludi, L., Cotti G., et al. 1994, *J. Mol. Spectrosc.*, 167, 468.

- Cernicharo, J., 1985, ATM "A Program to compute atmospheric absorption for frequencies below 1000 GHz", IRAM Internal Report No. 52.
- Cernicharo, J., 2012, in ECLA-2011: Proceedings of the European Conference on Laboratory Astrophysics. European Astronomical Society Publications Series, 2012.
- Chernin, L. M., Masson, C. R., & Fuller, G. A., 1994, *ApJ*, 436, 741.
- Clark, F. O., & Johnson, D. R., 1974, *ApJ*, 191, L87.
- Clark, W. W., & DeLucia, F. C., 1976, *J. Mol. Spectrosc.*, 60, 332.
- Codella, C., & Bachiller, R., 1999, *A&A*, 350, 659-671.
- Codella, C., & Scappini, F., 2003, *MNRAS*, 344, 1257.
- Dreizler, H. & Dendl, G., 1964, *Naturforsch.*, 19a, 512.
- Fuente, A., Rodríguez-Franco, A., García-Burillo, S. et al. 2003, *A&A*, 406, 899-913.
- Gezari, D. Y., Backman, D. E. & Werner, M. W., 1998 *ApJ*, 509, 283.
- Goicoechea, J. R., Cernicharo, J., Lerate, M. R., et al. 2006, *ApJ*, 641, L49-L52.
- Goldreich, P. & Kwan, J., 1974, *ApJ*, 189, 441-453.
- Goldsmith, Paul F. & Langer, William D., 1999, *ApJ*, 517, 209.
- Gómez, L., Rodríguez, L. F., Loinard, L., & Lizano, S., 2005, *ApJ*, 635, 1166-1172.
- Gottlieb, C. A., & Ball, John A., 1973, *ApJ*, 184, L59.
- Guélin, M., Brouillet, N., Cernicharo, J., et al. 2008, *Ap&SS*, 313, 45-51.
- Hatchell, J., Thompson, M. A., Millar, T. J., & MacDonald, G. H., 1998, *A&A*, 338, 713.
- Jiménez-Serra, I., Martín-Pintado, J., Rodríguez-Franco, A., Martín, S., 2005, *ApJ*, 627, L121.
- Joo, D. L., Clouthier, D. J., Chan, C. P., et al. 1995, *J. Mol. Spectrosc.*, 171, 113-124.
- Joo, D. L., Harjanto, H., & Clouthier, D. J., 1996, *J. Mol. Spectrosc.*, 178, 78-83.
- Kirchhoff, W. H., 1969, *J. Am. Chem. Soc.*, 91, 2437.
- Klaus, Th., Saleck, A. H., Belov S. P., et al. 1996, *J. Mol. Spectrosc.*, 180, 197.
- Lee, C. F., Hasegawa, T. I., Hirano, N., Palau, A., et al. 2010, *ApJ*, 713.
- Lattanzi, V., Gottlieb, C. A., Thaddeus, P., et al. 2011, *A&A*, 533, L11.
- Lique, F., Spielfiedel, A., Dhont, G., & Feautrier, N., 2006, *A&A*, 458, 331-337.
- Lique, F., & Spielfiedel, A., 2007, *AA*, 462, 1179.
- Lovas, F. J., Suenram, R. D., Ogata, T., and Yamamoto, S., 1992, *ApJ*, 399, 325.
- Maki & Kuritsyn, 1990, *J. Mol. Spectrosc.*, 144, 242.
- Marcelino, N., Tercero, B., Cernicharo, J., et al. in prep.
- Marconi, M. L., Mendis, D. A., Mitchell, D. L., et al. 1991, *ApJ*, 378, 756.
- Margules, L., et al. 2010, *J. Mol. Spectrosc.*, 260, 23.
- Martin-Drumel, M. A., 2012, PhD thesis, University Paris.
- Mauersberger, R., Henkel, C., Langer, N., & Chin, Y. N., 1996, *A&A*, 313, L1-L4.
- McCarthy, M. C., Thorwirth, S., Gottlieb, C. A., & Thaddeus, P., 2004, *J. Chem. Phys.* 126, 4096-4097.
- McCarthy, M. C., Thorwirth, S., Gottlieb, C. A., & Thaddeus, P., 2004, *J. Chem. Phys.* 121, 632.
- Menten, K. M., Reid, M. J., Forbrich, J., & Brunthaler, A., 2007, *A&A*, 474, 515-520.
- Meschi, D.J. & Myers, R. J., 1959, *J. Mol. Spectrosc.*, 3, 405.
- Müller, H. S. P., Farhoomand, J., Cohen E. A., et al. 2000, *J. Mol. Spectrosc.*, 232, 213.
- Müller, H. S. P., Thorwirth, S., Roth, D. A., & Winnewisser, G., 2001, *AA*, 370, L49.
- Müller & Brünken, 2005, *J. Mol. Spectrosc.*, 232, 213.
- Palau, A., Sánchez-Monge, Á., Busquet, G., et al. 2010, *A&A*, 510, A5.
- Pardo, J. R. & Encrenaz, Pierre J., 2001, *IAU Symposium*, Vol. 196.
- Patel, D., Margolese, D. & Dykea, T. R., 1979, *J. Chem. Phys.*, 70, 2740.
- Penn, R. E. & Olsen, R. J., 1976, *J. Mol. Spectrosc.*, 61, 21-28.
- Persson, C. M., Olofsson, A. O. H., Koning, N., et al. 2007, *A&A*, 476, 807-828.
- Pickett, H. M., Poynter, R. L., Cohen, E. A., et al. 1998, *JQSRT*, 60, 5.
- Plambeck, R. L., Wright, M. C. H., Welch, W. J., et al. 1982, *ApJ*, 259, 617-624.
- Plambeck, R. L., Wright, M. C. H., Friedel, D. N., et al., 2009, *ApJ*, 704, L25.
- Powell, F. X. & Lide, D. R., et al., 1964, *J. Chem. Phys.*, 41, 1413.
- Rawling, J. M. C. & Yates, J. A., 2001, *M.N.R.A.S.*, 326, 1423.
- Schilke, P., Benford, D. J., Hunter, T. R., et al. 2001, *ApJ*, 132, 281.
- Schultz, A. S. B., Colgan, S. W. J., Erickson, E. F., et al. 1999, *ApJ*, 511, 282-289.
- Scoville, N., Kleinmann, S. G., Hall, D. N. B., & Ridgway, S. T., 1983, *ApJ*, 275, 201-224.
- Sedo, G., Schultz, J., & Leopold, K. R., 2008, *J. Mol. Spectrosc.*, 251, 4-8.
- Sutton, E. C., Peng, R., Danchi, W. C., et al. 1995, *AJSS*, 97, 455.
- Tafalla, M., Santiago-García, J., Hacar, A., & Bachiller, R., 2010, *A&A*, 522, A91.
- Tercero, B., Cernicharo, J., Pardo, J. R., & Goicoechea, J. R., 2010, *A&A*, 517, id.A96.
- Tercero, B., Vincent, L., Cernicharo, J., et al. 2011, *A&A*, 528, A26.
- Thorwirth, S., McCarthy, M. C., Gottlieb, C. A., et al. 2005, *J. Chem. Phys.*, 123, 54326.
- Thorwirth, S., Theulé, P., Gottlieb, C. A., et al. 2006, *J. Mol. Struct.*, 795, 219-229.
- Thorwirth, S., Mück, L. A., Gauss, F., et al. 2011, *J. Chem. Phys. Lett.* 2, 1228.
- Tiemann, E., *J. Phys. Chem.*, 3, 259.
- Tiemann, E., 1982, *J. Mol. Spectrosc.*, 91, 60.
- Tyblewski, M., Ha, T. K., Bauder, A., et al. 1986, *J. Mol. Spectrosc.*, 115, 353-365.
- Turner, B. E., 1991, *ApJ*, 76, 617.
- Turner, B. E., Chan, Kin-Wing, Green, S., & Lubowich, D. A., 1992, *ApJ*, 399, 114.
- Turner, B. E., 1994, *ApJ*, 430, 727.
- Viti, S. & Williams, David A., 1999, *M.N.R.A.S.*, 305, 755.
- Viti, S., Caselli, P., Hartquist, T. W., & Williams, D. A., 2001, *A&A* 370, 1017-1025.
- Viti, S., Collings, M. P., Dever, J. W., et al. 2004a, *M.N.R.A.S.*, 354, 1141.
- Viti, S., Codella, C., Benedettini, M., & Bachiller, R., 2004b, *M.N.R.A.S.*, 350, 1029.
- White, G. J. & Phillips, J. P., 1983, *MNRAS*, 203.
- Wilson, T. L., Gaume, R. A., Gensheimer, P., & Johnston, K. J., 2000, *ApJ*, 538, 665.
- Winnewisser, G., Winnewisser, M., & Gordy, W., 1966, *Bull. Amer. Phys. Soc.*, 11, 312.
- Wright M. C. H., Plambeck R. L., & Wilner D. J., 1996, *ApJ*, 469, 216-237.
- Zapata, L. A., Schmid-Burgk, J., & Menten, K. M., 2011a, *A&A*, 529, A24.

Table A.1. SO emission line parameters obtained from Gaussian fits.

Species/ Transition	Plateau			High-velocity plateau			Hot core			Extended ridge			20.5 km s ⁻¹ component		
	v_{LSR} (km s ⁻¹)	Δv (km s ⁻¹)	T_{A}^* (K)	v_{LSR} (km s ⁻¹)	Δv (km s ⁻¹)	T_{A}^* (K)	v_{LSR} (km s ⁻¹)	Δv (km s ⁻¹)	T_{A}^* (K)	v_{LSR} (km s ⁻¹)	Δv (km s ⁻¹)	T_{A}^* (K)	v_{LSR} (km s ⁻¹)	Δv (km s ⁻¹)	T_{A}^* (K)
SO 2 ₂ -1 ₁	6.8	27±3	3.86	10.8	34±1	5.00	5.5	11.2±0.3	2.20	8.8	6.5±0.4	1.10	20.5	8.5±0.5	0.91
SO 2 ₃ -1 ₂	6.6	27±1	6.70	11.7	35±1	11.0	5.5	10.5±0.5	4.20	8.5	5.6±0.2	1.51	21.0	7.5±0.4	0.93
SO 3 ₂ -2 ₁	6.8	27±5	7.00	11.8	34±2	7.15	5.3	11.5±0.8	3.70	9.0	5.4±0.2	1.50	20.5	7.5±0.4	1.58
SO 3 ₄ -2 ₃	6.0	27±3	10.45	11.4	37±4	16.0	5.9	9.0±0.3	3.70	20.5	7.5±0.3	1.50
SO 4 ₃ -3 ₂	6.6	23±1	11.50	11.0	36±4	13.2	5.5	8.4±0.5	7.10	21.6	7.5±0.4	2.25
SO 4 ₄ -3 ₃	6.0	25±2	18.00	11.9	36±3	17.9	4.5	10.0±0.2	5.00	21.5	7.5±0.3	4.00
SO 5 ₄ -4 ₃	6.7	24±5	10.93	12.7	37±1	12.0	5.7	9.5±0.4	10.0	21.5	7.5±0.5	2.88
SO 5 ₅ -4 ₄	6.4	28±4	18.00	12.9	42±4	11.0	3.9	9.4±0.5	5.50	20.0	8.3±0.6	5.00
SO 5 ₆ -4 ₅	6.3	28±4	16.95	13.5	39±2	14.0	4.3	9.3±0.4	8.50	8.3	5.9±0.3	2.00
SO 6 ₅ -5 ₄	6.0	29±3	20.00	12.5	36±1	10.5	3.5	7.5±0.6	6.30	9.0	4.0±0.2	3.49
SO 6 ₆ -5 ₅	6.7	35±3	12.62	11.7	35±2	8.99	8.5	6.1±0.5	1.26
SO 6 ₇ -5 ₆	6.0	33±4	20.00	13.3	37±4	16.0	1.5	12.0±0.5	8.80	21.5	8.5±0.5	5.24

Notes. The fit errors are provided by CLASS. v_{LSR} is the LSR central velocity, Δv is the line width, and T_{A}^* is the antenna temperature.

Table A.2. SO₂ parameters from Gaussian fits (lines at 1.3 mm).

Transition	Plateau			High-velocity plateau			Hot core			Compact ridge			Extended ridge			20.5 km s ⁻¹ component			
	v _{LSR} (km s ⁻¹)	Δv (km s ⁻¹)	T _A [*] (K)	v _{LSR} Δv	T _A [*]	v _{LSR} Δv	v _{LSR} Δv	T _A [*]	v _{LSR} Δv	T _A [*]	v _{LSR} Δv	T _A [*]	v _{LSR} Δv	T _A [*]	v _{LSR} Δv	T _A [*]	v _{LSR} Δv	T _A [*]	
1.3 mm																			
3 _(2,2) -2 _(1,1)	6.4	26±1	5.50	12.9	35±3	5.00	5.0	10.0±0.2	6.60	21.0	8.0±0.4	3.50
4 _(2,2) -3 _(1,3)	6.0	25±1	6.00	12.6	33±5	4.60	4.5	8.0±0.4	5.47	22	7.5±0.5	2.60
4 _(3,1) -4 _(2,2)	6.0	25±1	2.40	11.5	32±3	3.60	3.7	8.9±0.4	1.61	7.8	4.1±0.5	1.37	21.0	8.0±0.3	0.69
5 _(2,4) -4 _(1,3)	5.9	26±1	7.00	12.8	38±5	6.40	3.8	12.2±0.3	7.90	20.5	8.0±0.3	3.86
6 _(4,2) -7 _(3,5)	6.0	24±2	1.00	11.5	29±1	1.40	5.0	7.0±0.5	3.30	20.5	8.0±0.3	0.14
7 _(2,6) -6 _(1,5)	6.0	25±1	5.00	12.8	35±2	3.50	5.0	11.0±0.2	2.50	20.5	7.5±0.4	2.00
7 _(3,5) -7 _(2,6)	6.0	23±2	3.00	12.9	33±2	3.30	4.5	9.6±0.3	0.55	7.5	5.0±0.3	1.31	20.5	7.5±0.4	0.60
7 _(4,4) -8 _(3,5)	6.3	24±1	2.80	11.6	33±1	1.42	4.4	7.7±0.5	1.40	20.5	7.5±0.4	0.43
11 _(1,11) -10 _(0,10)	6.0	30±4	7.00	12.0	35±1	9.50	4.0	11.9±0.2	9.00	7.7	4.9±0.3	2.00	20.5	7.5±0.5	2.70
11 _(2,10) -11 _(1,11)	6.0	25±3	7.00	12.9	33±4	4.40	5.0	8.4±0.3	7.00	21.0	7.5±0.4	2.00
11 _(3,9) -11 _(2,10)	6.0	25±2	3.56	12.7	35±6	4.30	5.7	9.0±0.3	3.02	21.0	8.0±0.3	1.31
11 _(5,7) -12 _(4,8)	6.2	25±2	1.23	11.7	31±1	1.10	5.5	7.5±0.5	0.88	20.5	7.0±0.5	0.21
13 _(1,13) -12 _(0,12)	6.0	25±3	11.00	12.7	38±3	10.6	5.9	10.0±0.2	9.15	21.0	8.0±0.2	2.99
13 _(3,11) -13 _(2,12)	6.0	28±1	10.50	10.8	30±1	10.4
14 _(3,11) -14 _(2,12)	6.6	27±4	6.50	12.9	32±1	5.0	4.5	9.3±0.2	10.0	7.2	5.5±0.2	1.46
14 _(6,8) -15 _(5,11)	6.9	25±2	1.60	5.0	7.2±0.4	1.54	19.3	7.5±0.3	0.37
15 _(3,13) -15 _(2,14)	6.0	24±2	4.20	11.6	35±1	3.90	5.5	8.6±0.2	1.92	21.0	7.5±0.4	1.30
16 _(1,15) -15 _(2,14)	5.9	25±3	4.00	12.6	33±2	4.30	4.8	10.0±0.1	4.89	21.5	7.5±0.3	2.05
16 _(1,15) -16 _(0,16)	6.0	24±2	3.50	12.3	34±3	3.30	5.7	13.0±0.5	4.42	7.0	4.0±0.5	0.49	20.5	7.5±0.4	1.67
16 _(3,13) -16 _(2,14)	6.0	25±3	5.79	12.0	34±3	2.50	4.9	9.0±0.3	5.57	21.0	7.5±0.4	1.50
18 _(3,15) -18 _(2,16)	6.0	24±1	4.50	12.3	32±1	5.00	4.5	10.3±0.2	5.10	20.5	7.5±0.3	1.98
20 _(3,17) -20 _(2,18)	6.0	28±3	5.00	12.5	41±3	3.60	4.8	9.1±0.3	6.09	20.5	8.5±0.2	1.54
20 _(7,13) -21 _(6,16)	6.0	20±1	0.40	11.5	24±2	0.45	5.2	6.0±0.6	0.77
24 _(3,21) -24 _(2,22)	6.0	27±3	3.00	11.5	36±1	0.98	5.3	8.8±0.3	4.38
26 _(3,23) -26 _(2,24)	6.9	25±4	3.50	5.0	7.8±0.5	3.95
28 _(4,24) -28 _(3,25)	6.3	23±3	2.65	12.4	27±1	1.85	4.0	8.7±0.3	3.76

Notes. The fit errors are provided by CLASS. v_{LSR} is the LSR central velocity, Δv is the line width, and T_A^{*} is the antenna temperature. The units of v_{LSR}, Δv, and T_A^{*} are (km s⁻¹), (km s⁻¹), and (K), respectively, in all the cases.

Table A.3. SO₂ parameters from Gaussian fits (lines at 2–3 mm).

Transition	Plateau			High-velocity plateau			Hot core			Compact ridge			Extended ridge			20.5 km s ⁻¹ component	
	v_{LSR} (km s ⁻¹)	Δv (km s ⁻¹)	T_{A}^* (K)	v_{LSR} Δv	T_{A}^*	v_{LSR} Δv	v_{LSR} Δv	T_{A}^*	v_{LSR} Δv	T_{A}^*	v_{LSR} Δv	v_{LSR} Δv	T_{A}^*	v_{LSR} Δv	v_{LSR} Δv	T_{A}^*	
2 mm																	
2 _(2,0) -2 _(1,1)	6.0	22±2	4.00	11.7	32±2	3.00	5.5	9.0±0.3	1.20	20.5	7.5±0.3	1.15	
3 _(2,2) -3 _(1,3)	6.0	25±4	4.40	12.5	32±2	4.10	5.5	9.1±0.3	5.37	20.5	7.5±0.2	1.00	
5 _(1,5) -4 _(0,4)	6.0	24±1	6.09	11.7	33±1	6.40	5.5	8.0±0.2	2.97	8.0	3.6±0.5	21.0	7.0±0.2	1.50	
5 _(2,4) -5 _(1,5)	6.0	26±1	5.00	12.0	32±3	8.00	5.5	9.2±0.9	5.51	20.5	7.5±0.3	1.00	
6 _(2,4) -6 _(1,5)	6.0	25±1	5.94	11.6	33±3	5.50	5.5	11.1±0.3	3.05	8.0	6.2±0.3	20.5	7.5±0.2	1.80	
7 _(1,7) -6 _(0,6)	6.0	25±3	8.00	12.0	33±2	10.0	5.8	9.0±0.1	8.16	20.5	7.5±0.1	3.00	
7 _(2,6) -7 _(1,7)	6.0	25±1	6.00	12.3	34±3	6.60	5.5	8.8±0.1	6.32	21.0	7.5±0.3	2.10	
8 _(2,6) -8 _(1,7)	6.0	23±1	5.70	12.7	34±3	6.00	5.7	7.0±0.4	5.48	9.5	5.1±0.3	
10 _(0,10) -9 _(1,9)	6.0	25±1	11.0	11.9	35±2	8.00	4.0	10.0±0.5	5.00	8.0	3.0±0.5	4.49	...	20.5	7.5±0.1	2.50	
12 _(1,11) -12 _(0,12)	6.0	25±1	3.92	12.1	33±3	4.20	5.5	11.7±0.7	2.46	9.0	6.1±0.5	0.84	1.40	
14 _(1,13) -14 _(0,14)	6.0	25±1	6.00	11.7	32±5	6.93	5.0	10.0±0.3	4.50	7.3	4.5±0.5	1.96	...	20.5	7.5±0.2	2.00	
14 _(2,12) -14 _(1,13)	6.2	23±2	6.50	11.9	34±5	6.40	5.8	8.2±0.2	4.89	9.0	5.4±0.3	1.44	2.00	
16 _(2,14) -16 _(1,15)	6.0	25±3	6.00	11.6	33±3	5.50	5.5	10.2±0.2	4.05	7.0	6.0±0.2	0.20	...	20.5	7.5±0.2	1.80	
18 _(2,16) -18 _(1,17)	6.0	24±3	6.50	11.6	32±2	6.00	5.0	10.3±0.2	3.00	7.5	6.1±0.2	1.72	...	20.5	7.5±0.3	1.59	
3 mm																	
8 _(1,7) -8 _(0,8)	6.0	22±1	3.67	11.3	32±1	4.40	5.5	9.1±0.2	1.15	8.0	5.5±0.4	2.21	...	20.5	7.5±0.4	0.90	
8 _(3,5) -9 _(2,8)	6.0	24±2	0.82	11.7	30±3	1.10	5.8	10.0±0.2	0.83	
10 _(1,9) -10 _(0,10)	6.0	24±1	3.98	11.4	32±3	6.00	5.5	10.9±0.1	3.50	8.6	5.5±0.4	1.19	1.50	

Notes. The fit errors are provided by CLASS. v_{LSR} is the LSR central velocity, Δv is the line width, and T_{A}^* is the antenna temperature. The units of v_{LSR} , Δv , and T_{A}^* are (km s⁻¹), (km s⁻¹), and (K), respectively, in all the cases.

Table A.4. Rotational temperatures, T_{rot} , and column densities, N , obtained from rotational diagrams.

Component	$T_{\text{rot}}(\text{SO})$ (K)	$N(\text{SO}) \times 10^{15}$ (cm^{-2})	$C_{\tau}(\text{SO})$	$T_{\text{rot}}(\text{SO}_2)$ (K)	$N(\text{SO}_2) \times 10^{15}$ (cm^{-2})	$C_{\tau}(\text{SO}_2)$
Extended ridge (ER)	107±40	0.017±0.001	1.00-1.02	83±40	0.023±0.009	1.04-1.15
Compact ridge (CR)	80±30	1.2±0.2	1.00-1.63
High-velocity plateau (HVP)	111±15	3.9±0.5	1.01-2.12	110±20	9.5±0.6	1.0-1.60
Plateau (PL)	130±20	4.6±0.2	1.01-1.11	120±20	13±1	1.01-1.69
Hot core (HC)	288±90	18±1	1.02-1.64	190±60	33±3	1.00-1.71
20.5 km s ⁻¹ comp.	51±10	0.014±0.02	1.06-1.36	90±20	4.6±0.1	1.00-1.58

Notes. C_{τ} is the range of optical depths in each component.

Table A.5. Isotopologue ratios and molecular ratios.

Ratio	Extended ridge (ER)	Compact ridge (CR)	High-velocity plateau (HVP)	Plateau (PL)	Hot core (HC1)	20.5 km s ⁻¹ component	Solar isotopic abundance
Isotopologues ratios							
$\text{SO}_2/^{34}\text{SO}_2$	2±1	2±1	20±13	16±10	10±8	5±3	23
$\text{SO}_2/^{33}\text{SO}_2$	7±4	17±10	137±90	19±13	29±19	20±14	127
$\text{SO}_2/\text{SO}^{18}\text{O}$	12±8	40±26	151±100	164±100	67±48	...	500
$\text{SO}_2/\text{SO}^{17}\text{O}$	34±27	180±110	1300±900	334±200	111±80	...	2625
$^{34}\text{SO}_2/^{33}\text{SO}_2$	3±2	7±4	7±4	1.2±0.8	3±2	4±3	5.5
$^{34}\text{SO}_2/\text{SO}^{18}\text{O}$	5±3	17±11	8±5	10±6	7±5
$^{33}\text{SO}_2/\text{SO}^{18}\text{O}$	2±1	2±1	1.1±0.7	8±6	2±1
$\text{SO}/^{34}\text{SO}$	3±1	...	11±5	1.7±0.8	4±2	1.4±0.6	23
$\text{SO}/^{33}\text{SO}$	180±80	10±5	26±14	8±4	127
$\text{SO}/\text{S}^{18}\text{O}$	188±90	50±30	18±9	...	500
$^{34}\text{SO}/^{33}\text{SO}$	16±7	6±3	6±3	6±3	5.5
$^{34}\text{SO}/\text{S}^{18}\text{O}$	17±8	30±15	4±2
$^{33}\text{SO}/\text{S}^{18}\text{O}$	1.1±0.6	5±3	0.7±0.5
Molecular ratios							
SO/SO_2	0.08±0.05	...	0.3±0.2	0.5±0.3	0.09±0.06	29±16	...
$^{34}\text{SO}/^{34}\text{SO}_2$	0.07±0.04	...	0.6±0.3	5±3	0.2±0.1	97±49	...
$^{33}\text{SO}/^{33}\text{SO}_2$	0.3±0.1	1.0±0.6	0.10±0.05	71±40	...
$\text{S}^{18}\text{O}/\text{SO}^{18}\text{O}$	0.3±0.1	2±1	0.3±0.2

Table A.6. Molecular abundances, X .

Region	Species	X ($\times 10^{-8}$)
Extended Ridge ^(a)	SO	0.02
	SO ₂	0.31
Compact Ridge ^(b)	SO	...
	SO ₂	1.60
Plateau ^(c)	SO	2.38
	SO ₂	4.76
High velocity Plateau ^(d)	SO	72.5
	SO ₂	210
Hot core ^(e)	SO	2.14
	SO ₂	23.8
20.5 km s ⁻¹ component ^(f)	SO	5.00
	SO ₂	0.17

Notes. Derived molecular abundances, X , assuming:

^(a) $N_{\text{H}_2}=7.5 \times 10^{22} \text{ cm}^{-2}$, ^(b) $N_{\text{H}_2}=7.5 \times 10^{22} \text{ cm}^{-2}$, ^(c) $N_{\text{H}_2}=2.1 \times 10^{23} \text{ cm}^{-2}$, ^(d) $N_{\text{H}_2}=6.2 \times 10^{22} \text{ cm}^{-2}$, ^(e) $N_{\text{H}_2}=4.2 \times 10^{23} \text{ cm}^{-2}$, ^(f) $N_{\text{H}_2}=1.0 \times 10^{23} \text{ cm}^{-2}$.

Table A.7. Column density upper limits for undetected sulfur-bearing molecules in Orion KL.

Molecule	Column density $\leq N \times 10^{14}$ (cm^{-2})	Dipole moment (D)	References for spectroscopic constants
SO ⁺	2.5	2.30	1
(<i>cis</i>)-HOSO ⁺	0.36	$\mu_a=1.74$ $\mu_b=0.49$	2
SSO	7.6	$\mu_a=0.87$ $\mu_b=1.18$	3, 4
OSiS	0.63	1.47	5
S ₃	10	0.51	6
S ₄	7.0	0.87	6
H ₂ SO ₄	1.3	$\mu_c=2.96$	7
CH ₃ SOCH ₃	1.0	$\mu_b=3.94$ $\mu_c=0.4$	8, 9
H ₂ CSO	0.3	$\mu_a=2.95$ $\mu_b=0.50$	10, 11
HNSO	4.1	$\mu_a=0.89$ $\mu_b=0.18$	12, 13
o-H ₂ S ₂	1.6	0.69	14
SSH	0.71	$\mu_a=1.16$ $\mu_b=0.83$	1
CH ₃ SSH	2.6	$\mu_a=1.08$ $\mu_b=1.22$ $\mu_c=0.76$	15
(<i>tr</i>)-HCSSH	0.36	1.53	16

References. (1) CDMS catalog; (2) Lattanzi et al. (2011); (3) Thorwirth et al. (2006); (4) Meschi et al. (1959); (5) Thorwirth et al. (2011); (6) Thorwirth et al. (2005); (7) Sedo et al. (2008); (8) Dreizler & Dendl (1964); (9) Margules et al. (2010); (10) Joo et al. (1995); (11) Penn & Olsen (1976); (12) Joo et al. (1996); (13) Kirchoff (1969); (14) Behrend et al. (1990); (15) Tyblewski et al. (1997); (16) Bak et al. (1978).

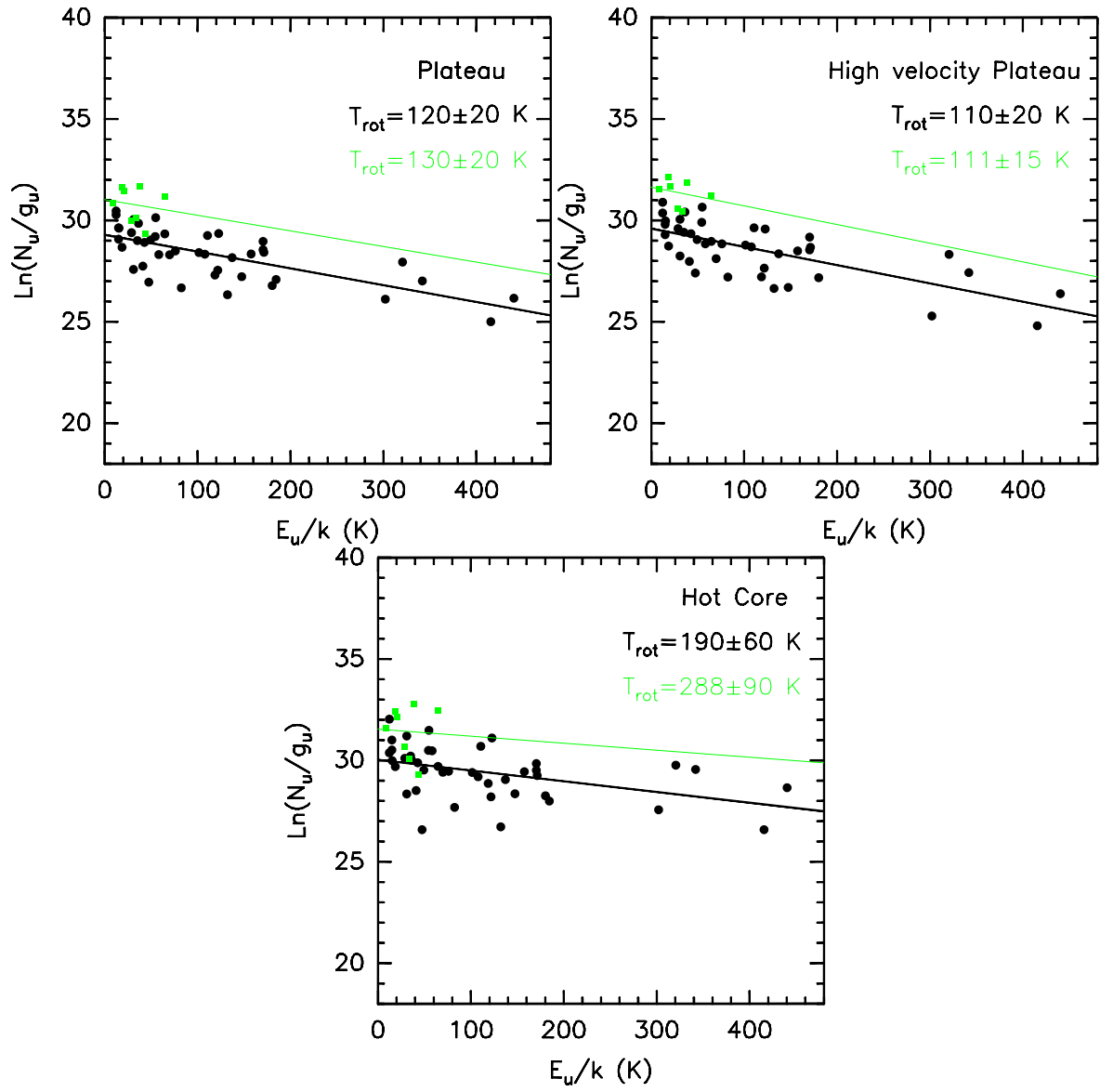


Fig. A.1. Rotational diagrams for the plateau, high-velocity plateau, and hot core components. Black dots for SO_2 and green dots for SO . The black and green lines are the best linear fits to the SO_2 and SO points, respectively.

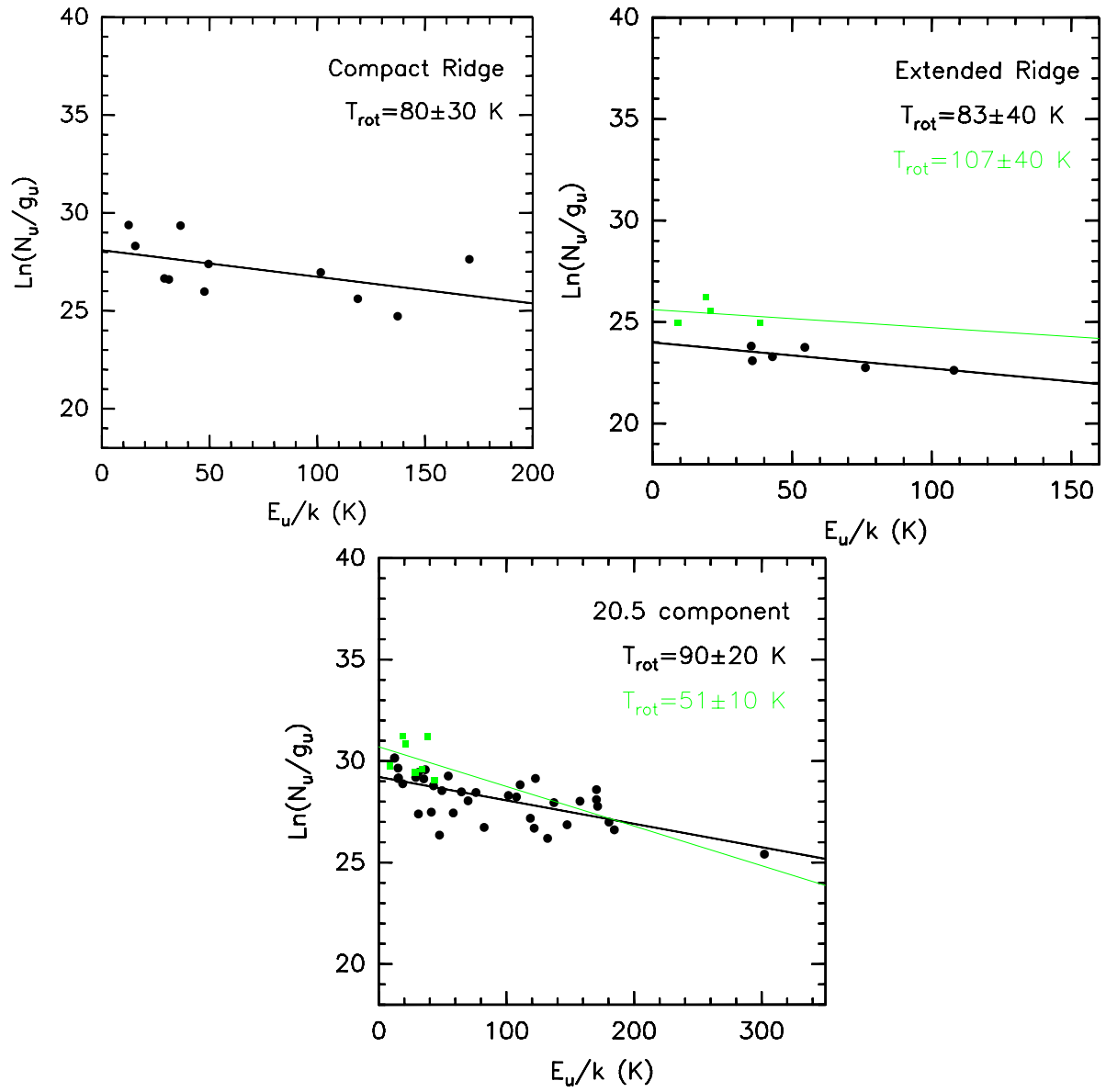


Fig. A.2. Rotational diagrams for the compact ridge, extended ridge, and 20.5 km s^{-1} component. Black dots for SO_2 and green dots for SO . The black and green lines are the best linear fits to the SO_2 and SO points, respectively.

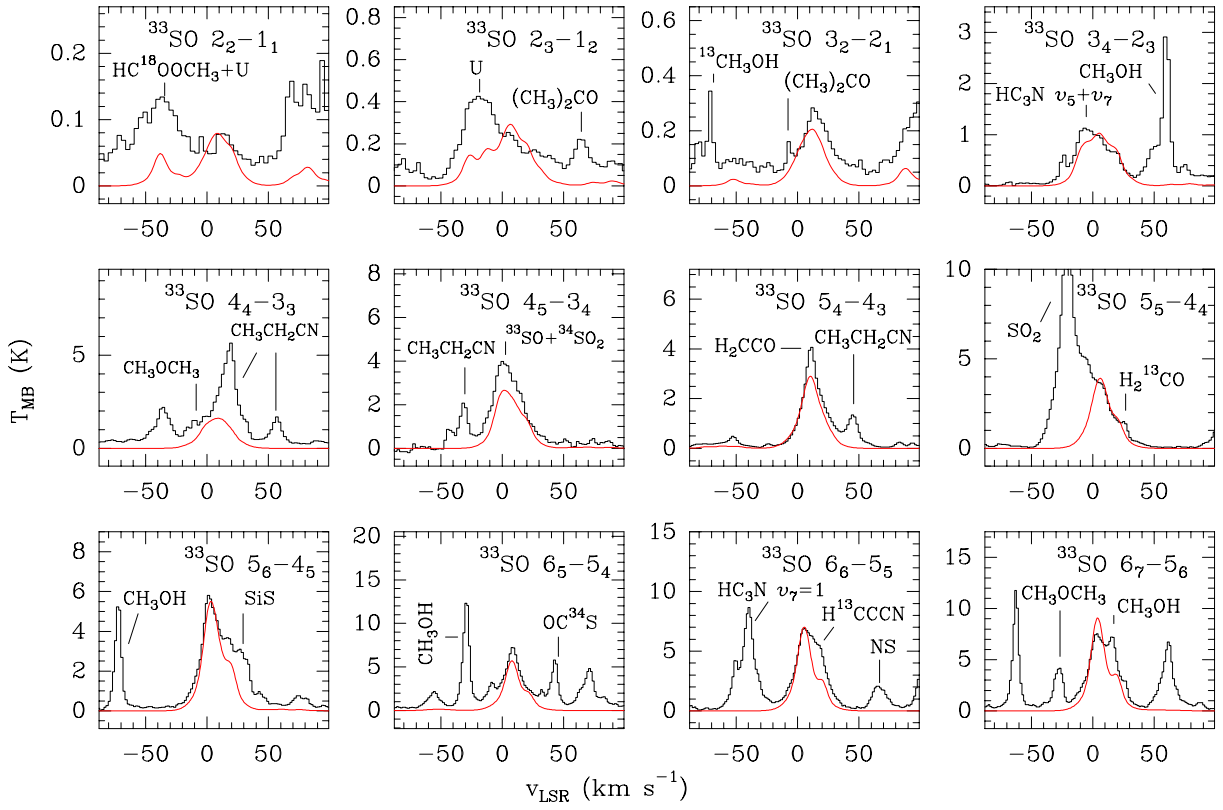


Fig. A.3. Observed lines of ^{33}SO (black histogram) and best fit LVG model results (red).

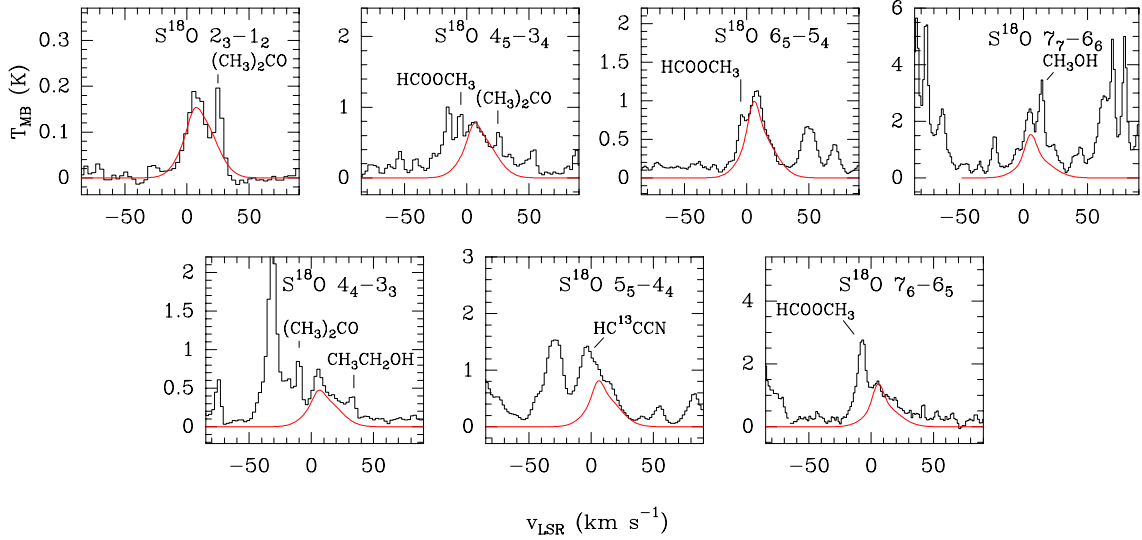


Fig. A.4. Observed lines of S^{18}O (black histogram) and best fit LVG model results (red).

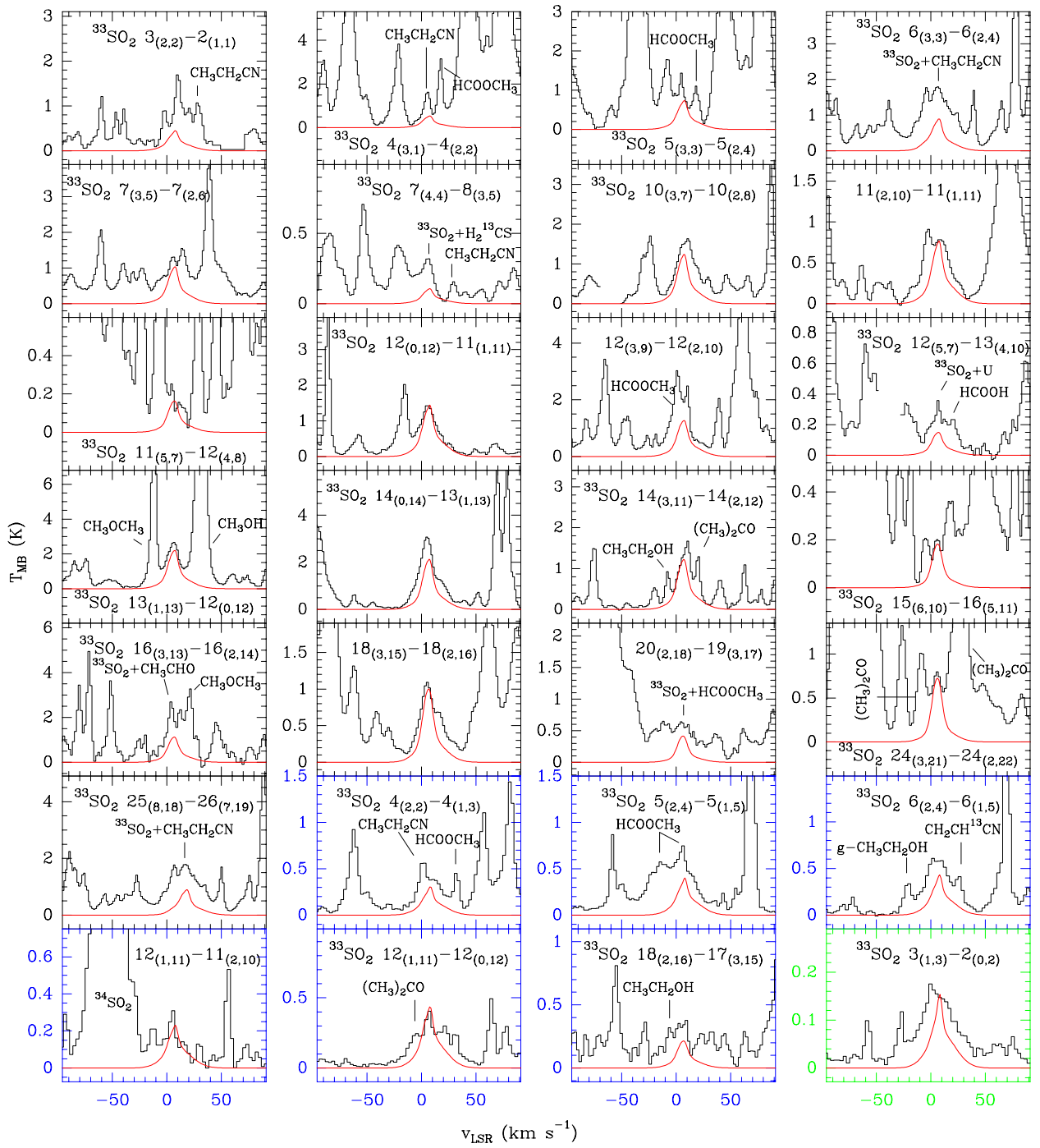


Fig. A.5. Observed lines of $^{33}\text{SO}_2$ (black histogram) and best fit LTE model (red). Boxes in black, blue, and green correspond to frequencies at 1.3, 2, and 3 mm, respectively.

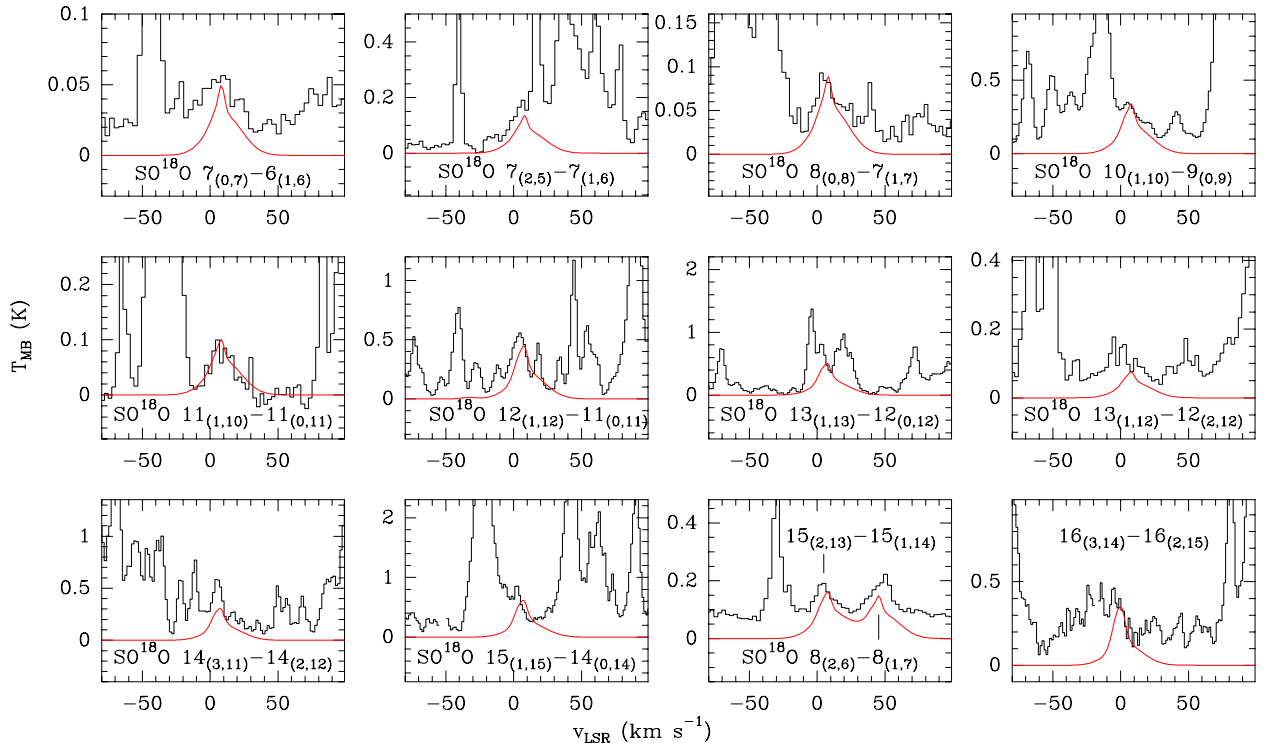


Fig. A.6. Observed lines of SO^{18}O (black histogram) and best fit LTE model (red).

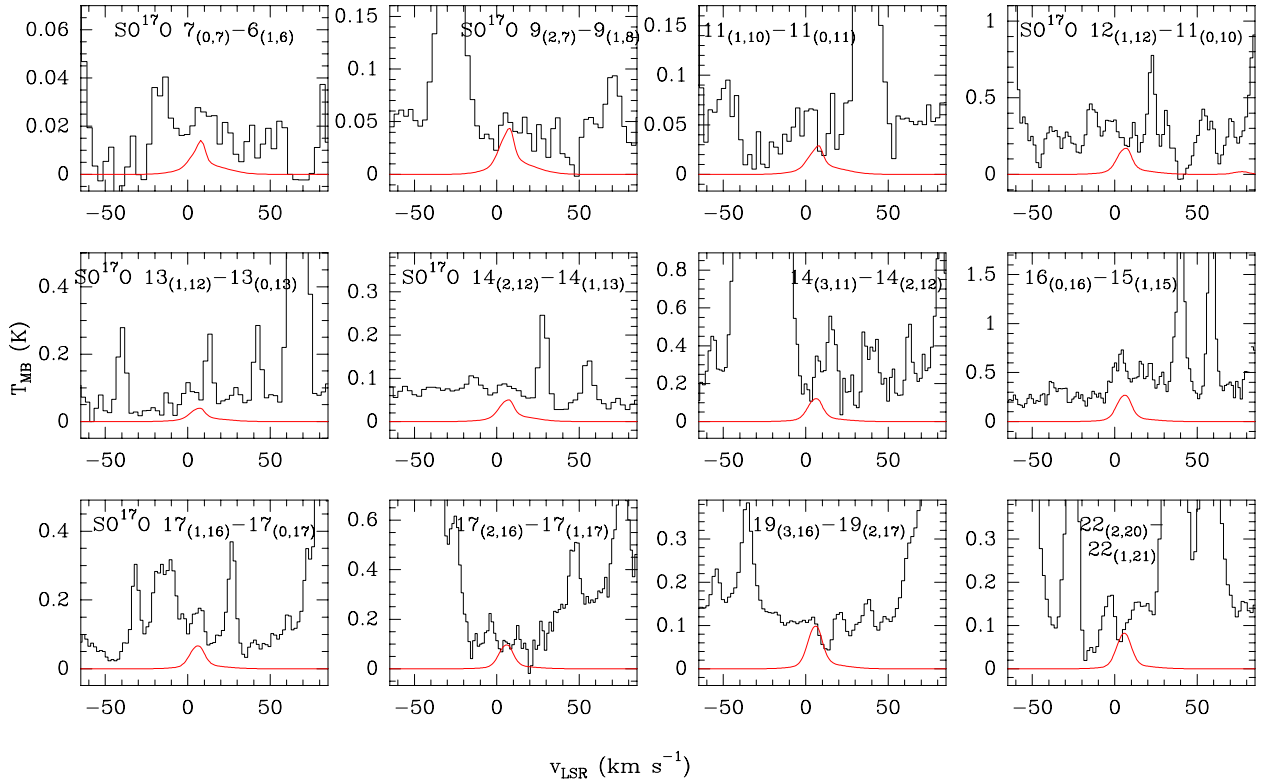


Fig. A.7. Observed lines of SO^{17}O (black histogram) and best fit LTE model (red).

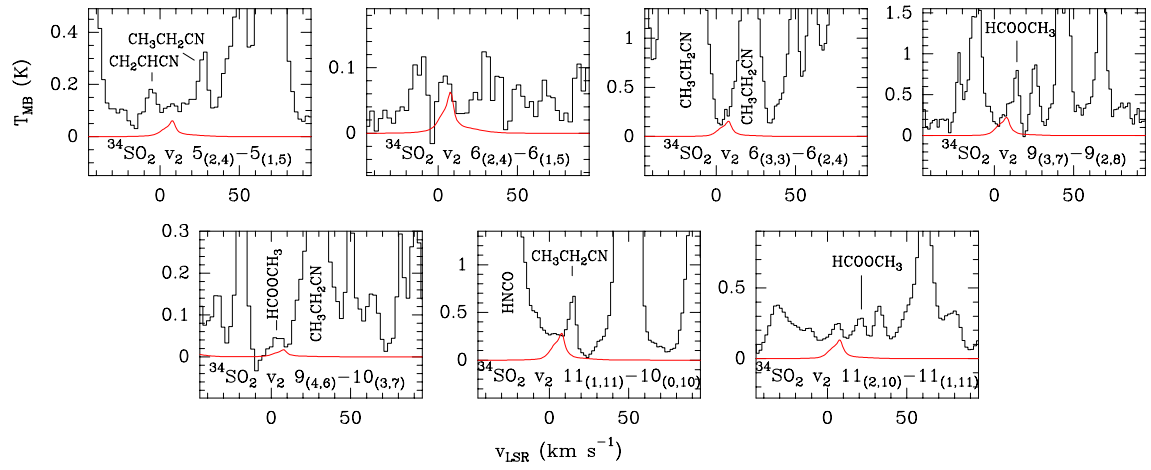


Fig. A.8. Observed lines of $^{34}\text{SO}_2$ $v_2=1$ (black histogram) and best fit LTE model (red).

Table A.8. Observed lines of SO and its isotopologues.

Species	Transition $N_J-N'_J$	Predicted freq. (MHz)	S_{ij}	E_u (K)	Observed freq. (MHz)	Observed v_{LSR} (km s ⁻¹)	Observed T_A^* (K)	Blended with
SO	2 ₂ -1 ₁	86093.958	1.50	19.3	86094.4	7.4	11.73	
SO	2 ₃ -1 ₂	99299.887	2.93	38.6	99300.4	7.4	22.52	
SO	5 ₄ -4 ₄	100029.550	0.36	38.6	100030.5	6.2	5.90	CH ₃ CH ₂ CN
SO	3 ₂ -2 ₁	109252.181	1.51	21.1	109252.5	8.1	18.38	
SO	6 ₅ -5 ₅	136634.660	0.28	50.7	136636.4	5.2	7.98	CH ₃ OCH ₃
SO	3 ₄ -2 ₃	138178.654	3.94	15.9	138178.9	8.5	29.4	
SO	4 ₃ -3 ₂	158971.811	2.69	28.7	158972.6	7.5	30.99	
SO	4 ₄ -3 ₃	172181.403	3.75	33.8	172182.7	6.7	39.33	
SO	7 ₆ -6 ₆	174928.886	0.22	64.9	174931.4	4.7	9.43	HCOOCH ₃
SO	5 ₄ -4 ₃	206176.013	3.78	38.6	206177.5	6.8	31.82	
SO	8 ₇ -7 ₇	214357.054	0.19	81.2	214359.9	5.0	6.95	CH ₃ OCH ₃ , ¹³ CH ₃ CN CH ₃ CH ₂ CN ν_{13}/ν_{21}
SO	5 ₅ -4 ₄	215220.650	4.80	44.1	215223.6	4.9	33.22	
SO	5 ₆ -4 ₅	219949.389	5.95	35.0	219951.1	6.7	38.65	
SO	2 ₁ -1 ₂	236452.293	0.012	15.8	236455.1	5.4	1.02	H ₂ C ³⁴ S
SO	3 ₂ -2 ₃	246404.588	0.012	21.1	246406.9	6.2	1.62	³³ SO
SO	6 ₅ -5 ₄	251825.759	4.84	50.7	two peaks 251826.5 251829.5	8.1 4.6	35.11 35.11	CH ₃ OH
SO	9 ₈ -8 ₈	254573.628	0.16	99.7	two peaks 254571.5 254577.4	11.5 4.6	6.30 8.92	HCOOCH ₃
SO	6 ₆ -5 ₅	258255.826	5.83	56.5	258255.2	9.7	25.94	
SO	6 ₇ -5 ₆	261843.705	6.95	47.6	two peaks 261844.5 261849.5	9.0 2.4	40.10 41.06	
SO	4 ₃ -3 ₄	267197.745	0.0095	28.7	267202.5	3.7	4.47	HCN $\nu_2=1$
³⁴ SO	2 ₂ -1 ₁	84410.684	1.50	19.2	84411.4	6.5	0.96	
³⁴ SO	5 ₄ -4 ₄	96781.825	0.36	38.1	96783.4	4.1	0.27	
³⁴ SO	2 ₃ -1 ₂	97715.405	2.93	9.1	97716.3	6.3	2.93	HCOOCH ₃
³⁴ SO	3 ₂ -2 ₁	106743.363	1.51	20.9	106744.4	6.1	2.17	H ₃₉ α
³⁴ SO	6 ₅ -5 ₅	132432.200	0.28	49.9	132437.5	-3.0	0.96	HCOOCH ₃
³⁴ SO	3 ₄ -2 ₃	135775.651	3.94	15.6	135777.4	5.1	6.29	
³⁴ SO	4 ₃ -3 ₂	155506.801	2.69	28.4	155508.7	5.3	5.11	
³⁴ SO	4 ₄ -3 ₃	168815.109	3.75	33.4	168817.5	4.8	6.01	
³⁴ SO	7 ₆ -6 ₆	169787.430	0.22	63.8	169791.6	1.6	0.77	NH ₂ CHO
³⁴ SO	4 ₅ -3 ₄	175352.753	4.94	24.0	175354.9	5.3	10.3	
³⁴ SO	5 ₄ -4 ₃	201846.655	3.78	38.1	201849.3	5.1	6.35	
³⁴ SO	8 ₇ -7 ₇	208292.093	0.19	79.9	208297.1	1.8	0.46	
³⁴ SO	5 ₅ -4 ₄	211013.019	4.80	43.5	211015.7	5.2	12.1	
³⁴ SO	5 ₆ -4 ₅	215839.916	5.95	34.4	215842.2	5.8	13.4	CH ₃ CH ₂ CN ν_{13}/ν_{21} HCOOCH ₃ $\nu_t=1$
³⁴ SO	2 ₁ -1 ₂	237107.766	0.01	15.8	237112.6	2.9	0.25	U line
³⁴ SO	3 ₂ -2 ₃	246135.724	0.01	20.9	246137.8	6.5	0.07	CH ₃ CH ₂ ¹³ CN
³⁴ SO	6 ₅ -5 ₄	246663.394	4.83	49.9	246666.3	5.5	10.9	
³⁴ SO	9 ₈ -8 ₈	247598.441	0.16	98.0	247598.5	8.9	0.62	(CH ₃) ₂ CO
³⁴ SO	6 ₆ -5 ₅	253207.017	5.83	55.7	253210.3	5.1	11.8	CH ₃ OH
³⁴ SO	6 ₇ -5 ₆	256877.810	6.95	46.7	256880.2	6.2	15.5	
³⁴ SO	4 ₃ -3 ₄	265866.874	0.01	28.4	265884.5	-10.9	34.8	HCN
³³ SO	2 ₂ -1 ₁	85225.608	1.50	19.3	85224.3	13.6	0.06	
³³ SO	5 ₄ -4 ₄	98350.735	0.36	38.3	98353.5	0.6	<0.02	
³³ SO	2 ₃ -1 ₂	98483.142	2.93	9.2	98484.3	5.5	0.18	U
³³ SO	3 ₂ -2 ₁	107956.681	1.51	21.0	107955.2	13.1	0.20	(CH ₃) ₂ CO
³³ SO	6 ₅ -5 ₅	134463.407	0.28	50.3	CH ₃ CH ₂ CN ($\nu=0$ and ν_{13}/ν_{21})
³³ SO	3 ₄ -2 ₃	136939.179	3.94	15.7	136941.4	4.1	0.70	HC ₃ N $\nu_5+\nu_7$
³³ SO	4 ₃ -3 ₂	157183.674	2.69	28.5	CH ₃ OH
³³ SO	4 ₄ -3 ₃	170444.835	3.75	33.6	CH ₃ CH ₂ CN

Table A.8. continued.

Species	Transition $N_J-N'_J$	Predicted freq. (MHz)	S_{ij}	E_u (K)	Observed freq. (MHz)	Observed v_{LSR} (km s ⁻¹)	Observed T_A^* (K)	Blended with
³³ SO	7 ₆ -6 ₆	172273.415	0.22	64.4	172267.6	19.1	0.64	U line
³³ SO	4 ₅ -3 ₄	176927.358	4.94	24.2	176926.4	10.6	2.15	
					176932.5	0.5	2.66	
³³ SO	5 ₄ -4 ₃	203942.465	3.78	38.3	203940.6	11.7	2.74	H ₂ CCO
³³ SO	8 ₇ -7 ₇	211225.385	1.87	80.5	H ₂ CO
³³ SO	5 ₅ -4 ₄	213050.062	4.80	43.8	213052.3	5.9	2.09	SO ₂ , H ₂ ¹³ CO
³³ SO	5 ₆ -4 ₅	217829.254	5.95	34.7	217834.6	1.6	3.23	SiS
³³ SO	2 ₁ -1 ₂	236786.517	0.01	15.8	
³³ SO	3 ₂ -2 ₃	246260.056	0.01	21.0	CH ₃ CH ₂ CN
³³ SO	6 ₅ -5 ₄	249162.733	4.83	50.3	249162.5	9.3	4.05	CH ₃ CH ₂ CN $v_{20}=1$
³³ SO	9 ₈ -8 ₈	250972.610	0.16	98.8	CH ₃ OH
³³ SO	6 ₆ -5 ₅	255651.300	5.83	56.1	255654.1	5.7	3.71	H ¹³ CCCN
³³ SO	6 ₇ -5 ₆	259281.738	6.95	47.1	259286.5	3.5	4.16	CH ₃ OH
³³ SO	4 ₃ -3 ₄	266504.551	0.01	28.5	266510.4	2.4	0.18	
¹⁸ O	5 ₄ -4 ₄	87876.593	0.36	36.6	87877.5	5.9	0.03	(CH ₃) ₂ CO
¹⁸ O	2 ₃ -1 ₂	93267.376	2.94	8.7	93268.5	5.4	0.17	(CH ₃) ₂ CO
¹⁸ O	3 ₂ -2 ₁	99803.663	1.51	20.5	99804.5	6.5	0.07	HCCCN $v_6=1$
¹⁸ O	4 ₃ -3 ₂	145874.497	2.69	27.5	CH ₃ CH ₂ CN v_{13}/v_{21}
¹⁸ O	7 ₆ -6 ₆	155591.913	0.23	60.9	CH ₃ CH ₂ CN v_{13}/v_{21}
¹⁸ O	4 ₄ -3 ₃	159428.315	3.75	32.4	159429.9	6.0	0.54	
¹⁸ O	4 ₅ -3 ₄	166285.312	4.95	22.9	166286.7	6.5	0.52	
¹⁸ O	5 ₅ -4 ₄	199280.161	4.80	42.0	199283.5	4.0	0.68	HC ¹³ CCN
¹⁸ O	5 ₆ -4 ₅	204387.945	5.95	32.7	SO ₂
¹⁸ O	9 ₈ -8 ₈	228271.646	0.16	93.1	228271.3	9.5	0.21	HCOOCH ₃
¹⁸ O	6 ₅ -5 ₄	232265.872	4.83	47.8	232267.3	7.2	0.64	HCOOCH ₃
¹⁸ O	2 ₁ -1 ₂	239102.492	0.11	15.7	CH ₃ CN
¹⁸ O	6 ₆ -5 ₅	239128.519	5.83	53.4	CH ₃ CN
¹⁸ O	6 ₇ -5 ₆	243039.305	6.95	44.4	243042.5	5.1	1.34	CH ₂ DCN
¹⁸ O	3 ₂ -2 ₃	245638.780	0.01	20.5	245641.5	5.7	0.24	
¹⁸ O	4 ₃ -3 ₄	262447.093	0.01	27.5	262448.5	7.4	0.12	HCOO ¹³ CH ₃
¹⁸ O	10 ₉ -9 ₉	265637.956	0.01	112.1	265642.6	3.8	0.08	
¹⁸ O	7 ₆ -6 ₅	273858.128	5.87	60.9	273861.3	5.5	0.85	HCOOCH ₃
¹⁸ O	7 ₇ -6 ₆	278972.690	6.86	66.8	278976.6	4.8	1.02	CH ₃ OH

Notes. Emission lines of SO and its isotopologues in the frequency range of the 30-m Orion KL survey. Column 1 indicates the species, Col.2 the quantum numbers of the line transition, Col. 3 gives the assumed rest frequencies, Col. 4 the line strength, Col. 5 the energy of the upper level, Col. 6 observed frequency assuming a v_{LSR} of 9.0 km s⁻¹, Col. 7 the observed radial velocities, Col. 8 the peak line antenna temperature, and Col. 9 the blended species.

Table A.9. Observed lines of SO₂, its isotopologues, and vibrationally excited states.

Species/Transition $J_{K_a,K_c} - J'_{K'_a,K'_c}$	Predicted freq. (MHz)	S_{ij}	E_u (K)	Observed freq. (MHz)	Observed v_{LSR} (km s ⁻¹)	Observed T_A^* (K)
SO ₂ 34 _{8,26} -35 _{7,29}	82409.542	5.20	704.4	82410.5	5.5	0.08
SO ₂ 13 _{4,10} -14 _{3,11}	82951.936	1.93	123.0	82952.5	7.0	2.18
SO ₂ 8 _{1,7} -8 _{0,8}	83688.092	6.38	36.7	83688.5	7.5	11.0
SO ₂ 32 _{5,27} -31 _{6,26}	84320.877	5.05	549.4	84321.5	6.8	0.25
SO ₂ 43 _{7,37} -42 _{8,34}	85247.002	6.77	992.8	85248.5	3.7	0.03
SO ₂ 39 _{9,31} -40 _{8,32}	86153.761	5.97	916.2	¹
SO ₂ 8 _{3,5} -9 _{2,8}	86639.090	1.13	55.2	86639.4	7.9	2.65
SO ₂ 20 _{2,18} -21 _{1,21}	86828.940	0.27	207.8	86830.4 ²	4.0	0.25
SO ₂ 32 _{5,29} -32 _{6,26}	87926.274	5.16	579.2	³
SO ₂ 44 _{10,34} -45 _{9,37}	90005.126	6.73	1155.7	90005.5	7.8	0.02
SO ₂ 25 _{3,23} -24 _{4,20}	90548.146	3.26	320.9	90549.5	4.5	1.16
SO ₂ 18 _{5,13} -19 _{4,16}	91550.440	2.69	218.7	91551.5 ⁴	5.5	2.55
SO ₂ 23 _{6,18} -24 _{5,19}	94064.694	3.46	342.2	94065.5	6.4	0.81
SO ₂ 38 _{6,32} -37 _{7,31}	97466.369	6.00	772.6	97467.6	5.2	0.09
SO ₂ 7 _{3,5} -8 _{2,6}	97702.334	0.94	47.8	97703.5 ^{5,6}	5.4	3.61
SO ₂ 33 _{3,31} -32 _{4,28}	97994.088	2.01	535.8	97996.5 ⁷	1.6	0.24
SO ₂ 28 _{7,21} -29 _{6,24}	98976.292	4.23	493.7	98977.5	5.3	0.43
SO ₂ 29 _{4,26} -28 _{5,23}	99392.512	4.37	440.7	99393.5	6.0	0.76
SO ₂ 2 _{2,0} -3 _{1,3}	100878.107	0.16	12.6	100878.5	7.8	1.21
SO ₂ 33 _{8,26} -34 _{7,27}	102690.061	4.99	673.0	102690.4	8.0	0.15
SO ₂ 49 _{8,42} -48 _{9,39}	102707.256	7.73	1286.5	102708.6	5.1	0.02
SO ₂ 3 _{1,3} -2 _{0,2}	104029.419	2.01	7.7	104030.0	7.3	12.5
SO ₂ 16 _{2,14} -15 _{3,13}	104033.582	2.99	137.5	⁸
SO ₂ 10 _{1,9} -10 _{0,10}	104239.299	6.70	54.7	104239.5 ^{5,6}	8.4	14.0
SO ₂ 38 _{9,29} -39 _{8,32}	106674.825	5.76	880.2	106676.5 ⁹	4.3	0.13
SO ₂ 27 _{3,25} -26 _{4,22}	107060.210	3.10	369.4	107061.5 ¹⁰	5.4	1.38
SO ₂ 12 _{2,8} -13 _{3,11}	107843.470	1.70	111.0	107844.5	6.1	3.98
SO ₂ 42 _{4,38} -43 _{3,41}	108915.425	0.76	887.0	¹¹
SO ₂ 39 _{6,34} -38 _{7,31}	108955.919	6.14	808.3	108956.6	7.1	0.08
SO ₂ 17 _{5,13} -18 _{4,14}	109757.585	2.48	202.1	109758.5 ^{1,12}	6.5	2.78
SO ₂ 43 _{10,34} -44 _{9,35}	110363.835	6.52	1115.1	¹³
SO ₂ 31 _{3,29} -30 _{4,26}	111755.021	2.42	476.9	111756.4	5.3	0.49
SO ₂ 44 _{7,37} -43 _{8,36}	111875.546	6.95	1033.8	111876.6	6.2	0.04
SO ₂ 29 _{3,27} -28 _{4,24}	114565.369	2.81	421.4	114566.5	6.0	0.75
SO ₂ 22 _{6,16} -23 _{5,19}	115317.555	3.24	321.1	115318.5	6.5	1.25
SO ₂ 42 _{10,32} -43 _{9,35}	130679.975	6.31	1075.5	130680.5	7.8	0.04
SO ₂ 31 _{4,28} -30 _{5,25}	130859.427	4.49	497.0	130860.5	6.5	0.84
SO ₂ 12 _{1,11} -12 _{0,12}	131014.841	6.64	76.4	131015.5	7.5	12.7
SO ₂ 16 _{5,11} -17 _{4,14}	131274.861	2.26	186.4	131276.4	5.5	2.89
SO ₂ 14 _{2,12} -14 _{1,13}	132744.832	11.7	108.1	132745.5	7.5	18.1
SO ₂ 8 _{2,6} -8 _{1,7}	134004.812	5.69	43.1	134005.5	7.5	17.1
SO ₂ 47 _{11,37} -48 _{10,38}	134203.832	7.08	1333.6	134205.2	5.9	0.06
SO ₂ 21 _{6,16} -22 _{5,17}	134943.290	3.03	300.8	134944.5	6.3	1.69
SO ₂ 5 _{1,5} -4 _{0,4}	135696.017	3.13	15.7	135696.5	7.9	17.3
SO ₂ 34 _{5,29} -33 _{6,28}	135963.028	5.41	612.0	135964.5	5.8	0.50
SO ₂ 5 _{3,3} -6 _{2,4}	139355.030	0.50	35.9	139356.4	6.1	5.14
SO ₂ 26 _{7,19} -27 _{6,22}	139474.500	3.80	443.0	139476.3	5.1	1.29
SO ₂ 6 _{2,4} -6 _{1,5}	140306.166	3.83	29.2	140307.0	7.2	14.4
SO ₂ 16 _{2,14} -16 _{1,15}	143057.080	13.0	137.5	143058.8	5.4	15.4
SO ₂ 31 _{8,24} -32 _{7,25}	143357.818	4.57	613.1	143358.9 ⁴	6.7	4.27
SO ₂ 51 _{8,44} -50 _{9,41}	145970.266	8.08	1380.0	¹⁴
SO ₂ 40 _{6,34} -39 _{7,33}	146393.711	6.35	846.1	146396.4 ⁷	3.5	0.18
SO ₂ 10 _{4,6} -11 _{3,9}	146550.044	1.27	89.8	146551.3	6.4	4.02
SO ₂ 4 _{2,2} -4 _{1,3}	146605.519	2.27	19.0	146606.5	7.0	10.9
SO ₂ 36 _{9,27} -37 _{8,30}	147239.288	5.34	811.1	147240.2	7.1	0.14
SO ₂ 15 _{5,11} -16 _{4,12}	150381.071	2.04	171.7	150382.6	6.0	3.61
SO ₂ 41 _{6,36} -40 _{7,33}	150486.942	6.45	883.4	¹⁵

Table A.9. continued.

Species/Transition $J_{K_a,K_c} - J'_{K'_a,K'_c}$	Predicted freq. (MHz)	S_{ij}	E_u (K)	Observed freq. (MHz)	Observed v_{LSR} (km s ⁻¹)	Observed T_A^* (K)
SO ₂ 41 _{10,32} -42 _{9,33}	150878.808	6.10	1036.8	¹⁶
SO ₂ 2 _{2,0} -2 _{1,1}	151378.663	0.87	12.6	151380.1	6.2	7.98
SO ₂ 43 _{4,40} -42 _{5,37}	153677.158	2.50	909.7	⁵
SO ₂ 46 _{11,35} -47 _{10,38}	154373.328	6.87	1290.3	154367.6 ¹⁷	20.1	0.09
SO ₂ 20 _{6,14} -21 _{5,17}	155389.625	2.81	281.4	155391.4	5.6	3.29
SO ₂ 33 _{4,30} -32 _{5,27}	157135.255	4.47	556.9	157137.7	4.3	1.00
SO ₂ 3 _{2,2} -3 _{1,3}	158199.781	1.44	15.3	158201.4	5.9	13.4
SO ₂ 46 _{7,39} -45 _{8,38}	158845.079	7.30	1118.3	158846.5 ¹⁸	6.3	0.17
SO ₂ 25 _{7,19} -26 _{6,20}	159447.934	3.58	419.1	159450.1	4.9	1.56
SO ₂ 18 _{2,16} -18 _{1,17}	160342.971	13.6	170.8	160343.9	7.3	16.4
SO ₂ 4 _{3,1} -5 _{2,4}	160543.024	0.30	31.3	160543.6	7.9	3.96
SO ₂ 10 _{0,10} -9 _{1,9}	160827.841	6.43	49.7	160828.5	7.8	26.3
SO ₂ 18 _{2,16} -17 _{3,15}	163119.379	3.72	170.8	163121.4	5.3	11.1
SO ₂ 30 _{8,22} -31 _{7,25}	163567.675	4.35	584.6	163569.5	5.7	0.73
SO ₂ 14 _{1,13} -14 _{0,14}	163605.533	6.41	101.8	163606.5	7.2	18.5
SO ₂ 37 _{5,33} -36 _{6,30}	163924.734	5.63	710.8	⁵
SO ₂ 9 _{4,6} -10 _{3,7}	165123.634	1.05	80.6	165125.2	6.2	7.24
SO ₂ 5 _{2,4} -5 _{1,5}	165144.652	2.46	23.6	165145.7	7.1	17.7
SO ₂ 7 _{1,7} -6 _{0,6}	165225.452	4.43	27.1	165226.4	7.3	25.3
SO ₂ 44 _{4,40} -45 _{3,43}	166387.129	0.66	969.1	¹
SO ₂ 35 _{9,27} -36 _{8,28}	167367.348	5.12	777.9	167368.9	6.2	0.27
SO ₂ 24 _{2,22} -25 _{1,25}	168790.063	0.18	292.8	^{1,5}
SO ₂ 34 _{3,31} -35 _{2,34}	170293.819	0.41	581.9	⁴
SO ₂ 14 _{5,9} -15 _{4,12}	170754.546	1.82	157.9	170756.5	5.6	4.99
SO ₂ 40 _{10,30} -41 _{9,33}	171018.058	5.89	999.0	⁴
SO ₂ 47 _{7,41} -46 _{8,38}	171036.705	7.43	1161.5	171038.9 ^{5,19}	5.2	0.29
SO ₂ 19 _{6,14} -20 _{5,15}	175101.318	2.59	263.0	175103.9	4.6	4.34
SO ₂ 7 _{2,6} -7 _{1,7}	175275.722	3.30	35.5	175277.6	5.8	18.2
SO ₂ 41 _{4,38} -40 _{5,35}	176295.902	3.01	832.2	176297.6 ⁵	6.1	0.43
SO ₂ 35 _{4,32} -34 _{5,29}	176466.255	4.30	620.4	176468.9	4.5	1.42
SO ₂ 20 _{3,17} -20 _{2,18}	197142.060	15.4	217.2	197144.9 ⁴	4.7	14.4
SO ₂ 39 _{5,35} -38 _{6,32}	197585.319	5.74	782.1	⁴
SO ₂ 49 _{12,38} -50 _{11,39}	197709.365	7.21	1478.6	197711.0 ⁶	6.5	0.10
SO ₂ 42 _{6,36} -41 _{7,35}	198847.847	6.67	923.6	⁶
SO ₂ 23 _{7,17} -24 _{6,18}	199415.871	3.15	373.9	199418.6	4.9	2.25
SO ₂ 24 _{3,21} -24 _{2,22}	200287.422	19.4	302.4	200289.9	5.3	8.35
SO ₂ 16 _{1,15} -16 _{0,16}	200809.321	6.17	130.7	200811.2	6.2	11.4
SO ₂ 12 _{0,12} -11 _{1,11}	203391.484	8.43	70.1	203391.9	8.4	17.5
SO ₂ 28 _{8,20} -29 _{7,23}	203570.093	3.92	530.2	203570.6 ⁷	8.3	2.02
SO ₂ 18 _{3,15} -18 _{2,16}	204246.762	13.0	180.6	204249.4	5.1	13.9
SO ₂ 7 _{4,4} -8 _{3,5}	204384.191	0.63	65.0	204387.0 ²¹	4.9	5.43
SO ₂ 11 _{2,10} -11 _{1,11}	205300.539	4.55	70.2	205302.3	6.4	17.7
SO ₂ 33 _{9,25} -34 _{8,26}	207421.450	4.69	714.3	^{5,6}
SO ₂ 48 _{7,41} -47 _{8,40}	208302.827	7.63	1206.7	²
SO ₂ 3 _{2,2} -2 _{1,1}	208700.337	1.67	15.3	two peaks: 208692.4 208702.4	20.4 6.0	10.3 16.5
SO ₂ 53 _{5,49} -52 _{6,46}	209874.382	2.96	1381.3	⁵
SO ₂ 12 _{5,7} -13 _{4,10}	209936.041	1.39	133.0	209938.7	5.2	5.51
SO ₂ 38 _{10,28} -39 _{9,31}	211053.096	5.46	926.3	211054.6	6.9	0.08
SO ₂ 26 _{3,23} -26 _{2,24}	213068.427	20.4	350.8	213071.1 ²²	5.2	11.0
SO ₂ 49 _{7,43} -48 _{8,40}	213703.045	7.72	1251.5	⁵
SO ₂ 43 _{11,33} -44 _{10,34}	214451.816	6.23	1166.0	214454.9 ¹⁷	4.7	0.11
SO ₂ 16 _{3,13} -16 _{2,14}	214689.395	10.6	147.8	214692.3	4.9	13.6
SO ₂ 17 _{6,12} -18 _{5,13}	214728.280	2.16	229.0	214731.2	4.9	4.52
SO ₂ 26 _{2,24} -27 _{1,27}	215094.516	0.15	340.6	⁴
SO ₂ 22 _{2,20} -22 _{1,21}	216643.304	13.2	248.5	two peaks:

Table A.9. continued.

Species/Transition $J_{K_a, K_c} - J'_{K'_a, K'_c}$	Predicted freq. (MHz)	S_{ij}	E_u (K)	Observed freq. (MHz)	Observed v_{LSR} (km s ⁻¹)	Observed T_A^* (K)
				216636.1	19.0	4.49
				216646.1	5.1	10.3
SO ₂ 22 _{7,15} -23 _{6,18}	219275.970	2.93	352.8	219278.6	5.4	3.05
SO ₂ 11 _{1,11} -10 _{0,10}	221965.221	7.71	60.4	221967.4	6.1	44.2
SO ₂ 36 _{3,33} -37 _{2,36}	222869.135	0.36	648.6	222871.2	6.2	0.09
SO ₂ 27 _{8,20} -28 _{7,21}	223434.487	3.70	504.4	223436.4	6.4	1.29
SO ₂ 6 _{4,2} -7 _{3,5}	223883.568	0.43	58.6	223886.2	5.5	5.57
SO ₂ 20 _{2,18} -19 _{3,17}	224264.815	4.62	207.8	224267.3	5.7	12.7
SO ₂ 46 _{4,42} -47 _{3,45}	224473.442	0.59	1054.6	⁴
SO ₂ 13 _{2,12} -13 _{1,13}	225153.705	4.97	93.0	two peaks:
				225146.2	19.0	8.47
				225156.1	5.8	16.2
SO ₂ 14 _{3,11} -14 _{2,12}	226300.028	8.61	119.0	226302.2	6.1	21.6
SO ₂ 41 _{5,37} -40 _{6,34}	226508.309	5.72	857.0	226509.9	6.9	0.36
SO ₂ 32 _{9,23} -33 _{8,26}	227335.786	4.47	684.0	227337.4	6.9	0.74
SO ₂ 11 _{5,7} -12 _{4,8}	229347.627	1.17	122.0	229349.9	6.0	3.10
SO ₂ 45 _{6,40} -44 _{7,37}	229749.763	6.89	1044.8	¹⁶
SO ₂ 37 _{10,28} -38 _{9,29}	230965.232	5.24	891.3	230968.5	4.8	0.15
SO ₂ 28 _{3,25} -28 _{2,26}	234187.057	20.7	403.1	two peaks:
				234185.5	11.0	1.95
				234189.5	5.9	2.33
SO ₂ 42 _{11,31} -43 _{10,34}	234352.997	6.01	1126.4	234357.6 ¹⁷	3.1	0.31
SO ₂ 16 _{6,10} -17 _{5,13}	234421.582	1.94	213.3	234426.3 ⁴	3.0	6.75
SO ₂ 4 _{2,2} -3 _{1,3}	235151.721	1.71	19.0	two peaks:
				235144.5	18.2	8.85
				235153.5	6.7	15.4
SO ₂ 16 _{1,15} -15 _{2,14}	236216.688	6.05	130.7	236219.0 ²³	6.1	12.6
SO ₂ 12 _{3,9} -12 _{2,10}	237068.834	6.90	94.0	two peaks:
				237061.0	18.9	8.51
				237071.5	5.6	14.1
SO ₂ 47 _{12,36} -48 _{11,37}	237501.891	6.78	1389.2	⁶
SO ₂ 17 _{3,15} -18 _{0,18}	238166.384	0.12	162.9	238169.5	5.1	0.55
SO ₂ 21 _{7,15} -22 _{6,16}	238992.525	2.71	332.5	two peaks:
				238989.5	12.8	1.79
				238995.5	5.3	3.53
SO ₂ 15 _{3,13} -16 _{0,16}	239832.819	0.10	132.5	²⁴
SO ₂ 18 _{1,17} -18 _{0,18}	240942.792	5.99	163.1	two peaks:
				240940.0	12.5	10.3
				240946.1	4.9	11.5
SO ₂ 51 _{5,47} -50 _{6,44}	241044.688	3.54	1285.2	¹⁶
SO ₂ 5 _{2,4} -4 _{1,3}	241615.798	2.12	23.6	two peaks:
				241608.0	18.7	12.9
				241620.5 ^{3,4}	3.2	20.3
SO ₂ 19 _{3,17} -20 _{0,20}	242997.814	0.13	197.0	243000.5	5.7	1.06
SO ₂ 5 _{4,2} -6 _{3,3}	243087.646	0.25	53.1	243090.2	5.9	2.91
SO ₂ 26 _{8,18} -27 _{7,21}	243245.422	3.48	479.6	243248.9	4.7	1.01
SO ₂ 14 _{0,14} -13 _{1,13}	244254.220	10.5	93.9	two peaks:
				244245.2	20.1	15.3
				244256.4	6.3	24.6
SO ₂ 26 _{3,23} -25 _{4,22}	245339.234	4.86	350.8	245342.6	4.9	6.56
SO ₂ 10 _{3,7} -10 _{2,8}	245563.423	5.44	72.7	245565.5	6.5	18.6
SO ₂ 31 _{9,23} -32 _{8,24}	247169.754	4.25	654.5	^{16,25}
SO ₂ 15 _{2,14} -15 _{1,15}	248057.403	5.27	119.3	248060.1	5.7	18.2
SO ₂ 13 _{3,11} -14 _{0,14}	248436.938	0.74	105.8	248440.2 ^{4,21}	5.1	2.44
SO ₂ 10 _{5,5} -11 _{4,8}	248830.822	0.96	111.9	248833.5	5.8	8.35
SO ₂ 43 _{5,39} -42 _{6,36}	248995.137	5.54	935.6	248997.5	6.2	0.45
SO ₂ 36 _{10,26} -37 _{9,29}	250816.770	5.03	857.2	^{26,27}
SO ₂ 13 _{1,13} -12 _{0,12}	251199.676	9.63	82.2	251201.3	7.1	29.9

Table A.9. continued.

Species/Transition $J_{K_a, K_c} - J'_{K'_a, K'_c}$	Predicted freq. (MHz)	S_{ij}	E_u (K)	Observed freq. (MHz)	Observed v_{LSR} (km s ⁻¹)	Observed T_A^* (K)
SO ₂ 8 _{3,5} -8 _{2,6}	251210.586	4.14	55.2	⁸
SO ₂ 32 _{4,28} -31 _{5,27}	252563.897	5.37	531.1	252566.4	6.0	2.03
SO ₂ 21 _{3,19} -22 _{0,22}	253753.446	0.14	234.7	253757.4 ¹⁶	4.3	12.8
SO ₂ 38 _{5,33} -37 _{6,32}	253935.893	6.11	749.1	253940.0 ²³	4.2	3.63
SO ₂ 15 _{6,10} -16 _{5,11}	253956.563	1.72	198.6	253959.6	5.4	6.22
SO ₂ 41 _{11,31} -42 _{10,32}	254194.858	5.80	1087.7	²⁸
SO ₂ 6 _{3,3} -6 _{2,4}	254280.537	2.89	41.4	254282.7 ²³	6.5	28.1
SO ₂ 24 _{2,22} -24 _{1,23}	254283.322	12.7	292.8	⁸
SO ₂ 4 _{3,1} -4 _{2,2}	255553.303	1.61	31.3	255554.5	7.6	17.5
SO ₂ 51 _{7,45} -50 _{8,42}	255595.369	7.97	1345.2	²⁹
SO ₂ 44 _{6,38} -43 _{7,37}	255818.422	6.99	1005.1	255819.5	7.7	0.21
SO ₂ 3 _{3,1} -3 _{2,2}	255958.045	0.89	27.6	255959.6	7.2	13.8
SO ₂ 5 _{3,3} -5 _{2,4}	256246.946	2.26	35.9	256248.3	7.4	19.6
SO ₂ 7 _{3,5} -7 _{2,6}	257099.967	3.48	47.8	257101.3	7.4	31.2
SO ₂ 46 _{12,34} -47 _{11,37}	257318.855	6.57	1346.0	⁴
SO ₂ 32 _{4,28} -32 _{3,29}	258388.714	25.5	531.1	258391.4	5.9	2.08
SO ₂ 20 _{7,13} -21 _{6,16}	258666.959	2.49	313.2	258669.5	6.1	1.57
SO ₂ 9 _{3,7} -9 _{2,8}	258942.200	4.65	63.5	258943.4	7.6	9.56
SO ₂ 30 _{4,26} -30 _{3,27}	259599.446	23.3	471.5	259602.5	5.5	3.25
SO ₂ 49 _{5,45} -48 _{6,42}	260269.339	4.15	1192.5	⁶
SO ₂ 50 _{7,43} -49 _{8,42}	261062.785	7.93	1299.0	¹⁶
SO ₂ 27 _{4,24} -28 _{1,27}	261091.176	0.31	388.0	261096.4 ⁵	3.0	0.89
SO ₂ 11 _{3,9} -11 _{2,10}	262256.907	5.78	82.8	262258.9	6.7	26.1
SO ₂ 4 _{4,0} -5 _{3,3}	262333.965	0.10	48.5	262341.4	0.5	2.17
SO ₂ 28 _{2,26} -29 _{1,29}	262524.931	0.13	391.8	262528.8 ³⁰	4.6	0.27
SO ₂ 25 _{8,18} -26 _{7,19}	262969.717	3.26	455.6	262972.5	5.8	1.09
SO ₂ 45 _{5,41} -44 _{6,38}	263216.484	5.21	1017.7	263218.9	6.3	0.20
SO ₂ 30 _{3,27} -30 _{2,28}	263543.954	20.3	459.1	263546.4 ¹²	6.2	3.99
SO ₂ 25 _{4,22} -26 _{1,25}	263897.868	0.28	339.0	263900.5	6.0	0.35
SO ₂ 11 _{3,9} -12 _{0,12}	264165.962	0.04	82.8	264171.5	2.7	1.18
SO ₂ 29 _{4,26} -30 _{1,29}	265461.469	0.33	440.7	265465.1 ²⁵	4.9	0.54
SO ₂ 34 _{4,30} -34 _{3,31}	265481.970	27.1	594.7	265485.1 ^{4,23}	5.5	1.93
SO ₂ 47 _{6,42} -46 _{7,39}	265608.359	6.99	1131.1	265610.6	6.5	0.20
SO ₂ 30 _{9,21} -31 _{8,24}	266943.308	4.04	625.9	266944.5 ³²	7.7	1.05
SO ₂ 47 _{5,43} -46 _{6,40}	267428.351	4.73	1103.4	267433.8 ¹⁰	2.9	0.11
SO ₂ 13 _{3,11} -13 _{2,12}	267537.453	6.87	105.8	267538.5	7.8	13.1
SO ₂ 28 _{4,24} -28 _{3,25}	267719.839	20.6	415.9	267723.5	4.9	4.24
SO ₂ 9 _{5,5} -10 _{4,6}	268168.331	0.76	102.7	two peaks: 268165.1 268171.4	12.6 5.6	2.75 4.36
SO ₂ 23 _{3,21} -24 _{0,24}	269786.414	0.14	276.0	269789.5	5.6	0.78
SO ₂ 35 _{10,26} -36 _{9,27}	270605.490	4.81	824.1	270608.5	5.7	0.24
SO ₂ 7 _{2,6} -6 _{1,5}	271529.016	2.67	35.5	271530.1	7.8	24.5
SO ₂ 37 _{5,33} -38 _{2,36}	271726.167	0.53	710.8	³³
SO ₂ 14 _{6,8} -15 _{5,11}	273462.663	1.51	184.8	273466.4	4.9	3.12
SO ₂ 17 _{2,16} -17 _{1,17}	273752.962	5.48	149.2	two peaks: 273744.5 273754.5	18.3 7.3	5.64 8.77
SO ₂ 40 _{11,29} -41 _{10,32}	273982.611	5.58	1050.0	273981.5 ⁴	10.2	0.51
SO ₂ 47 _{6,42} -48 _{3,45}	274075.204	0.79	1131.1	³⁴
SO ₂ 35 _{5,31} -36 _{2,34}	274521.579	0.49	643.1	274522.6 ^{6,35}	7.9	3.12
SO ₂ 23 _{4,20} -24 _{1,23}	274525.462	0.23	293.7	⁸
SO ₂ 15 _{3,13} -15 _{2,14}	275240.185	7.88	132.5	275242.6	6.4	21.6
SO ₂ 38 _{3,35} -39 _{2,38}	275375.696	0.32	718.7	^{7,13}
SO ₂ 31 _{4,28} -32 _{1,31}	276254.571	0.33	497.0	276257.6	5.7	0.70
SO ₂ 45 _{6,40} -46 _{3,43}	276301.223	0.74	1044.8	¹
SO ₂ 39 _{5,35} -40 _{2,38}	276558.354	0.56	782.1	^{12,36}

Table A.9. continued.

Species/Transition $J_{K_a,K_c} - J'_{K'_a,K'_c}$	Predicted freq. (MHz)	S_{ij}	E_u (K)	Observed freq. (MHz)	Observed v_{LSR} (km s ⁻¹)	Observed T_A^* (K)
SO ₂ 39 _{5,35} -40 _{2,38}	276558.354	0.56	782.1	^{12,36}
SO ₂ 45 _{12,34} -46 _{11,35}	277085.908	6.35	1303.6	^{9,37}
SO ₂ 19 _{7,13} -20 _{6,14}	278250.961	2.27	294.8	278255.1 ⁴	4.5	7.82
SO ₂ 49 _{6,44} -50 _{3,47}	279766.567	0.81	1221.0	¹⁷
SO ₂ 26 _{4,22} -26 _{3,23}	280807.245	18.0	364.3	280810.5 ³⁸	5.5	4.56
³⁴ SO ₂ 10 _{1,9} -9 _{2,8}	82124.347	2.45	54.6	82125.5	4.8	0.32
³⁴ SO ₂ 8 _{1,7} -8 _{0,8}	83043.821	6.26	36.6	83044.5	6.6	0.90
³⁴ SO ₂ 33 _{3,31} -32 _{4,28}	85972.412	1.74	533.7	85973.3 ⁷	5.9	0.07
³⁴ SO ₂ 7 _{3,5} -8 _{2,6}	88720.563	0.94	47.0	88721.5	5.8	0.16
³⁴ SO ₂ 30 _{3,27} -31 _{2,30}	89308.378	0.51	458.0	^{6,39}
³⁴ SO ₂ 26 _{4,22} -25 _{5,21}	92428.871	4.10	362.6	92427.5 ³²	13.4	0.33
³⁴ SO ₂ 17 _{5,18} -18 _{4,14}	93852.067	2.47	199.7	93854.5 ⁷	1.2	0.32
³⁴ SO ₂ 20 _{2,18} -21 _{1,21}	94250.841	0.25	207.2	94251.5 ^{40,41}	6.9	0.04
³⁴ SO ₂ 2 _{2,0} -3 _{1,3}	95810.413	0.16	12.2	95811.5	5.6	0.04
³⁴ SO ₂ 12 _{4,8} -13 _{3,11}	95922.816	1.70	109.5	95924.5	3.7	0.22
³⁴ SO ₂ 25 _{3,23} -24 _{4,20}	96075.299	3.10	319.5	^{5,42}
³⁴ SO ₂ 22 _{6,16} -23 _{5,19}	96193.856	3.24	317.6	96195.5	3.9	0.05
³⁴ SO ₂ 27 _{7,21} -28 _{6,22}	96204.065	4.01	463.1	96205.5	4.5	0.02
³⁴ SO ₂ 3 _{1,3} -2 _{0,2}	102031.880	2.02	7.6	102032.5	7.2	0.70
³⁴ SO ₂ 10 _{1,9} -10 _{0,10}	104391.706	6.52	54.6	104392.5	6.7	1.38
³⁴ SO ₂ 31 _{3,29} -30 _{4,26}	104914.698	2.14	475.0	104915.5	6.7	0.04
³⁴ SO ₂ 33 _{5,29} -32 _{6,26}	106374.262	5.10	576.3	^{4,36}
³⁴ SO ₂ 32 _{5,27} -31 _{6,26}	107567.843	5.02	546.7	⁴³
³⁴ SO ₂ 27 _{3,25} -26 _{4,22}	109260.509	2.89	367.9	⁴⁴
³⁴ SO ₂ 29 _{4,26} -28 _{5,23}	111902.795	4.27	438.6	111904.5	4.4	0.06
³⁴ SO ₂ 11 _{4,8} -12 _{3,9}	112532.318	1.49	98.5	112533.5	5.9	0.23
³⁴ SO ₂ 29 _{3,27} -28 _{4,24}	112577.899	2.55	419.7	112577.7 ¹⁷	9.5	0.02
³⁴ SO ₂ 6 _{3,3} -7 _{2,6}	114574.435	0.71	40.6	114576.5 ^{31,34}	3.6	0.29
³⁴ SO ₂ 16 _{2,14} -15 _{3,13}	115291.389	3.04	137.1	⁷
³⁴ SO ₂ 21 _{6,16} -22 _{5,17}	115722.150	3.03	297.4	115724.5	2.9	0.09
³⁴ SO ₂ 16 _{5,11} -17 _{4,14}	115744.668	2.26	184.1	115746.5	4.3	0.14
³⁴ SO ₂ 5 _{3,3} -6 _{2,4}	130584.304	0.50	35.1	130585.5	6.3	0.27
³⁴ SO ₂ 12 _{1,11} -12 _{0,12}	132114.053	6.41	76.2	132115.1	6.6	1.32
³⁴ SO ₂ 5 _{1,5} -4 _{0,4}	133471.429	3.14	15.5	133472.6	6.4	1.53
³⁴ SO ₂ 22 _{2,20} -23 _{1,23}	134417.591	0.19	247.8	⁴
³⁴ SO ₂ 10 _{4,6} -11 _{3,9}	134535.253	1.27	88.4	134538.5 ⁶	1.8	0.96
³⁴ SO ₂ 15 _{5,11} -16 _{4,12}	134703.279	2.04	169.4	134705.5 ⁶	4.1	0.57
³⁴ SO ₂ 6 _{2,4} -6 _{1,5}	134826.248	3.88	28.8	134827.5 ⁶	6.2	1.75
³⁴ SO ₂ 12 _{1,11} -11 _{2,10}	134873.798	3.46	76.2	134874.5	7.4	0.78
³⁴ SO ₂ 22 _{3,19} -21 _{4,18}	135566.286	3.71	256.9	135567.5	6.3	0.23
³⁴ SO ₂ 20 _{6,14} -21 _{5,17}	136343.660	2.81	278.0	136346.3	3.2	0.10
³⁴ SO ₂ 25 _{7,19} -26 _{6,20}	136847.952	3.58	414.4	136849.5	5.6	0.13
³⁴ SO ₂ 30 _{8,22} -31 _{7,25}	137520.630	4.35	578.4	¹⁷
³⁴ SO ₂ 4 _{2,2} -4 _{1,3}	141158.940	2.29	18.7	141160.2	6.3	1.31
³⁴ SO ₂ 31 _{4,28} -30 _{5,25}	141195.794	4.34	494.8	141198.7	2.8	0.08
³⁴ SO ₂ 16 _{2,14} -16 _{1,15}	141653.405	12.8	137.1	141653.5 ⁵	8.8	4.34
³⁴ SO ₂ 35 _{5,31} -34 _{6,28}	144436.662	5.34	640.1	144438.8	4.6	0.11
³⁴ SO ₂ 2 _{2,0} -2 _{1,1}	146020.420	0.87	12.2	146023.5 ^{5,36}	2.7	1.12
³⁴ SO ₂ 28 _{4,24} -27 _{5,23}	149209.906	4.50	414.3	149212.6 ¹	3.6	0.16
³⁴ SO ₂ 4 _{3,1} -5 _{2,4}	151917.559	0.30	30.5	151917.5 ³²	9.1	1.01
³⁴ SO ₂ 9 _{4,6} -10 _{3,7}	152953.645	1.05	79.2	152955.5 ⁶	5.4	0.93
³⁴ SO ₂ 3 _{2,2} -3 _{1,3}	153015.053	1.44	15.0	153016.4	6.4	0.94
³⁴ SO ₂ 14 _{5,9} -15 _{4,12}	155232.875	1.82	155.6	155235.0	4.9	0.39
³⁴ SO ₂ 19 _{6,14} -20 _{5,15}	156033.446	2.59	259.7	156035.2	5.6	0.55
³⁴ SO ₂ 24 _{7,17} -25 _{6,20}	157058.684	3.36	391.4	¹⁶

Table A.9. continued.

Species/Transition $J_{K_a, K_c} - J'_{K'_a, K'_c}$	Predicted freq. (MHz)	S_{ij}	E_u (K)	Observed freq. (MHz)	Observed v_{LSR} (km s ⁻¹)	Observed T_A^* (K)
³⁴ SO ₂ 29 _{8,22} -30 _{7,23}	157588.146	4.13	550.8	157590.5	4.5	0.11
³⁴ SO ₂ 5 _{2,4} -5 _{1,5}	160143.612	2.45	23.2	160142.6 ⁴⁵	10.9	2.60
³⁴ SO ₂ 18 _{2,16} -18 _{1,17}	160802.573	13.2	170.3	160804.5	5.4	2.13
³⁴ SO ₂ 34 _{5,29} -33 _{6,28}	161392.836	5.37	609.3	⁴
³⁴ SO ₂ 10 _{0,10} -9 _{1,9}	162020.378	6.52	49.5	162021.3	7.3	2.77
³⁴ SO ₂ 7 _{1,7} -6 _{0,6}	162775.882	4.45	26.9	162775.5 ⁵	9.7	5.90
³⁴ SO ₂ 33 _{4,30} -32 _{5,27}	164323.365	4.25	554.6	164324.0	7.8	0.09
³⁴ SO ₂ 14 _{1,13} -14 _{0,14}	165620.729	6.17	101.5	165622.5	5.8	1.88
³⁴ SO ₂ 3 _{3,1} -4 _{2,2}	170284.815	0.13	26.8	⁴
³⁴ SO ₂ 7 _{2,6} -7 _{1,7}	170546.952	3.29	35.1	170548.9 ⁶	5.6	2.29
³⁴ SO ₂ 8 _{4,4} -9 _{3,7}	173207.298	0.84	70.9	173210.2	4.0	0.63
³⁴ SO ₂ 13 _{5,9} -14 _{4,10}	174576.459	1.60	142.7	⁵
³⁴ SO ₂ 18 _{2,16} -17 _{3,15}	174850.251	3.81	170.3	174851.5 ^{5,46}	6.9	1.45
³⁴ SO ₂ 18 _{6,12} -19 _{5,15}	176093.351	2.37	242.2	176096.4	3.8	0.74
³⁴ SO ₂ 23 _{7,17} -24 _{6,18}	176940.267	3.15	369.3	176944.5	1.8	0.54
³⁴ SO ₂ 28 _{8,20} -29 _{7,23}	177647.037	3.92	524.1	177648.5	6.5	0.45
³⁴ SO ₂ 22 _{7,15} -23 _{6,18}	196854.461	2.93	348.2	196856.1	6.5	0.22
³⁴ SO ₂ 24 _{3,21} -24 _{2,22}	197044.107	19.3	301.5	197046.1 ^{4,6}	6.0	1.20
³⁴ SO ₂ 27 _{8,20} -28 _{7,21}	197555.307	3.70	498.4	⁴
³⁴ SO ₂ 32 _{9,23} -33 _{8,26}	198018.213	4.47	676.2	⁵
³⁴ SO ₂ 24 _{3,21} -23 _{4,20}	198348.517	4.28	301.5	198351.1	5.1	0.29
³⁴ SO ₂ 11 _{2,11} -11 _{1,11}	201376.485	4.50	69.7	201379.9	3.9	2.14
³⁴ SO ₂ 3 _{2,3} -3 _{1,1}	203225.060	1.67	15.0	203226.9	6.3	1.01
³⁴ SO ₂ 16 _{1,15} -16 _{0,16}	203504.216	5.93	130.3	203506.9	5.0	1.22
³⁴ SO ₂ 12 _{0,12} -11 _{1,11}	204136.230	8.54	69.9	204138.2	6.1	4.03
³⁴ SO ₂ 16 _{3,13} -16 _{2,14}	204525.183	10.9	146.9	204525.6 ⁷	8.4	2.71
³⁴ SO ₂ 39 _{5,35} -38 _{6,32}	210817.577	5.53	778.8	⁵
³⁴ SO ₂ 30 _{4,26} -29 _{5,25}	211418.824	4.92	469.9	211419.9 ¹	7.5	0.13
³⁴ SO ₂ 6 _{4,2} -7 _{3,5}	211762.760	0.43	57.2	211764.8	6.1	0.20
³⁴ SO ₂ 26 _{3,23} -26 _{2,24}	212981.206	20.0	349.9	212983.7	5.5	1.19
³⁴ SO ₂ 11 _{5,7} -12 _{4,8}	213807.332	1.17	119.8	213811.1	3.7	0.45
³⁴ SO ₂ 16 _{6,10} -17 _{5,13}	215468.142	1.94	210.0	215471.2	4.7	0.35
³⁴ SO ₂ 14 _{3,11} -14 _{2,12}	215999.732	8.75	118.1	216002.4 ³⁴	5.3	3.59
³⁴ SO ₂ 21 _{7,15} -22 _{6,16}	216593.474	2.71	328.0	216596.1	5.4	0.30
³⁴ SO ₂ 26 _{8,18} -27 _{7,21}	217412.916	3.48	473.6	³⁸
³⁴ SO ₂ 31 _{9,23} -32 _{8,24}	217902.356	4.25	646.8	217903.6	7.3	0.11
³⁴ SO ₂ 11 _{1,11} -10 _{0,10}	219355.012	7.79	60.1	two peaks: 219347.5 219357.3	19.3 5.9	1.83 4.49
³⁴ SO ₂ 36 _{5,31} -35 _{6,30}	220451.861	5.72	676.0	220453.7	6.5	0.12
³⁴ SO ₂ 22 _{2,20} -22 _{1,21}	221114.901	12.7	247.8	221117.4	5.6	1.40
³⁴ SO ₂ 13 _{2,12} -13 _{1,13}	221735.717	4.89	92.5	221738.7 ³⁴	5.0	2.36
³⁴ SO ₂ 26 _{2,24} -27 _{1,27}	225583.126	0.14	339.6	225587.4 ⁶	3.3	1.03
³⁴ SO ₂ 12 _{3,9} -12 _{2,10}	227031.884	6.98	93.1	227034.9	5.0	3.61
³⁴ SO ₂ 4 _{2,2} -3 _{1,3}	229857.629	1.70	18.7	229859.9 ^{4,20}	6.0	2.63
³⁴ SO ₂ 15 _{3,13} -16 _{0,16}	229866.232	0.10	131.6	¹⁶
³⁴ SO ₂ 17 _{3,15} -18 _{0,18}	229888.286	0.12	161.9	229889.9	6.9	0.12
³⁴ SO ₂ 5 _{4,2} -6 _{3,3}	230933.358	0.25	51.7	230934.9	7.0	0.22
³⁴ SO ₂ 10 _{5,5} -11 _{4,8}	233296.401	0.96	109.7	233301.3 ⁴⁸	2.7	0.19
³⁴ SO ₂ 15 _{6,10} -16 _{5,11}	235004.013	1.72	195.4	235006.5	5.8	0.40
³⁴ SO ₂ 5 _{2,4} -4 _{1,3}	235927.500	2.13	23.2	235933.5 ⁵	1.4	1.91
³⁴ SO ₂ 10 _{3,7} -10 _{2,8}	235951.921	5.48	71.9	235954.6	5.6	2.54
³⁴ SO ₂ 20 _{2,18} -19 _{3,17}	236225.098	4.77	207.2	⁴⁹
³⁴ SO ₂ 20 _{7,13} -21 _{6,16}	236295.678	2.49	308.7	236300.1 ^{36,50}	3.4	0.29
³⁴ SO ₂ 19 _{3,17} -20 _{0,20}	236428.774	0.13	195.9	236432.6	4.2	0.24
³⁴ SO ₂ 13 _{3,11} -14 _{0,14}	236871.403	0.08	104.9	236874.5	5.1	0.19

Table A.9. continued.

Species/Transition $J_{K_a, K_c} - J'_{K'_a, K'_c}$	Predicted freq. (MHz)	S_{ij}	E_u (K)	Observed freq. (MHz)	Observed v_{LSR} (km s ⁻¹)	Observed T_A^* (K)
³⁴ SO ₂ 25 _{8,18} -26 _{7,19}	237169.109	3.26	449.7	⁴
³⁴ SO ₂ 28 _{3,25} -28 _{2,26}	237521.028	20.0	402.1	237523.9	5.4	1.06
³⁴ SO ₂ 30 _{9,21} -31 _{8,24}	237721.815	4.03	618.3	³²
³⁴ SO ₂ 16 _{1,15} -15 _{2,14}	241509.049	6.25	130.3	241512.6	4.6	2.71
³⁴ SO ₂ 8 _{3,5} -8 _{2,6}	241985.451	4.15	54.4	^{4,6}
³⁴ SO ₂ 18 _{1,17} -18 _{0,18}	243935.963	5.77	162.6	243938.5	5.9	1.38
³⁴ SO ₂ 14 _{0,14} -13 _{0,13}	244481.520	10.6	93.5	244484.5	5.3	4.51
³⁴ SO ₂ 15 _{2,14} -15 _{1,15}	245178.728	5.17	118.7	245181.4	5.7	1.96
³⁴ SO ₂ 6 _{3,3} -6 _{2,4}	245302.240	2.90	40.6	245305.1	5.5	2.06
³⁴ SO ₂ 4 _{3,1} -4 _{2,2}	246686.119	1.62	30.5	246687.5	7.3	1.63
³⁴ SO ₂ 3 _{3,1} -3 _{2,2}	247127.390	0.89	26.8	two peaks: 247128.9 ¹⁸ 247133.9
					7.2	0.67
					1.1	0.49
³⁴ SO ₂ 5 _{3,3} -5 _{2,4}	247440.298	2.26	35.1	247442.7	6.1	1.33
³⁴ SO ₂ 7 _{3,5} -7 _{2,6}	248364.769	3.48	47.0	248367.7	5.5	3.07
³⁴ SO ₂ 13 _{1,13} -12 _{0,12}	248698.698	9.73	81.8	248702.5	4.4	5.83
³⁴ SO ₂ 21 _{3,19} -22 _{0,22}	248855.716	0.13	233.5	248856.5 ¹⁶	8.1	1.04
³⁴ SO ₂ 30 _{4,26} -30 _{3,27}	249099.208	23.7	469.9	249101.3 ³²	6.5	0.80
³⁴ SO ₂ 4 _{4,0} -5 _{3,3}	250156.048	0.10	47.1	250163.9	-0.4	0.75
³⁴ SO ₂ 9 _{3,7} -9 _{2,8}	250358.384	4.66	62.6	two peaks: 250351.4 250362.0 ⁴
					17.4	1.19
					4.7	2.57
³⁴ SO ₂ 11 _{3,9} -12 _{0,12}	251176.574	0.05	81.9	⁴⁹
³⁴ SO ₂ 25 _{4,22} -26 _{1,25}	251438.065	0.28	337.2	⁶
³⁴ SO ₂ 27 _{4,24} -28 _{1,27}	251639.934	0.31	386.1	¹⁶
³⁴ SO ₂ 32 _{4,28} -32 _{3,29}	251758.330	25.6	529.6	251760.5	6.4	0.31
³⁴ SO ₂ 9 _{5,5} -10 _{4,6}	252615.371	0.76	100.5	252618.4	5.4	0.47
³⁴ SO ₂ 11 _{3,9} -11 _{2,10}	253936.319	5.79	81.9	253940.0 ⁴⁹	4.7	3.63
³⁴ SO ₂ 28 _{4,24} -28 _{3,25}	254277.643	21.2	414.3	⁴⁹
³⁴ SO ₂ 14 _{6,8} -15 _{5,11}	254516.775	1.51	181.6	254519.5 ¹⁸	5.8	0.38
³⁴ SO ₂ 19 _{7,13} -20 _{6,14}	255892.295	2.27	290.3	255896.5	4.1	0.18
³⁴ SO ₂ 24 _{8,16} -25 _{7,19}	256864.330	3.04	426.7	⁵¹
³⁴ SO ₂ 29 _{9,21} -30 _{8,22}	257466.731	3.81	590.8	¹³
³⁴ SO ₂ 29 _{4,26} -30 _{1,29}	258889.599	0.32	438.6	258893.6	4.4	0.08
³⁴ SO ₂ 23 _{4,20} -24 _{1,23}	259022.539	0.24	291.9	⁵²
³⁴ SO ₂ 13 _{3,11} -13 _{2,12}	259617.206	6.87	104.9	259618.5 ^{5,7,34}	7.5	2.28
³⁴ SO ₂ 24 _{2,22} -24 _{1,23}	260326.950	12.2	292.0	260331.4 ^{4,7}	3.9	3.34
³⁴ SO ₂ 23 _{4,20} -24 _{1,23}	259022.539	0.24	291.9	⁵²
³⁴ SO ₂ 34 _{4,30} -34 _{3,31}	263436.078	26.7	593.1	263441.4 ¹⁸	2.9	0.46
³⁴ SO ₂ 26 _{3,23} -25 _{4,22}	264682.899	4.98	349.9	³
³⁴ SO ₂ 26 _{4,22} -26 _{3,23}	265488.694	18.5	362.6	265485.1 ^{4,49}	13.1	1.93
³⁴ SO ₂ 7 _{2,6} -6 _{1,25}	265554.053	2.68	35.1	265555.2	7.7	1.06
³⁴ SO ₂ 23 _{3,21} -24 _{0,24}	266469.801	0.13	274.7	266470.1	8.7	0.24
³⁴ SO ₂ 33 _{5,29} -34 _{2,32}	267094.152	0.45	576.3	267097.6	5.1	0.26
³⁴ SO ₂ 15 _{3,13} -15 _{2,14}	267871.064	7.85	131.6	267872.5 ³⁹	7.4	1.74
³⁴ SO ₂ 30 _{3,27} -30 _{2,28}	270229.677	19.5	458.0	270231.4 ⁷	7.1	0.52
³⁴ SO ₂ 17 _{2,16} -17 _{1,17}	271410.227	5.36	148.5	271413.9 ¹⁸	4.9	1.19
³⁴ SO ₂ 8 _{5,3} -9 _{4,6}	271916.826	0.56	92.3	271928.5 ⁴⁷	-3.9	0.72
³⁴ SO ₂ 31 _{4,28} -32 _{1,31}	272363.869	0.32	494.8	¹⁶
³⁴ SO ₂ 9 _{3,7} -10 _{0,10}	272625.742	0.02	62.6	³⁴
³⁴ SO ₂ 28 _{2,26} -29 _{1,29}	272789.518	0.12	390.7	272794.5	3.5	0.13
³⁴ SO ₂ 13 _{6,8} -14 _{5,9}	273929.985	1.29	168.7	273931.5	7.3	0.43
³⁴ SO ₂ 21 _{4,18} -22 _{1,21}	274940.961	0.18	250.4	274942.6	7.2	0.72
³⁴ SO ₂ 18 _{7,11} -19 _{6,14}	275434.219	2.06	272.9	275441.4 ³²	1.2	0.89
³⁴ SO ₂ 23 _{8,16} -24 _{7,17}	276484.001	2.82	404.7	²⁴
³⁴ SO ₂ 6 _{2,4} -5 _{1,5}	276999.606	1.85	28.8	277001.3	7.2	1.61

Table A.9. continued.

Species/Transition $J_{K_a,K_c} - J'_{K'_a,K'_c}$	Predicted freq. (MHz)	S_{ij}	E_u (K)	Observed freq. (MHz)	Observed v_{LSR} (km s ⁻¹)	Observed T_A^* (K)
³⁴ SO ₂ 28 _{9,19} -29 _{8,22}	277150.593	3.60	564.1	277154.0	5.3	0.14
³⁴ SO ₂ 33 _{10,24} -34 _{9,25}	277470.086	4.37	751.2	277471.3 ^{53,54}	7.7	0.57
³⁴ SO ₂ 32 _{4,28} -31 _{5,27}	278835.214	5.43	529.6	278834.5 ⁴³	9.8	0.56
³⁴ SO ₂ 17 _{3,15} -17 _{2,16}	279075.261	8.72	161.9	279076.3 ⁵	7.9	3.39
³⁴ SO ₂ 15 _{1,15} -14 _{0,14}	279429.979	11.8	107.0	279433.8 ^{6,18}	4.9	5.67
³⁴ SO ₂ 24 _{4,20} -24 _{3,21}	280407.893	15.9	314.9	280412.6 ⁶	4.0	2.09
³³ SO ₂ 8 _{3,5} -9 _{2,8}	82380.654	1.13	54.8	82380.5	9.6	0.03
³³ SO ₂ 26 _{4,22} -25 _{5,21}	82777.117	4.11	363.4	⁴
³³ SO ₂ 8 _{1,7} -8 _{0,8}	83345.818	6.32	36.7	83347.5	3.0	0.06
³³ SO ₂ 18 _{5,13} -19 _{4,16}	83540.669	2.68	217.4	83541.5	6.0	0.01
³³ SO ₂ 23 _{6,18} -24 _{5,19}	84025.261	3.46	340.4	¹⁷
³³ SO ₂ 28 _{7,21} -29 _{6,24}	87241.461	4.22	491.2	⁵
³³ SO ₂ 33 _{8,26} -34 _{7,27}	89094.697	4.99	669.8	89096.4	3.3	0.01
³³ SO ₂ 20 _{2,18} -21 _{1,21}	90595.537	0.26	207.5	³³
³³ SO ₂ 33 _{3,31} -32 _{4,28}	92105.596	1.87	534.7	noise level
³³ SO ₂ 7 _{3,5} -8 _{2,6}	93072.174	0.94	47.4	93073.5	4.7	0.04
³³ SO ₂ 25 _{3,23} -24 _{4,20}	93533.322	3.18	320.2	93535.5	2.0	0.03
³³ SO ₂ 32 _{5,27} -31 _{6,26}	96205.274	5.03	548.0	96208.5 ³⁴	...	0.05
³³ SO ₂ 33 _{5,29} -32 _{6,26}	97491.820	5.13	577.7	97493.7	3.2	0.02
³³ SO ₂ 2 _{2,0} -3 _{1,3}	98261.870	0.16	12.4	^{34,43}
³³ SO ₂ 17 _{5,13} -18 _{4,14}	101560.254	2.48	200.9	⁷
³³ SO ₂ 12 _{4,8} -13 _{3,11}	101688.876	1.70	110.2	⁴
³³ SO ₂ 3 _{1,3} -2 _{0,2}	103000.258	2.02	7.7	103003.4	-0.1	0.11
³³ SO ₂ 10 _{1,9} -10 _{0,10}	104301.966	6.61	54.6	¹⁶
³³ SO ₂ 22 _{6,16} -23 _{5,19}	105452.527	3.24	319.3	105456.6 ⁶	-2.0	0.13
³³ SO ₂ 29 _{4,26} -28 _{5,23}	105943.555	4.32	439.6	105944.5	6.3	0.02
³³ SO ₂ 27 _{7,21} -28 _{6,22}	107245.759	4.01	465.5	107246.5	6.9	0.02
³³ SO ₂ 27 _{3,25} -26 _{4,22}	108383.700	2.99	368.6	³⁰
³³ SO ₂ 31 _{3,29} -30 _{4,26}	108514.453	2.28	475.9	¹⁹
³³ SO ₂ 32 _{8,24} -33 _{7,27}	109681.906	4.78	639.4	⁶
³³ SO ₂ 16 _{2,14} -15 _{3,13}	109828.514	3.02	137.3	109829.5	6.3	0.11
³³ SO ₂ 29 _{3,27} -28 _{4,24}	113783.648	2.67	420.5	¹⁷
³³ SO ₂ 14 _{2,12} -14 _{1,13}	131191.102	11.7	107.9	131192.7	5.4	0.36
³³ SO ₂ 8 _{2,6} -8 _{1,7}	131247.049	5.73	43.0	131249.5	3.4	0.32
³³ SO ₂ 12 _{1,11} -12 _{0,12}	131561.786	6.53	76.3	131562.6 ⁴⁷	7.1	0.29
³³ SO ₂ 12 _{1,11} -11 _{2,10}	132084.974	3.42	76.3	132086.4 ^{5,55}	5.8	0.22
³³ SO ₂ 5 _{1,5} -4 _{0,4}	134550.979	3.14	15.6	134550.1 ⁴	11.0	2.72
³³ SO ₂ 5 _{3,3} -6 _{2,4}	134830.627	0.50	35.5	^{6,23}
³³ SO ₂ 35 _{5,31} -34 _{6,28}	136073.824	5.39	641.6	136075.1	6.2	0.02
³³ SO ₂ 31 _{2,28} -30 _{5,25}	136345.497	4.41	495.9	²³
³³ SO ₂ 6 _{2,4} -6 _{1,5}	137478.134	3.85	29.0	137481.4	1.9	0.43
³³ SO ₂ 10 _{4,6} -11 _{3,9}	140348.741	1.27	89.1	140350.1	6.1	0.11
³³ SO ₂ 16 _{2,14} -16 _{1,15}	142281.376	12.9	137.3	142281.4	8.9	0.40
³³ SO ₂ 15 _{5,11} -16 _{4,12}	142295.587	2.04	170.5	¹⁷
³³ SO ₂ 4 _{2,2} -4 _{1,3}	143795.870	2.28	18.8	two peaks: 143795.5 143799.5	9.8 1.4	0.27 0.48
³³ SO ₂ 20 _{6,14} -21 _{5,17}	145564.070	2.81	279.7	⁵⁶
³³ SO ₂ 25 _{7,19} -26 _{6,20}	147793.083	3.58	416.7	147795.5	4.1	0.11
³³ SO ₂ 2 _{2,0} -2 _{1,1}	148614.406	0.87	12.4	⁵
³³ SO ₂ 34 _{5,29} -33 _{6,28}	148926.741	5.39	610.6	¹⁷
³³ SO ₂ 30 _{8,22} -31 _{7,25}	150134.771	4.35	581.4	¹⁶
³³ SO ₂ 3 _{2,2} -3 _{1,3}	155523.945	1.44	15.2	two peaks: 155523.5 155526.4	9.9 4.3	0.27 0.24
³³ SO ₂ 4 _{3,1} -5 _{2,4}	156091.249	0.30	30.9	⁹

Table A.9. continued.

Species/Transition $J_{K_a, K_c} - J'_{K'_a, K'_c}$	Predicted freq. (MHz)	S_{ij}	E_u (K)	Observed freq. (MHz)	Observed v_{LSR} (km s ⁻¹)	Observed T_A^* (K)
³³ SO ₂ 9 _{4,6} -10 _{3,7}	158845.420	1.05	79.9	158846.5 ⁴⁹	7.0	0.17
³³ SO ₂ 18 _{2,16} -18 _{1,17}	160513.715	13.4	170.5	³¹
³³ SO ₂ 33 _{4,30} -32 _{5,27}	161071.892	4.36	555.7	⁴
³³ SO ₂ 10 _{0,10} -9 _{1,9}	161452.956	6.48	49.6	161452.6 ^{4,32}	9.7	2.53
³³ SO ₂ 5 _{2,4} -5 _{1,5}	162562.342	2.45	23.4	162564.5	5.0	0.51
³³ SO ₂ 14 _{5,9} -15 _{4,12}	162745.229	1.82	156.7	162748.5 ⁵	3.0	0.48
³³ SO ₂ 7 _{1,7} -6 _{0,6}	163964.985	4.44	27.0	⁵
³³ SO ₂ 14 _{1,13} -14 _{0,14}	164626.053	6.29	101.6	164626.5	8.2	0.37
³³ SO ₂ 19 _{6,14} -20 _{5,15}	165265.989	2.59	261.3	⁴
³³ SO ₂ 24 _{7,17} -25 _{6,20}	167953.648	3.36	393.7	167954.6 ³⁴	7.3	0.14
³³ SO ₂ 18 _{2,16} -17 _{3,15}	169164.044	3.76	170.5	169167.6	2.7	0.23
³³ SO ₂ 29 _{8,22} -30 _{7,23}	170176.428	4.13	553.8	¹⁷
³³ SO ₂ 7 _{2,6} -7 _{1,7}	172832.024	3.29	35.3	172831.5	9.9	0.57
³³ SO ₂ 24 _{2,22} -25 _{1,25}	173951.097	0.17	292.4	²⁵
³³ SO ₂ 3 _{3,1} -4 _{2,2}	174505.972	0.13	27.2	174506.5	8.1	0.37
³³ SO ₂ 7 _{4,4} -8 _{3,5}	198125.389	0.63	64.3	198127.4 ⁵⁵	6.0	0.22
³³ SO ₂ 24 _{3,21} -24 _{2,22}	198479.747	19.3	301.9	198482.4	5.0	0.52
³³ SO ₂ 18 _{3,15} -18 _{2,16}	199340.675	13.1	180.1	199343.6	4.6	0.54
³³ SO ₂ 30 _{4,26} -29 _{5,25}	199653.586	4.92	470.7	⁴
³³ SO ₂ 12 _{5,7} -13 _{4,10}	201927.690	1.39	131.9	201929.4	6.5	0.19
³³ SO ₂ 16 _{1,15} -16 _{0,16}	202188.357	6.04	130.5	202194.4 ^{5,57}	0.0	0.89
³³ SO ₂ 11 _{2,10} -11 _{1,11}	203266.908	4.53	70.0	203268.2	7.1	0.47
³³ SO ₂ 12 _{0,12} -11 _{1,11}	203790.096	8.49	70.0	203793.3	4.3	0.83
³³ SO ₂ 17 _{6,12} -18 _{5,13}	204932.906	2.16	227.3	⁷
³³ SO ₂ 3 _{2,2} -2 _{1,1}	205876.481	1.67	15.2	205876.1 ^{4,58}	9.6	1.06
³³ SO ₂ 36 _{5,31} -35 _{6,30}	206591.663	5.74	677.2	⁶
³³ SO ₂ 22 _{7,15} -23 _{6,18}	207708.782	2.93	350.4	⁷
³³ SO ₂ 16 _{3,13} -16 _{2,14}	209431.260	10.8	147.4	209434.9 ⁵⁹	3.8	1.15
³³ SO ₂ 27 _{8,20} -28 _{7,21}	210085.250	3.70	501.3	210088.7	4.1	0.16
³³ SO ₂ 32 _{9,23} -33 _{8,26}	212214.107	4.47	680.0	noisy spectrum
³³ SO ₂ 26 _{3,23} -26 _{2,24}	212860.266	20.2	350.3	212862.3 ⁷	6.1	0.18
³³ SO ₂ 6 _{4,2} -7 _{3,5}	217628.603	0.43	57.9	217629.8	7.4	0.18
³³ SO ₂ 22 _{2,20} -22 _{1,21}	218878.861	12.9	248.1	218879.9 ⁶⁰	7.6	0.43
³³ SO ₂ 11 _{1,11} -10 _{0,10}	220619.071	7.75	60.2	⁵⁷
³³ SO ₂ 14 _{3,11} -14 _{2,12}	220987.225	8.68	118.5	220986.2 ^{5,24,60}	10.4	0.92
³³ SO ₂ 11 _{5,7} -12 _{4,8}	221328.839	1.17	120.9	221332.4	4.2	0.14
³³ SO ₂ 13 _{2,12} -13 _{1,13}	223378.596	4.93	92.7	⁴
³³ SO ₂ 16 _{6,10} -17 _{5,13}	224641.972	1.94	211.6	⁴
³³ SO ₂ 21 _{7,15} -22 _{6,16}	227436.553	2.71	330.2	⁵⁶
³³ SO ₂ 26 _{8,18} -27 _{7,21}	229919.132	3.48	476.5	229919.9 ¹⁷	8.0	0.11
³³ SO ₂ 20 _{2,18} -19 _{3,17}	230438.867	4.69	207.5	230442.4 ⁵	4.4	0.24
³³ SO ₂ 12 _{3,9} -12 _{2,10}	231898.417	6.94	93.5	231904.9 ^{7,10,61}	0.6	0.41
³³ SO ₂ 31 _{9,23} -32 _{8,24}	232073.029	4.25	650.5	^{36,39}
³³ SO ₂ 4 _{2,2} -3 _{1,3}	232419.835	1.71	18.8	¹⁶
³³ SO ₂ 17 _{3,15} -18 _{0,18}	233838.726	0.12	162.4	233840.5	6.7	0.12
³³ SO ₂ 15 _{3,13} -16 _{0,16}	234641.219	0.10	132.0	234647.7	0.7	0.09
³³ SO ₂ 28 _{3,25} -28 _{2,26}	235726.867	20.3	402.5	¹⁷
³³ SO ₂ 5 _{4,2} -6 _{3,3}	236815.676	0.25	52.4	^{5,6}
³³ SO ₂ 5 _{2,4} -4 _{1,3}	238683.410	2.12	23.4	¹³
³³ SO ₂ 16 _{1,15} -15 _{2,14}	238967.956	6.15	130.5	¹³
³³ SO ₂ 19 _{3,17} -20 _{0,20}	239546.722	0.13	196.4	¹⁷
³³ SO ₂ 10 _{3,7} -10 _{2,8}	240612.356	5.46	72.3	240614.9	5.8	0.77
³³ SO ₂ 10 _{5,5} -11 _{4,8}	240814.508	0.96	110.8	240819.9 ¹⁷	2.3	0.43
³³ SO ₂ 13 _{3,11} -14 _{0,14}	242429.337	0.76	105.4	⁹
³³ SO ₂ 18 _{1,17} -18 _{0,18}	242489.055	5.88	162.8	^{4,16}

Table A.9. continued.

Species/Transition $J_{K_a,K_c} - J'_{K'_a,K'_c}$	Predicted freq. (MHz)	S_{ij}	E_u (K)	Observed freq. (MHz)	Observed v_{LSR} (km s ⁻¹)	Observed T_A^* (K)
³³ SO ₂ 15 _{6,10} -16 _{5,11}	244177.299	1.72	196.9	244178.9	7.0	0.10
³³ SO ₂ 14 _{0,14} -13 _{1,13}	244388.890	1.06	93.7	244392.0 ⁵⁹	5.2	1.53
³³ SO ₂ 8 _{3,5} -8 _{2,6}	246455.769	4.15	54.8	246457.6 ⁵	6.8	1.00
³³ SO ₂ 15 _{2,14} -15 _{1,15}	246558.644	5.22	119.0	⁶²
³³ SO ₂ 20 _{7,13} -21 _{6,16}	247124.476	2.49	310.9	247128.9 ¹⁷	3.6	0.67
³³ SO ₂ 6 _{3,3} -6 _{2,4}	249650.188	2.90	41.0	249652.5	6.2	0.99
³³ SO ₂ 25 _{8,18} -26 _{7,19}	249659.233	3.26	452.6	249660.5 ¹⁰	7.5	0.89
³³ SO ₂ 25 _{8,17} -26 _{7,20}	249664.196	3.26	452.6	249668.5	3.8	0.41
³³ SO ₂ 13 _{1,13} -12 _{0,12}	249907.904	9.68	82.0	249909.4	7.2	1.33
³³ SO ₂ 4 _{3,1} -4 _{2,2}	250978.790	1.61	30.9	250981.5 ⁶	5.8	0.80
³³ SO ₂ 21 _{3,19} -22 _{0,22}	251161.805	0.13	234.1	¹⁶
³³ SO ₂ 3 _{3,1} -3 _{2,2}	251401.862	0.89	27.2	251408.9 ⁴³	0.6	0.48
³³ SO ₂ 5 _{3,3} -5 _{2,4}	251702.803	2.26	35.5	251706.5 ⁵	4.6	0.72
³³ SO ₂ 30 _{9,21} -31 _{8,24}	251869.264	4.03	622.0	¹⁶
³³ SO ₂ 7 _{3,5} -7 _{2,6}	252591.694	3.48	47.4	252594.5	5.7	0.64
³³ SO ₂ 30 _{4,26} -30 _{3,27}	253982.798	23.5	470.7	²⁹
³³ SO ₂ 9 _{3,7} -9 _{2,8}	254510.018	4.65	63.0	254518.8 ²³	-1.3	0.38
³³ SO ₂ 32 _{4,28} -32 _{3,29}	254706.303	25.6	530.3	⁵⁶
³³ SO ₂ 26 _{3,23} -25 _{4,22}	255285.450	4.92	350.3	255288.8	5.1	0.04
³³ SO ₂ 4 _{4,0} -5 _{3,3}	256049.817	0.10	47.8	^{5,53}
³³ SO ₂ 24 _{2,22} -24 _{1,23}	257349.346	12.5	292.4	¹³
³³ SO ₂ 11 _{3,9} -11 _{2,10}	257957.223	5.79	82.4	257959.0	6.9	0.32
³³ SO ₂ 9 _{5,5} -10 _{4,6}	260142.516	0.76	101.6	260141.4 ^{5,9}	10.3	0.71
³³ SO ₂ 28 _{4,24} -28 _{3,25}	260651.733	20.9	415.1	⁵
³³ SO ₂ 13 _{3,11} -13 _{2,12}	263439.631	6.87	105.4	263441.4 ²³	7.0	0.46
³³ SO ₂ 14 _{6,8} -15 _{5,11}	263686.350	1.51	183.1	263688.5 ⁶³	6.6	0.36
³³ SO ₂ 34 _{4,30} -31 _{3,31}	264112.472	26.9	593.9	264115.1	6.0	0.33
³³ SO ₂ 32 _{4,28} -31 _{5,27}	265999.703	5.40	530.3	³²
³³ SO ₂ 23 _{4,20} -24 _{1,23}	266389.236	0.23	292.8	³²
³³ SO ₂ 19 _{7,13} -20 _{6,14}	266714.606	2.27	292.5	266720.5 ⁴⁷	2.4	0.77
³³ SO ₂ 30 _{3,27} -30 _{2,28}	266817.889	19.9	458.5	⁵
³³ SO ₂ 23 _{3,21} -24 _{0,24}	268010.417	0.13	275.4	⁴
³³ SO ₂ 7 _{2,6} -6 _{1,5}	268450.516	2.68	35.3	268455.1	3.9	0.35
³³ SO ₂ 24 _{8,17} -25 _{7,18}	269336.898	3.04	429.6	269338.8	6.9	0.32
³³ SO ₂ 24 _{8,16} -25 _{7,19}	269339.793	3.04	429.6	⁸
³³ SO ₂ 38 _{5,33} -37 _{6,32}	269919.292	6.10	747.8	269922.5 ⁴¹	5.4	0.09
³³ SO ₂ 15 _{3,13} -15 _{2,14}	271420.818	7.87	132.0	271413.9 ²³	16.6	1.19
³³ SO ₂ 29 _{9,21} -30 _{8,22}	271595.561	3.82	594.4	271599.4	4.8	0.16
³³ SO ₂ 17 _{2,16} -17 _{1,17}	272529.988	5.42	148.9	272532.5	6.2	0.35
³³ SO ₂ 26 _{4,22} -26 _{3,23}	272834.379	18.3	363.4	272836.5	6.7	0.36
³³ SO ₂ 34 _{10,24} -35 _{9,27}	273528.762	4.59	787.0	273531.5	6.0	0.14
³³ SO ₂ 6 _{2,4} -5 _{1,5}	279434.518	1.86	29.0	^{7,23}
³³ SO ₂ 8 _{5,3} -9 _{4,6}	279451.477	0.56	93.3	279456.5	3.6	0.47
³³ SO ₂ 15 _{1,15} -14 _{0,14}	280557.119	11.7	107.2	⁴
SO ¹⁸ O 19 _{5,15} -20 _{4,16}	80417.639	2.91	225.1	noise level
SO ¹⁸ O 8 _{3,6} -9 _{2,7}	80709.124	1.17	52.9	⁷
SO ¹⁸ O 19 _{5,14} -20 _{4,17}	83312.870	2.91	225.1	³¹
SO ¹⁸ O 2 _{1,2} -1 _{0,1}	84094.060	1.50	4.9	84094.5	7.4	0.02
SO ¹⁸ O 16 _{2,14} -15 _{3,13}	86720.509	2.95	130.1	86722.3	2.8	0.03
SO ¹⁸ O 7 _{0,7} -6 _{1,6}	87752.674	3.73	24.1	⁶⁴
SO ¹⁸ O 9 _{1,8} -9 _{0,9}	88201.737	6.75	42.8	88202.5 ⁴	...	0.06
SO ¹⁸ O 26 _{3,24} -25 _{4,21}	88869.508	3.38	326.4	88870.4	6.0	0.02
SO ¹⁸ O 26 _{6,19} -25 _{5,20}	88950.657	3.68	347.0	noise level
SO ¹⁸ O 8 _{3,5} -9 _{2,8}	90082.440	1.13	52.9	90082.6	8.5	0.02
SO ¹⁸ O 24 _{6,18} -25 _{5,21}	90093.680	3.68	347.0	noise level

Table A.9. continued.

Species/Transition $J_{K_a, K_c} - J'_{K'_a, K'_c}$	Predicted freq. (MHz)	S_{ij}	E_u (K)	Observed freq. (MHz)	Observed v_{LSR} (km s ⁻¹)	Observed T_A^* (K)
SO ¹⁸ O 11 _{1,10} -10 _{2,9}	90833.653	2.81	61.5	90835.5	2.9	0.02
SO ¹⁸ O 13 _{4,10} -14 _{3,11}	91008.626	1.93	117.4	³⁶
SO ¹⁸ O 22 _{3,19} -21 _{4,18}	94940.503	3.67	243.9	³²
SO ¹⁸ O 13 _{4,9} -14 _{3,12}	95583.519	1.92	117.4	noise level
SO ¹⁸ O 27 _{3,25} -26 _{4,22}	97271.829	3.31	349.7	97273.5 ⁶⁵	...	0.02
SO ¹⁸ O 10 _{1,9} -10 _{0,10}	98201.071	6.89	51.7	98201.5	7.7	0.07
SO ¹⁸ O 28 _{4,24} -27 _{5,23}	98879.028	4.52	393.7	98881.4	1.8	0.02
SO ¹⁸ O 3 _{1,3} -2 _{0,2}	100072.226	2.01	7.4	⁵⁶
SO ¹⁸ O 18 _{5,14} -19 _{4,15}	100152.038	2.70	208.5	100152.6 ^{1,34}	7.3	0.07
SO ¹⁸ O 2 _{2,0} -3 _{1,3}	100241.696	0.16	12.2	⁶⁶
SO ¹⁸ O 7 _{3,5} -8 _{2,6}	101189.989	0.94	45.9	¹⁶
SO ¹⁸ O 18 _{5,13} -19 _{4,16}	102098.856	2.69	208.5	102099.5	7.1	0.01
SO ¹⁸ O 28 _{3,26} -27 _{4,23}	103761.584	3.21	373.9	103761.5 ¹⁷	9.2	0.04
SO ¹⁸ O 7 _{3,4} -8 _{2,7}	107207.806	0.92	45.9	107210.5 ⁶⁷	1.5	0.06
SO ¹⁸ O 29 _{3,27} -28 _{4,24}	108156.775	3.07	398.9	108158.5	4.2	0.03
SO ¹⁸ O 23 _{6,18} -24 _{5,19}	108397.195	3.47	326.1	108398.5	5.4	0.02
SO ¹⁸ O 8 _{0,8} -7 _{1,7}	108695.341	4.54	30.9	108697.5 ¹⁶	3.0	0.05
SO ¹⁸ O 23 _{6,17} -24 _{5,20}	109165.615	3.46	326.1	³¹
SO ¹⁸ O 11 _{1,1} -11 _{0,11}	109636.196	6.93	61.5	109637.5	5.4	0.07
SO ¹⁸ O 12 _{4,9} -13 _{3,10}	110819.438	1.71	106.1	110820.5 ⁵³	6.1	0.06
SO ¹⁸ O 12 _{4,8} -13 _{3,11}	113802.293	1.70	106.1	⁷
SO ¹⁸ O 17 _{2,15} -16 _{3,14}	113985.361	3.28	145.3	⁴
SO ¹⁸ O 4 _{1,4} -3 _{0,3}	115401.986	2.55	10.7	115404.5	2.5	0.08
SO ¹⁸ O 5 _{1,5} -4 _{0,4}	130142.719	3.12	14.9	130146.4	0.5	0.13
SO ¹⁸ O 11 _{4,8} -12 _{3,9}	130201.251	1.49	95.7	⁶
SO ¹⁸ O 8 _{2,6} -8 _{1,7}	131766.987	5.61	41.1	131767.6	7.6	0.13
SO ¹⁸ O 15 _{2,13} -15 _{1,14}	131783.379	12.5	115.7	131785.5 ⁶⁸	4.2	0.14
SO ¹⁸ O 11 _{4,7} -12 _{3,10}	132076.129	1.49	95.7	132076.4 ¹⁷	8.4	0.09
SO ¹⁸ O 7 _{2,5} -7 _{1,6}	134717.922	4.66	34.0	134719.6	5.3	0.14
SO ¹⁸ O 16 _{2,14} -16 _{1,15}	136657.242	13.1	130.1	⁵
SO ¹⁸ O 13 _{1,12} -13 _{0,13}	136749.392	6.80	83.8	136751.1	5.3	0.21
SO ¹⁸ O 6 _{2,4} -6 _{1,5}	137821.359	3.79	27.9	137824.5	2.2	0.20
SO ¹⁸ O 16 _{5,12} -17 _{4,13}	138730.445	2.26	178.1	138730.5 ¹⁷	8.9	0.12
SO ¹⁸ O 16 _{5,11} -17 _{4,14}	139548.900	2.26	178.1	139551.4	3.6	0.11
SO ¹⁸ O 5 _{3,3} -6 _{2,4}	140259.456	0.50	34.6	⁵³
SO ¹⁸ O 5 _{2,3} -5 _{1,4}	140879.971	2.99	22.7	140880.5	7.9	0.11
SO ¹⁸ O 13 _{1,12} -12 _{2,11}	141009.800	3.85	83.8	141012.7	2.8	0.12
SO ¹⁸ O 18 _{2,16} -17 _{3,15}	141890.087	3.64	161.4	141891.6	5.8	0.08
SO ¹⁸ O 17 _{2,15} -17 _{1,16}	143096.211	13.6	145.3	¹⁶
SO ¹⁸ O 4 _{2,2} -4 _{1,3}	143714.712	2.26	18.3	143715.5	7.4	0.10
SO ¹⁸ O 6 _{1,6} -5 _{0,5}	144375.674	3.74	19.9	144377.6	5.0	0.14
SO ¹⁸ O 3 _{2,1} -3 _{1,2}	146171.277	1.57	14.8	¹
SO ¹⁸ O 21 _{6,16} -22 _{5,17}	146720.814	3.03	287.0	146725.4 ¹⁷	-0.4	0.03
SO ¹⁸ O 21 _{6,15} -22 _{5,18}	147048.896	3.03	287.0	³⁴
SO ¹⁸ O 2 _{2,0} -2 _{1,1}	148124.155	0.87	12.2	148125.1 ¹⁷	7.1	0.24
SO ¹⁸ O 10 _{4,7} -11 _{3,8}	149240.910	1.27	86.1	149241.3	8.2	0.08
SO ¹⁸ O 10 _{0,10} -9 _{1,9}	150298.672	6.34	47.0	150301.4	3.6	0.18
SO ¹⁸ O 10 _{4,6} -11 _{3,9}	150370.440	1.27	86.1	⁴⁹
SO ¹⁸ O 18 _{2,16} -18 _{1,17}	151170.878	13.9	161.4	151172.6 ⁴¹	5.6	0.13
SO ¹⁸ O 24 _{3,21} -23 _{4,20}	151524.215	4.17	285.9	151525.1	7.3	0.05
SO ¹⁸ O 2 _{2,1} -2 _{1,2}	152273.960	0.83	12.2	⁶⁹
SO ¹⁸ O 14 _{1,13} -14 _{0,14}	152276.995	6.68	96.2	152278.9	5.3	0.22
SO ¹⁸ O 3 _{2,2} -3 _{1,3}	154383.207	1.44	14.8	154385.1	5.3	0.11
SO ¹⁸ O 4 _{2,3} -4 _{1,4}	157205.792	1.98	18.3	157206.4	7.8	0.17
SO ¹⁸ O 15 _{5,11} -16 _{4,12}	157677.252	2.04	164.2	157679.5 ⁴⁰	4.7	0.11
SO ¹⁸ O 15 _{5,10} -16 _{4,13}	158186.297	2.04	164.2	⁴⁹

Table A.9. continued.

Species/Transition $J_{K_a,K_c} - J'_{K'_a,K'_c}$	Predicted freq. (MHz)	S_{ij}	E_u (K)	Observed freq. (MHz)	Observed v_{LSR} (km s ⁻¹)	Observed T_A^* (K)
SO ¹⁸ O 7 _{1,7} -6 _{0,6}	158202.045	4.40	25.7	⁴⁹
SO ¹⁸ O 4 _{3,2} -5 _{2,3}	159085.121	0.30	30.3	¹⁷
SO ¹⁸ O 4 _{3,1} -5 _{2,4}	160099.923	0.30	30.3	160102.7 ¹⁷	3.8	0.19
SO ¹⁸ O 5 _{2,4} -5 _{1,5}	160749.394	2.46	22.6	160750.5	6.9	0.19
SO ¹⁸ O 19 _{2,17} -19 _{1,18}	160926.624	14.0	178.4	160927.5	7.4	0.15
SO ¹⁸ O 6 _{2,5} -6 _{1,6}	165022.264	2.91	27.8	165023.9	6.0	0.14
SO ¹⁸ O 9 _{2,7} -8 _{2,6}	165236.094	8.55	49.0	⁴⁹
SO ¹⁸ O 20 _{6,15} -21 _{5,16}	165650.855	2.82	268.7	⁵
SO ¹⁸ O 20 _{6,14} -21 _{5,17}	165858.555	2.82	268.7	^{1,24}
SO ¹⁸ O 14 _{1,13} -13 _{2,12}	166375.483	4.45	96.2	166377.6 ^{70,71}	5.2	0.15
SO ¹⁸ O 9 _{4,6} -10 _{3,7}	168012.811	1.05	77.5	168014.5 ¹⁷	6.0	0.15
SO ¹⁸ O 9 _{4,5} -10 _{3,8}	168660.086	1.05	77.5	¹⁷
SO ¹⁸ O 15 _{1,14} -15 _{0,15}	168946.152	6.55	109.4	168947.5 ⁵³	6.6	0.21
SO ¹⁸ O 7 _{2,6} -7 _{1,7}	170032.391	3.32	33.9	⁵
SO ¹⁸ O 19 _{2,17} -18 _{3,16}	170334.178	4.04	178.4	⁴
SO ¹⁸ O 11 _{0,11} -10 _{1,10}	170740.229	7.31	56.3	⁴⁹
SO ¹⁸ O 8 _{1,8} -7 _{0,7}	171738.990	5.13	32.3	⁴
SO ¹⁸ O 20 _{2,18} -20 _{1,19}	172376.560	14.1	196.3	⁵
SO ¹⁸ O 25 _{7,19} -26 _{6,20}	173292.221	3.59	399.7	⁷
SO ¹⁸ O 25 _{7,18} -26 _{6,21}	173372.106	3.59	399.7	⁹
SO ¹⁸ O 8 _{2,7} -8 _{1,8}	175786.587	3.70	40.8	³
SO ¹⁸ O 14 _{5,10} -15 _{4,11}	176449.762	1.82	151.1	¹⁷
SO ¹⁸ O 14 _{5,9} -15 _{4,12}	176756.335	1.82	151.1	³⁴
SO ¹⁸ O 3 _{3,1} -4 _{2,2}	177592.074	0.13	26.8	177593.6 ⁷²	6.4	0.33
SO ¹⁸ O 3 _{3,0} -4 _{2,3}	178027.433	0.13	26.8	¹⁷
SO ¹⁸ O 25 _{3,22} -25 _{2,23}	196757.077	20.2	308.3	⁶
SO ¹⁸ O 11 _{2,10} -11 _{1,11}	197543.946	4.61	66.7	⁴
SO ¹⁸ O 19 _{3,16} -19 _{2,17}	198011.793	13.9	187.9	⁵
SO ¹⁸ O 10 _{1,10} -9 _{0,9}	198451.881	6.74	48.1	198454.9	4.4	0.23
SO ¹⁸ O 20 _{2,18} -19 _{3,17}	199209.147	4.48	196.3	¹⁷
SO ¹⁸ O 22 _{2,20} -22 _{1,21}	200212.306	13.8	234.8	200213.6	7.1	0.09
SO ¹⁸ O 26 _{3,23} -26 _{2,24}	202204.122	20.7	331.6	¹³
SO ¹⁸ O 3 _{2,2} -2 _{1,1}	202265.667	1.67	14.8	¹³
SO ¹⁸ O 18 _{3,15} -18 _{2,16}	202393.329	12.7	171.1	202393.2	9.2	0.11
SO ¹⁸ O 18 _{6,13} -19 _{5,14}	203148.227	2.38	234.8	203150.9	5.1	0.13
SO ¹⁸ O 18 _{6,12} -19 _{5,15}	203225.585	2.38	234.8	²³
SO ¹⁸ O 7 _{4,4} -8 _{3,5}	204989.937	0.63	62.7	204993.6	3.6	0.10
SO ¹⁸ O 17 _{1,16} -17 _{0,17}	205002.547	6.31	138.4	^{5,7}
SO ¹⁸ O 7 _{4,3} -8 _{3,6}	205164.732	0.63	62.7	205167.4 ²⁶	5.1	0.42
SO ¹⁸ O 12 _{2,11} -12 _{1,12}	206285.933	4.85	77.0	206286.2	8.6	0.28
SO ¹⁸ O 3 _{2,1} -2 _{1,2}	206589.735	1.60	14.8	⁷
SO ¹⁸ O 17 _{3,14} -17 _{2,15}	207401.220	11.5	155.2	^{4,7,73}
SO ¹⁸ O 27 _{3,24} -27 _{2,25}	209536.690	21.1	355.8	¹⁶
SO ¹⁸ O 13 _{0,13} -12 _{1,12}	210546.341	9.34	77.2	210548.7 ³⁴	5.6	1.23
SO ¹⁸ O 11 _{1,11} -10 _{0,10}	211873.232	7.63	57.2	211873.6 ⁶⁰	8.5	0.82
SO ¹⁸ O 26 _{3,23} -25 _{4,22}	211913.681	4.76	331.6	noisy spectrum
SO ¹⁸ O 16 _{3,13} -16 _{2,14}	212789.912	10.4	140.3	³²
SO ¹⁸ O 12 _{5,8} -13 _{4,9}	213591.909	1.39	127.7	213593.6	6.6	0.11
SO ¹⁸ O 12 _{5,7} -13 _{4,10}	213691.030	1.39	127.7	213694.9	3.6	0.09
SO ¹⁸ O 13 _{2,12} -13 _{1,13}	215756.356	5.05	88.2	215757.4 ⁴	7.6	0.51
SO ¹⁸ O 23 _{2,21} -23 _{1,22}	216415.486	13.6	255.3	216416.1 ⁹	8.1	0.16
SO ¹⁸ O 16 _{1,15} -15 _{2,14}	217102.694	5.86	123.5	⁷⁴
SO ¹⁸ O 4 _{2,3} -3 _{1,2}	218230.244	1.88	18.3	¹⁵
SO ¹⁸ O 15 _{3,12} -15 _{2,13}	218316.801	9.40	126.2	⁵⁶
SO ¹⁸ O 28 _{3,25} -28 _{2,26}	218793.885	21.3	380.9	218796.1	6.0	0.09
SO ¹⁸ O 17 _{6,12} -18 _{5,13}	221746.496	2.16	219.2	²³

Table A.9. continued.

Species/Transition $J_{K_a,K_c} - J'_{K'_a,K'_c}$	Predicted freq. (MHz)	S_{ij}	E_u (K)	Observed freq. (MHz)	Observed v_{LSR} (km s ⁻¹)	Observed T_A^* (K)
SO ¹⁸ O 17 _{6,11} -18 _{5,14}	221791.775	2.16	219.2	221794.9 ¹⁷	4.8	0.57
SO ¹⁸ O 6 _{4,3} -7 _{3,4}	223286.066	0.43	56.6	223287.4	7.2	0.09
SO ¹⁸ O 6 _{4,2} -7 _{3,5}	223365.572	0.43	56.6	223367.4 ⁴	6.5	0.15
SO ¹⁸ O 14 _{3,11} -14 _{2,12}	223753.919	8.47	113.1	223757.4	4.3	0.33
SO ¹⁸ O 18 _{1,17} -18 _{0,18}	223997.568	6.22	154.2	⁴
SO ¹⁸ O 12 _{1,12} -11 _{0,11}	225476.608	8.56	67.1	225479.8	4.8	0.33
SO ¹⁸ O 14 _{2,13} -14 _{1,14}	225937.235	5.23	100.2	225939.9	5.5	0.16
SO ¹⁸ O 4 _{2,2} -3 _{1,3}	227022.358	1.72	18.3	⁵
SO ¹⁸ O 21 _{2,19} -20 _{3,18}	228399.026	4.97	215.1	228403.5	3.1	0.06
SO ¹⁸ O 13 _{3,10} -13 _{2,11}	228899.481	7.61	100.8	228901.1 ²⁵	6.9	1.25
SO ¹⁸ O 22 _{7,16} -23 _{6,17}	229536.105	2.93	337.1	229541.1 ⁵	2.5	0.27
SO ¹⁸ O 22 _{7,15} -23 _{6,18}	229554.746	2.93	337.1	229557.4	5.5	0.12
SO ¹⁸ O 14 _{0,14} -13 _{1,13}	229854.843	10.4	88.9	²³
SO ¹⁸ O 29 _{3,26} -29 _{2,27}	229980.850	21.3	406.9	229984.9	3.7	0.15
SO ¹⁸ O 11 _{5,7} -12 _{4,8}	232008.234	1.17	117.3	⁴
SO ¹⁸ O 11 _{5,6} -12 _{4,9}	232060.800	1.17	117.3	232064.9	3.7	0.16
SO ¹⁸ O 17 _{3,15} -18 _{0,18}	233278.358	0.12	154.6	⁴
SO ¹⁸ O 5 _{2,4} -4 _{1,3}	233497.590	2.12	22.6	⁴
SO ¹⁸ O 12 _{3,9} -12 _{2,10}	233588.336	6.82	89.5	⁶
SO ¹⁸ O 24 _{2,22} -24 _{1,23}	233949.989	13.3	276.6	233950.5 ^{6,36}	8.3	0.27
SO ¹⁸ O 18 _{3,16} -19 _{0,19}	233967.257	0.13	170.3	⁶
SO ¹⁸ O 16 _{3,14} -17 _{0,17}	234113.397	0.11	139.8	⁵
SO ¹⁸ O 19 _{3,17} -20 _{0,20}	236122.215	0.14	186.8	¹⁷
SO ¹⁸ O 15 _{3,13} -16 _{0,16}	236522.092	0.10	125.9	⁵⁶
SO ¹⁸ O 15 _{2,14} -15 _{1,15}	236804.935	5.38	113.1	^{5,6}
SO ¹⁸ O 27 _{8,20} -28 _{7,21}	237018.562	3.70	481.6	237021.5	5.3	0.14
SO ¹⁸ O 27 _{8,19} -28 _{7,22}	237025.774	3.70	481.6	237026.5	8.1	0.17
SO ¹⁸ O 11 _{3,8} -11 _{2,9}	237700.285	6.09	79.0	237706.3	1.4	0.18
SO ¹⁸ O 13 _{1,13} -12 _{0,12}	239336.024	9.53	77.8	239340.2	3.8	0.45
SO ¹⁸ O 16 _{6,11} -17 _{5,12}	240261.313	1.94	204.4	³⁵
SO ¹⁸ O 16 _{6,10} -17 _{5,13}	240286.978	1.94	204.4	⁵
SO ¹⁸ O 10 _{3,7} -10 _{2,8}	241165.049	5.40	69.4	¹⁶
SO ¹⁸ O 5 _{4,2} -6 _{3,3}	241499.067	0.25	51.4	^{7,23}
SO ¹⁸ O 5 _{4,1} -6 _{3,4}	241530.882	0.25	51.4	⁷
SO ¹⁸ O 17 _{1,16} -16 _{2,15}	242215.554	6.66	138.4	⁴
SO ¹⁸ O 30 _{3,27} -30 _{2,28}	243063.849	21.2	433.8	243066.3	6.0	0.43
SO ¹⁸ O 27 _{3,24} -26 _{4,23}	243287.035	5.11	355.8	³⁴
SO ¹⁸ O 19 _{1,18} -19 _{0,19}	243374.811	6.15	170.7	243377.6	5.6	0.17
SO ¹⁸ O 33 _{4,29} -32 _{5,28}	243806.001	5.57	531.7	243810.5 ¹⁷	3.5	0.33
SO ¹⁸ O 9 _{3,6} -9 _{2,7}	243962.753	4.75	60.7	243965.5	5.6	0.41
SO ¹⁸ O 21 _{3,19} -22 _{0,22}	244570.319	0.14	222.4	³³
SO ¹⁸ O 8 _{3,5} -8 _{2,6}	246119.337	4.12	52.9	246122.6	5.0	0.32
SO ¹⁸ O 13 _{3,11} -14 _{0,14}	246199.086	0.07	100.7	⁵⁶
SO ¹⁸ O 7 _{3,4} -7 _{2,5}	247697.435	3.50	45.9	⁵
SO ¹⁸ O 6 _{2,5} -5 _{1,4}	248074.508	2.38	27.8	⁴⁹
SO ¹⁸ O 21 _{7,15} -22 _{6,16}	248124.713	2.71	318.0	248128.9 ¹⁷	3.9	0.35
SO ¹⁸ O 21 _{7,14} -22 _{6,17}	248135.684	2.71	318.0	no spectrum
SO ¹⁸ O 16 _{2,15} -16 _{1,16}	248330.358	5.50	126.8	248332.6	6.3	0.30
SO ¹⁸ O 5 _{2,3} -4 _{1,4}	248435.799	1.83	22.7	⁴
SO ¹⁸ O 15 _{0,15} -14 _{1,14}	248771.504	11.4	101.3	248772.5	7.8	0.75
SO ¹⁸ O 6 _{3,3} -6 _{2,4}	248784.360	2.89	39.8	⁵
SO ¹⁸ O 5 _{3,2} -5 _{2,3}	249479.459	2.26	34.6	249483.9 ^{7,71}	3.7	0.36
SO ¹⁸ O 4 _{3,1} -4 _{2,2}	249882.801	1.61	30.3	¹⁶
SO ¹⁸ O 3 _{3,0} -3 _{2,1}	250086.400	0.89	26.8	³⁹
SO ¹⁸ O 3 _{3,1} -3 _{2,2}	250231.226	0.89	26.8	250236.3	2.9	0.15

Table A.9. continued.

Species/Transition $J_{K_a,K_c} - J'_{K'_a,K'_c}$	Predicted freq. (MHz)	S_{ij}	E_u (K)	Observed freq. (MHz)	Observed v_{LSR} (km s ⁻¹)	Observed T_A^* (K)
SO ¹⁸ O 4 _{3,2} -4 _{2,3}	250315.128	1.61	30.3	6
SO ¹⁸ O 10 _{5,6} -11 _{4,7}	250345.658	0.96	107.7	23
SO ¹⁸ O 10 _{5,5} -11 _{4,8}	250371.975	0.96	107.7	23
SO ¹⁸ O 5 _{3,3} -5 _{2,4}	250481.005	2.26	34.6	250482.6 ^{19,26,27}	7.1	0.58
SO ¹⁸ O 22 _{3,20} -23 _{0,23}	250723.320	0.14	241.5	250726.5 ⁷²	5.2	0.08
SO ¹⁸ O 6 _{3,4} -6 _{2,5}	250767.445	2.87	39.8	no spectrum
SO ¹⁸ O 7 _{3,5} -7 _{2,6}	251218.717	3.47	45.9	49
SO ¹⁸ O 8 _{3,6} -8 _{2,7}	251883.714	4.06	52.9	16
SO ¹⁸ O 32 _{4,28} -32 _{3,29}	252312.209	25.2	502.2	252316.4	4.0	0.11
SO ¹⁸ O 33 _{4,29} -33 _{3,30}	252599.016	26.3	531.7	252601.5 ⁴¹	6.1	0.38
SO ¹⁸ O 25 _{2,23} -25 _{1,24}	252627.480	13.1	298.8	252633.5 ⁴	1.9	0.55
SO ¹⁸ O 9 _{3,7} -9 _{2,8}	252814.791	4.64	60.7	16
SO ¹⁸ O 12 _{3,10} -13 _{0,13}	253493.155	0.06	89.4	69
SO ¹⁸ O 14 _{1,14} -13 _{0,13}	253497.373	10.5	89.4	253501.3	4.4	0.28
SO ¹⁸ O 31 _{4,27} -31 _{3,28}	253792.638	24.1	473.7	253793.5 ¹⁷	8.0	0.21
SO ¹⁸ O 10 _{3,8} -10 _{2,9}	254066.518	5.21	69.4	254068.9 ⁴	6.2	0.93
SO ¹⁸ O 34 _{4,30} -34 _{3,31}	254792.758	27.2	562.1	12
SO ¹⁸ O 26 _{8,19} -27 _{7,20}	255656.625	3.48	458.1	22,75
SO ¹⁸ O 26 _{8,18} -27 _{7,21}	255660.974	3.48	458.1	22,75
SO ¹⁸ O 11 _{3,9} -11 _{2,10}	255694.394	5.78	78.9	62
SO ¹⁸ O 28 _{4,25} -29 _{1,28}	256635.956	0.32	392.1	256640.4	3.8	0.07
SO ¹⁸ O 27 _{4,24} -28 _{1,27}	256860.014	0.31	367.7	51
SO ¹⁸ O 30 _{4,26} -30 _{3,27}	256869.345	22.8	446.1	51
SO ¹⁸ O 12 _{3,10} -12 _{2,11}	257753.563	6.33	89.4	257754.5 ^{5,23}	7.9	0.28
SO ¹⁸ O 22 _{2,20} -21 _{3,19}	257780.402	5.51	234.8	257783.5 ²⁷	5.4	0.12
SO ¹⁸ O 31 _{3,28} -31 _{2,29}	257966.427	21.0	461.5	257968.5	6.6	0.19
SO ¹⁸ O 29 _{4,26} -30 _{1,29}	258050.529	0.34	417.4	5
SO ¹⁸ O 23 _{3,21} -24 _{0,24}	258063.984	0.14	261.4	5
SO ¹⁸ O 15 _{6,10} -16 _{5,11}	258703.135	1.72	190.5	5
SO ¹⁸ O 15 _{6,9} -16 _{5,12}	258717.168	1.72	190.5	258720.5	5.1	0.12
SO ¹⁸ O 26 _{4,23} -27 _{1,26}	258800.211	0.29	344.1	258802.5 ¹⁷	6.4	0.16
SO ¹⁸ O 35 _{4,31} -35 _{3,32}	259001.896	27.9	593.5	52
SO ¹⁸ O 29 _{2,27} -30 _{1,30}	259066.034	0.14	395.8	259070.1 ¹⁷	4.3	0.19
SO ¹⁸ O 4 _{4,1} -5 _{3,2}	259653.472	0.10	47.1	5
SO ¹⁸ O 4 _{4,0} -5 _{3,3}	259664.080	0.10	47.1	5
SO ¹⁸ O 13 _{3,11} -13 _{2,12}	260297.574	6.87	100.7	6
SO ¹⁸ O 17 _{2,16} -17 _{1,17}	260479.408	5.60	141.3	74
SO ¹⁸ O 30 _{4,27} -31 _{1,30}	261020.897	0.34	443.6	17
SO ¹⁸ O 29 _{4,25} -29 _{3,26}	261340.830	21.4	419.4	261341.4	8.3	0.48
SO ¹⁸ O 7 _{2,6} -6 _{1,5}	261972.250	2.67	33.9	261971.5 ^{17,41}	9.9	0.39
SO ¹⁸ O 11 _{3,9} -12 _{0,12}	262401.534	0.04	78.9	7
SO ¹⁸ O 25 _{4,22} -26 _{1,25}	262526.174	0.27	321.4	30,49
SO ¹⁸ O 31 _{9,23} -32 _{8,24}	262894.205	4.26	624.7	7
SO ¹⁸ O 31 _{9,22} -32 _{8,25}	262895.846	4.26	624.7	7
SO ¹⁸ O 20 _{1,19} -20 _{0,20}	262954.802	6.10	188.1	26
SO ¹⁸ O 14 _{3,12} -14 _{2,13}	263377.210	7.39	112.8	263377.6 ⁵	8.6	0.19
SO ¹⁸ O 36 _{4,32} -36 _{3,33}	265303.263	28.3	625.7	265302.7 ⁶⁸	9.6	0.17
SO ¹⁸ O 31 _{4,28} -32 _{1,31}	265460.709	0.35	470.6	25
SO ¹⁸ O 20 _{7,14} -21 _{6,15}	266646.030	2.49	299.8	266648.5	6.2	0.19
SO ¹⁸ O 20 _{7,13} -21 _{6,16}	266652.322	2.49	299.8	266653.5 ⁷⁷	7.7	0.24
SO ¹⁸ O 28 _{4,24} -28 _{3,25}	266977.664	20.1	393.7	266980.5	5.8	0.32
SO ¹⁸ O 18 _{1,17} -17 _{2,16}	266993.928	7.52	154.2	6
SO ¹⁸ O 15 _{3,13} -15 _{2,14}	267039.427	7.90	125.9	267043.9	4.0	0.17
SO ¹⁸ O 16 _{0,16} -15 _{1,15}	267322.270	12.5	114.5	no spectrum
SO ¹⁸ O 15 _{1,15} -14 _{0,14}	267979.833	11.5	101.7	267985.5	2.7	0.41

Table A.9. continued.

Species/Transition $J_{K_a,K_c} - J'_{K'_a,K'_c}$	Predicted freq. (MHz)	S_{ij}	E_u (K)	Observed freq. (MHz)	Observed v_{LSR} (km s ⁻¹)	Observed T_A^* (K)
SO ¹⁸ O 24 _{4,21} -25 _{1,24}	268096.198	0.24	299.6	268096.4 ¹⁷	8.8	0.31
SO ¹⁸ O 9 _{5,5} -10 _{4,6}	268618.479	0.76	99.0	268620.5	6.7	0.19
SO ¹⁸ O 9 _{5,4} -10 _{4,7}	268630.772	0.76	99.0	³¹
SO ¹⁸ O 6 _{2,4} -5 _{1,5}	270970.943	1.90	27.9	270974.5 ³⁴	5.1	0.39
SO ¹⁸ O 32 _{4,29} -33 _{1,32}	271281.411	0.35	498.5	⁷
SO ¹⁸ O 16 _{3,14} -16 _{2,15}	271326.403	8.37	139.8	271328.9 ³⁶	6.2	0.18
SO ¹⁸ O 26 _{2,24} -26 _{1,25}	272235.733	12.9	321.9	³¹
SO ¹⁸ O 10 _{3,8} -11 _{0,11}	272869.061	0.03	69.4	⁵⁶
SO ¹⁸ O 18 _{2,17} -18 _{1,18}	273213.674	5.69	156.7	273216.5	5.9	0.14
SO ¹⁸ O 27 _{4,23} -27 _{3,24}	273527.753	18.7	368.9	273528.6	8.1	0.24
SO ¹⁸ O 37 _{4,33} -37 _{3,34}	273740.474	28.6	658.9	⁴⁸
SO ¹⁸ O 25 _{8,18} -26 _{7,19}	274232.871	3.26	435.5	⁶⁹
SO ¹⁸ O 25 _{8,17} -26 _{7,20}	274235.442	3.26	435.5	274236.3	8.1	0.08
SO ¹⁸ O 32 _{3,29} -32 _{2,30}	274568.048	20.7	490.1	274568.5 ⁵	8.5	0.33
SO ¹⁸ O 8 _{2,7} -7 _{1,6}	275207.551	2.97	40.8	⁴⁹
SO ¹⁸ O 28 _{3,25} -27 _{4,24}	275282.312	5.49	380.9	275283.9	7.3	0.17
SO ¹⁸ O 23 _{4,20} -24 _{1,23}	275552.789	0.22	278.6	no spectrum
SO ¹⁸ O 25 _{3,23} -26 _{0,26}	276001.955	0.14	303.9	³²
SO ¹⁸ O 17 _{3,15} -17 _{2,16}	276274.719	8.82	154.6	276277.6	5.9	0.21
SO ¹⁸ O 34 _{4,30} -33 _{5,29}	276277.576	5.84	562.1	⁸
SO ¹⁸ O 14 _{6,9} -15 _{5,10}	277081.114	1.51	177.5	277086.3 ^{9,37}	3.4	0.36
SO ¹⁸ O 14 _{6,8} -15 _{5,11}	277088.479	1.51	177.5	277092.6	4.5	0.22
SO ¹⁸ O 26 _{4,22} -26 _{3,23}	280724.381	17.5	345.0	280727.5 ⁶⁸	5.7	0.25
SO ₂ $\nu_2=1$ 25 _{3,23} -24 _{4,20}	82488.410	3.28	1066.4	82489.5	5.0	0.02
SO ₂ $\nu_2=1$ 8 _{1,7} -8 _{0,8}	85208.089	6.40	781.9	85208.5	7.6	0.08
SO ₂ $\nu_2=1$ 24 _{6,18} -25 _{5,21}	88029.007	3.67	1111.3	88031.4 ¹⁷	0.7	0.04
SO ₂ $\nu_2=1$ 29 _{4,26} -28 _{5,23}	88888.803	4.39	1186.5	¹⁷
SO ₂ $\nu_2=1$ 13 _{4,10} -14 _{3,11}	91400.957	1.93	869.0	noise level
SO ₂ $\nu_2=1$ 8 _{3,5} -9 _{2,8}	92660.362	1.13	800.8	92661.5	5.4	0.03
SO ₂ $\nu_2=1$ 29 _{7,23} -30 _{6,24}	93456.549	4.44	1268.1	93457.5	6.1	0.02
SO ₂ $\nu_2=1$ 39 _{6,34} -38 _{7,31}	93474.213	6.15	1555.0	⁸⁸
SO ₂ $\nu_2=1$ 16 _{2,14} -15 _{3,13}	98264.696	2.99	882.8	98265.5 ⁶	6.4	0.17
SO ₂ $\nu_2=1$ 27 _{3,25} -26 _{4,22}	99177.397	3.14	1114.8	⁵
SO ₂ $\nu_2=1$ 18 _{5,13} -19 _{4,16}	102335.197	2.69	965.1	102337.0	3.7	0.06
SO ₂ $\nu_2=1$ 7 _{3,5} -8 _{2,6}	103699.749	0.94	793.5	103699.5 ¹⁷	9.6	0.09
SO ₂ $\nu_2=1$ 31 _{3,29} -30 _{4,26}	104210.533	2.47	1222.2	³²
SO ₂ $\nu_2=1$ 2 _{2,0} -3 _{1,3}	104518.097	0.16	757.9	104518.6 ⁴¹	7.5	0.02
SO ₂ $\nu_2=1$ 3 _{1,3} -2 _{0,2}	105117.218	2.01	752.9	105118.5	5.4	0.08
SO ₂ $\nu_2=1$ 10 _{1,9} -10 _{0,10}	105956.755	6.73	799.9	105957.5	6.9	0.16
SO ₂ $\nu_2=1$ 29 _{3,27} -28 _{4,24}	106870.586	2.85	1166.8	106870.5 ¹⁷	9.3	0.10
SO ₂ $\nu_2=1$ 23 _{6,18} -24 _{5,19}	107251.291	3.46	1089.2	107253.5 ⁶	2.8	0.25
SO ₂ $\nu_2=1$ 22 _{3,19} -21 _{4,18}	110003.703	3.68	1003.3	110004.5	6.9	0.04
SO ₂ $\nu_2=1$ 35 _{5,31} -34 _{6,28}	114050.625	5.45	1389.3	⁶
SO ₂ $\nu_2=1$ 28 _{7,21} -29 _{6,24}	114467.268	4.23	1241.3	114470.5 ³⁴	0.7	0.10
SO ₂ $\nu_2=1$ 12 _{2,10} -12 _{1,11}	131530.479	9.89	827.9	131531.4	6.9	0.21
SO ₂ $\nu_2=1$ 10 _{2,8} -10 _{1,9}	132594.603	7.77	806.3	132595.5	6.9	0.34
SO ₂ $\nu_2=1$ 12 _{1,11} -12 _{0,12}	133003.613	6.69	821.6	133005.1 ⁹⁰	5.5	0.19
SO ₂ $\nu_2=1$ 11 _{4,8} -12 _{3,9}	133271.748	1.49	846.0	⁷
SO ₂ $\nu_2=1$ 27 _{7,21} -28 _{6,22}	134483.137	4.01	1215.6	⁴
SO ₂ $\nu_2=1$ 14 _{2,12} -14 _{1,13}	135531.563	11.7	853.4	135532.6	6.7	0.31
SO ₂ $\nu_2=1$ 5 _{1,5} -4 _{0,4}	136675.406	3.13	760.8	136676.5	6.6	0.22
SO ₂ $\nu_2=1$ 8 _{2,6} -8 _{1,7}	137234.335	5.68	788.5	¹⁶
SO ₂ $\nu_2=1$ 32 _{8,24} -33 _{7,27}	140968.037	4.78	1391.0	³⁴
SO ₂ $\nu_2=1$ 16 _{5,11} -17 _{4,14}	142044.339	2.26	932.9	³⁶
SO ₂ $\nu_2=1$ 6 _{2,4} -6 _{1,5}	143663.844	3.83	774.5	143664.5 ¹	7.7	0.42

Table A.9. continued.

Species/Transition $J_{K_a,K_c} - J'_{K'_a,K'_c}$	Predicted freq. (MHz)	S_{ij}	E_u (K)	Observed freq. (MHz)	Observed v_{LSR} (km s ⁻¹)	Observed T_A^* (K)
SO ₂ $\nu_2=1$ 5 _{3,3} -6 _{2,4}	145331.342	0.51	781.5	145332.7	6.3	0.05
SO ₂ $\nu_2=1$ 16 _{2,14} -16 _{1,15}	145739.989	13.0	882.8	145741.5	5.9	0.39
SO ₂ $\nu_2=1$ 33 _{4,30} -32 _{5,27}	147129.710	4.51	1302.6	¹³
SO ₂ $\nu_2=1$ 21 _{6,16} -22 _{5,17}	148089.279	3.03	1047.8	¹⁶
SO ₂ $\nu_2=1$ 4 _{2,2} -4 _{1,3}	150060.477	2.27	764.4	150062.6	4.7	0.16
SO ₂ $\nu_2=1$ 37 _{5,33} -36 _{6,30}	151196.604	5.66	1456.9	¹⁷
SO ₂ $\nu_2=1$ 2 _{2,0} -2 _{1,1}	154896.423	0.87	757.9	154899.5 ¹⁷	3.0	0.25
SO ₂ $\nu_2=1$ 10 _{4,6} -11 _{3,9}	154925.408	1.27	835.8	154926.5	6.9	0.13
SO ₂ $\nu_2=1$ 26 _{7,19} -27 _{6,22}	154937.399	3.80	1190.7	154939.6	4.8	0.08
SO ₂ $\nu_2=1$ 18 _{2,16} -17 _{3,15}	157562.692	3.70	916.0	157563.9	6.7	0.16
SO ₂ $\nu_2=1$ 10 _{0,10} -9 _{1,9}	159887.299	6.41	794.8	⁴
SO ₂ $\nu_2=1$ 31 _{8,24} -32 _{7,25}	161118.533	4.57	1361.5	⁶
SO ₂ $\nu_2=1$ 15 _{5,11} -16 _{4,12}	161153.766	2.04	918.2	⁵
SO ₂ $\nu_2=1$ 3 _{2,2} -3 _{1,3}	161799.286	1.44	760.7	161802.5	3.1	0.37
SO ₂ $\nu_2=1$ 18 _{2,16} -18 _{1,17}	162976.601	13.6	916.0	162977.5	7.3	0.34
SO ₂ $\nu_2=1$ 14 _{1,13} -14 _{0,14}	165963.827	6.46	846.9	165964.6	7.7	0.42
SO ₂ $\nu_2=1$ 7 _{1,7} -6 _{0,6}	166061.130	4.43	772.2	²⁴
SO ₂ $\nu_2=1$ 4 _{3,1} -5 _{2,4}	166507.963	0.30	776.9	⁷³
SO ₂ $\nu_2=1$ 35 _{4,32} -34 _{5,29}	166834.689	4.35	1366.1	166836.5	5.7	0.05
SO ₂ $\nu_2=1$ 20 _{6,14} -21 _{5,17}	168508.840	2.81	1028.5	^{5,31}
SO ₂ $\nu_2=1$ 5 _{2,4} -5 _{1,5}	168826.259	2.46	768.9	⁵¹
SO ₂ $\nu_2=1$ 24 _{3,21} -23 _{4,20}	171566.838	4.21	1047.8	171567.5	7.9	0.13
SO ₂ $\nu_2=1$ 9 _{4,6} -10 _{3,7}	173495.943	1.05	826.6	²⁶
SO ₂ $\nu_2=1$ 25 _{7,19} -26 _{6,20}	174901.050	3.58	1166.8	174903.5 ⁷⁰	4.8	0.56
SO ₂ $\nu_2=1$ 30 _{4,26} -29 _{5,25}	176012.893	4.91	1217.2	176015.1 ⁴¹	5.3	0.37
SO ₂ $\nu_2=1$ 37 _{4,34} -36 _{5,31}	177865.345	4.04	1433.2	noisy spectrum
SO ₂ $\nu_2=1$ 22 _{3,19} -22 _{2,20}	199756.971	17.6	1003.3	199758.7 ⁵	6.5	0.62
SO ₂ $\nu_2=1$ 13 _{5,9} -14 _{4,10}	200888.344	1.60	891.5	¹⁶
SO ₂ $\nu_2=1$ 29 _{8,22} -30 _{7,23}	201308.491	4.14	1305.4	⁵
SO ₂ $\nu_2=1$ 20 _{3,17} -20 _{2,18}	201972.010	15.4	962.7	201974.4	5.4	0.40
SO ₂ $\nu_2=1$ 12 _{0,12} -11 _{1,11}	202562.326	8.41	815.2	202564.4	5.9	0.47
SO ₂ $\nu_2=1$ 16 _{1,15} -16 _{0,16}	203652.511	6.21	875.8	203654.4	6.2	0.44
SO ₂ $\nu_2=1$ 24 _{3,21} -24 _{2,22}	204331.692	19.4	1047.8	204333.2	6.8	0.28
SO ₂ $\nu_2=1$ 34 _{9,25} -35 _{8,28}	207420.884	4.91	1494.9	⁶
SO ₂ $\nu_2=1$ 18 _{6,12} -19 _{5,15}	208172.440	2.38	992.6	^{2,4,6}
SO ₂ $\nu_2=1$ 18 _{3,15} -18 _{2,16}	209433.722	12.9	926.1	209434.9 ¹⁸	7.4	1.15
SO ₂ $\nu_2=1$ 11 _{2,10} -11 _{1,11}	209454.261	4.56	815.5	209456.1	6.3	0.48
SO ₂ $\nu_2=1$ 3 _{2,2} -2 _{1,1}	212177.612	1.67	760.7	212179.9	5.7	0.14
SO ₂ $\nu_2=1$ 7 _{4,4} -8 _{3,5}	212726.193	0.63	811.0	212728.6 ³⁴	5.5	0.11
SO ₂ $\nu_2=1$ 23 _{7,17} -24 _{6,18}	214835.983	3.15	1121.7	214837.5 ⁵	7.0	0.25
SO ₂ $\nu_2=1$ 26 _{3,23} -26 _{2,24}	216758.559	20.5	1096.2	216759.9 ⁵	7.1	0.60
SO ₂ $\nu_2=1$ 20 _{2,18} -19 _{3,17}	218995.835	4.59	953.0	218997.4	6.9	0.31
SO ₂ $\nu_2=1$ 22 _{2,20} -22 _{1,21}	219465.546	13.3	993.7	219467.4 ^{4,7}	6.5	1.00
SO ₂ $\nu_2=1$ 16 _{3,13} -16 _{2,14}	220165.252	10.6	893.4	⁵
SO ₂ $\nu_2=1$ 12 _{5,7} -13 _{4,10}	220657.897	1.39	879.5	⁴
SO ₂ $\nu_2=1$ 28 _{8,20} -29 _{7,23}	221277.998	3.92	1278.7	⁵
SO ₂ $\nu_2=1$ 11 _{1,11} -10 _{0,10}	222424.457	7.70	805.5	222423.7 ^{5,7}	10.1	1.21
SO ₂ $\nu_2=1$ 17 _{6,12} -18 _{5,13}	227808.377	2.16	976.0	¹⁶
SO ₂ $\nu_2=1$ 13 _{2,12} -13 _{1,13}	229545.293	4.98	838.3	229548.6 ⁵⁴	4.7	0.22
SO ₂ $\nu_2=1$ 14 _{3,11} -14 _{2,12}	231980.527	8.58	864.6	⁷
SO ₂ $\nu_2=1$ 6 _{4,2} -7 _{3,5}	232210.300	0.43	804.6	³⁹
SO ₂ $\nu_2=1$ 16 _{1,15} -15 _{2,14}	233724.927	6.02	875.8	233728.8	4.0	0.25
SO ₂ $\nu_2=1$ 22 _{7,15} -23 _{6,18}	234679.037	2.93	1100.5	¹⁶
SO ₂ $\nu_2=1$ 26 _{3,23} -25 _{4,22}	237062.226	4.84	1096.2	¹⁸
SO ₂ $\nu_2=1$ 28 _{3,25} -28 _{2,26}	237602.207	20.8	1148.5	237603.6 ³²	7.2	0.51
SO ₂ $\nu_2=1$ 4 _{2,2} -3 _{1,3}	238697.756	1.72	764.4	238698.9	7.6	0.37
SO ₂ $\nu_2=1$ 38 _{5,33} -37 _{6,32}	239753.000	6.11	1495.2	¹⁶

Table A.9. continued.

Species/Transition $J_{K_a, K_c} - J'_{K'_a, K'_c}$	Predicted freq. (MHz)	S_{ij}	E_u (K)	Observed freq. (MHz)	Observed v_{LSR} (km s ⁻¹)	Observed T_A^* (K)
SO ₂ $\nu_2=1$ 11 _{5,7} -12 _{4,8}	240057.470	1.17	868.5	240060.5	5.3	0.07
SO ₂ $\nu_2=1$ 27 _{8,20} -28 _{7,21}	241126.743	3.70	1252.9	241128.6	6.7	0.13
SO ₂ $\nu_2=1$ 32 _{4,28} -31 _{5,27}	241193.824	5.36	1276.8	¹⁶
SO ₂ $\nu_2=1$ 12 _{3,9} -12 _{2,10}	242872.869	6.88	839.6	⁵
SO ₂ $\nu_2=1$ 14 _{0,14} -13 _{1,13}	243522.666	10.5	839.0	243523.9 ¹²	7.5	1.18
SO ₂ $\nu_2=1$ 18 _{1,17} -18 _{0,18}	244386.673	6.03	908.2	¹⁸
SO ₂ $\nu_2=1$ 5 _{2,4} - 4 _{1,3}	245002.780	2.12	768.9	245004.5	6.9	0.46
SO ₂ $\nu_2=1$ 32 _{9,23} -33 _{8,26}	247275.019	4.47	1433.3	³²
SO ₂ $\nu_2=1$ 16 _{6,10} -17 _{5,13}	247485.487	1.94	960.4	247490.1 ^{32,91}	3.4	0.29
SO ₂ $\nu_2=1$ 5 _{4,2} - 6 _{3,3}	251401.371	0.25	799.1	⁴³
SO ₂ $\nu_2=1$ 10 _{3,7} -10 _{2,8}	251428.540	5.43	818.3	251428.8 ⁶	8.7	1.04
SO ₂ $\nu_2=1$ 13 _{1,13} -12 _{0,12}	251450.180	9.61	827.3	251452.6 ^{6,34}	6.2	0.83
SO ₂ $\nu_2=1$ 15 _{2,14} -15 _{1,15}	252731.060	5.29	864.6	252733.5	6.1	0.47
SO ₂ $\nu_2=1$ 21 _{7,15} -22 _{6,16}	254381.132	2.71	1080.3	254385.1 ³⁶	4.3	0.20
SO ₂ $\nu_2=1$ 8 _{3,5} - 8 _{2,6}	257099.338	4.13	800.8	⁴⁹
SO ₂ $\nu_2=1$ 24 _{2,22} -24 _{1,23}	257420.276	12.8	1038.0	257422.7 ³¹	6.2	0.38
SO ₂ $\nu_2=1$ 10 _{5,5} -11 _{4,8}	259525.559	0.96	858.4	⁵
SO ₂ $\nu_2=1$ 6 _{3,3} - 6 _{2,4}	260176.150	2.89	787.0	260178.9	5.8	0.46
SO ₂ $\nu_2=1$ 26 _{8,18} -27 _{7,21}	260920.931	3.48	1228.1	260922.6	7.1	0.52
SO ₂ $\nu_2=1$ 4 _{3,1} - 4 _{2,2}	261450.266	1.61	776.9	261453.8	4.9	0.53
SO ₂ $\nu_2=1$ 3 _{3,1} - 3 _{2,2}	261855.237	0.89	773.3	⁴⁴
SO ₂ $\nu_2=1$ 5 _{3,3} - 5 _{2,4}	262144.899	2.26	781.5	262145.2	8.7	0.36
SO ₂ $\nu_2=1$ 7 _{3,5} - 7 _{2,6}	262999.768	3.48	793.5	263004.5 ²⁶	3.7	0.66
SO ₂ $\nu_2=1$ 32 _{4,28} -32 _{3,29}	264129.781	25.5	1276.8	264128.9 ¹⁷	10.1	0.19
SO ₂ $\nu_2=1$ 9 _{3,7} - 9 _{2,8}	264846.220	4.65	809.1	264849.5	5.3	0.22
SO ₂ $\nu_2=1$ 30 _{4,26} -30 _{3,27}	266030.564	23.2	1217.2	266032.6	6.7	0.42
SO ₂ $\nu_2=1$ 30 _{3,27} -30 _{2,28}	266815.527	20.5	1204.5	⁵
SO ₂ $\nu_2=1$ 15 _{6,10} -16 _{5,11}	267006.778	1.72	945.7	267008.5	7.1	0.15
SO ₂ $\nu_2=1$ 31 _{9,23} -32 _{8,24}	267091.922	4.25	1403.8	⁴⁷
SO ₂ $\nu_2=1$ 11 _{3,9} -11 _{2,10}	268169.791	5.78	828.4	⁴⁹
SO ₂ $\nu_2=1$ 34 _{4,30} -34 _{3,31}	270528.378	27.1	1340.3	⁵
SO ₂ $\nu_2=1$ 4 _{4,0} - 5 _{3,3}	270633.756	0.10	794.5	¹⁷
SO ₂ $\nu_2=1$ 13 _{3,11} -13 _{2,12}	273467.380	6.87	851.4	⁴⁹
SO ₂ $\nu_2=1$ 20 _{7,13} -21 _{6,16}	274039.760	2.49	1060.9	274041.3	7.3	0.05
SO ₂ $\nu_2=1$ 28 _{4,24} -28 _{3,25}	274778.408	20.5	1161.7	274780.5	6.7	0.36
SO ₂ $\nu_2=1$ 7 _{2,6} - 6 _{1,5}	274789.404	2.67	780.8	274791.5	6.8	0.27
SO ₂ $\nu_2=1$ 17 _{2,16} -17 _{1,17}	278755.123	5.50	894.5	278757.4	6.5	0.59
SO ₂ $\nu_2=1$ 9 _{5,5} -10 _{4,6}	278849.605	0.76	849.2	278851.5 ³⁶	7.0	0.49
SO ₂ $\nu_2=1$ 25 _{8,18} -26 _{7,19}	280629.381	3.26	1204.2	280631.5 ⁷³	6.7	0.40

Notes. Emission lines of SO₂, its isotopologues, and its vibrationally excited states present in the frequency range of the 30-m Orion KL survey. Column 1 indicates the species and the quantum numbers of the line transition, Col. 2 gives the assumed rest frequencies, Col. 3 the line strength, Col. 4 the energy of the upper level, Col. 5 observed frequency assuming a v_{LSR} of 9.0 km s⁻¹, Col. 6 the observed radial velocities, and Col. 7 the peak line antenna temperature.

(¹) Blended with HCOOCH₃ $\nu_7=1$. (²) Blended with CH₂DCN. (³) Blended with HNCO. (⁴) Blended with CH₃CH₂CN. (⁵) Blended with HCOOCH₃. (⁶) Blended with CH₃CH₂CN ν_{13}/ν_{21} . (⁷) Blended with CH₃OCH₃. (⁸) Blended with the previous transition. (⁹) Blended with g⁺-CH₃CH₂OH. (¹⁰) Blended with CH₃C¹⁵N. (¹¹) Blended with SiS. (¹²) Blended with NH₂CHO. (¹³) Blended with CH₃CN. (¹⁴) Blended with OCS. (¹⁵) Blended with H₂CO. (¹⁶) Blended with CH₃OH. (¹⁷) Blended with U line. (¹⁸) Blended with ³³SO₂. (¹⁹) Blended with CH₃¹³CH₂CN. (²⁰) Blended with SO¹⁸O. (²¹) Blended with S¹⁸O. (²²) Blended with ³³SO. (²³) Blended with ³⁴SO₂. (²⁴) Blended with CH₃CN $\nu_8=1$. (²⁵) Blended with HC₃N $\nu_7=2$. (²⁶) Blended with CH₃CHO. (²⁷) Blended with NO. (²⁸) Blended with ³⁰SiO. (²⁹) Blended with NS. (³⁰) Blended with ¹³CH₃CH₂CN. (³¹) Blended with ¹³CH₃OH. (³²) Blended with CH₂CHCN. (³³) Blended with HC¹³CCN. (³⁴) Blended with (CH₃)₂CO. (³⁵) Blended with H₂CS. (³⁶) Blended with t-CH₃CH₂OH. (³⁷) Blended with H¹⁵NCO. (³⁸) Blended with HCC¹³CN. (³⁹) Blended with ¹³CH₃CN. (⁴⁰) Blended with CH₂¹³CHCN. (⁴¹) Blended with CH₃CH₂C¹⁵N. (⁴²) Blended with OC³³S. (⁴³) Blended with CH₃CH₂CN $\nu_{20}=1$. (⁴⁴) Blended with SO. (⁴⁵) Blended with H₂CCO. (⁴⁶) Blended with CCH. (⁴⁷) Blended with CH₂CHCN $\nu_{11}=1$. (⁴⁸) Blended with NH₂CHO $\nu_{12}=1$. (⁴⁹) Blended with SO₂. (⁵⁰) Blended with H₂C³⁴S. (⁵¹) Blended with ³⁴SO. (⁵²) Blended with H¹³CN. (⁵³) Blended with H¹³COOCH₃. (⁵⁴) Blended with CH₂CHCN $\nu_{11}=2$. (⁵⁵) Blended with H₂¹³CS. (⁵⁶) Blended with HC₃N. (⁵⁷) Blended with CH₃¹³CN. (⁵⁸) Blended with g⁻-CH₃CH₂OH. (⁵⁹) Blended with SO₂ $\nu_2=1$. (⁶⁰) Blended with CH₂CHCN $\nu_{15}=1$. (⁶¹) Blended with H₃₀ α . (⁶²) Blended with HC₃N $\nu_7=1$. (⁶³) Blended with HN¹³CO. (⁶⁴) Blended with H¹³CO⁺. (⁶⁵) Blended with CS $\nu=1$. (⁶⁶) Blended with HC₃N $\nu_6=1$. (⁶⁷) Blended with H₆₅ ϵ . (⁶⁸) Blended with HCOO¹³CH₃. (⁶⁹) Blended with the next transition. (⁷⁰) Blended with CH₃CH₂¹³CN. (⁷¹) Blended with HNC¹⁸O. (⁷²) Blended with DCOOCH₃. (⁷³) Blended with CH₃OD. (⁷⁴) Blended with SiO. (⁷⁵) Blended with H¹³CCCN. (⁷⁶) Blended with SHD. (⁷⁷) Blended with c-C₂H₄O. (⁷⁸) Blended with CH₃OH $\nu_7=1$. (⁷⁹) Blended with HCC¹³CN $\nu_7=1$. (⁸⁰) Blended with HC₃CN $\nu_7+\nu_6$. (⁸¹) Blended with HC¹⁸OCH₃. (⁸²) Blended with HC₃¹⁵N. (⁸³) Blended with O¹³CS. (⁸⁴) Blended with CO. (⁸⁵) Blended with OC³⁴S. (⁸⁶) Blended with c-C₃H₂. (⁸⁷) Blended with HCOOH. (⁸⁸) Blended with C₃S. (⁸⁹) Blended with g⁺-g⁻-CH₃CH₂OH. (⁹⁰) Blended with ¹³CH₃CCH. (⁹¹) Blended with HDCS.